Energy Storage Materials 21 (2019) 308–334

Contents lists available at ScienceDirect

Energy Storage Materials

journal homepage: www.elsevier.com/locate/ensm

Recent progress on solid-state hybrid electrolytes for solid-state lithium batteries

Jianneng Liang, Jing Luo, Qian Sun, Xiaofei Yang, Ruying Li, Xueliang Sun *

Department of Mechanical and Materials Engineering, University of Western Ontario, London, Ontario, N6A 5B9, Canada

ARTICLE INFO

Keywords:
Solid-state electrolytes
Solid-state batteries
Hybrid electrolytes
Interface

ABSTRACT

Lithium batteries are promising energy storage systems for applications in electric vehicles. However, conventional liquid electrolytes inherit serious safety hazards including leakage, ignition and even explosion upon overheating. Solid-state electrolytes (SSEs) are considered as the ultimate solution to these safety concerns because of their excellent thermal and electrochemical stabilities. Nevertheless, few individual SSE has reached practical application standards due to incomprehensive performance. High ionic conductivity, low interfacial resistance, and high stability towards electrodes are difficult to achieve simultaneously with an individual SSE. Hybrid electrolytes rationally combining two or more types of SSEs with complementary advantages are promising for building feasible solid-state lithium batteries (SSLBs). Coupling desired soft electrolyte and stiff inorganic SSEs can ensure good electrode wettability, high ionic conductivity, and high mechanical strength to prevent lithium dendrite formation at the same time. In this review, comprehensive perspectives from the broad context of the importance of hybrid electrolytes to subtle design concepts are summarized. This review not only covers the introductory of classifications, synthesis methods, and ionic conductivity mechanism, but also crystallizes the strategies for enhancing the ionic conductivity of hybrid electrolyte, the understandings on the interfacial challenges of the electrolyte/electrolyte and electrolyte/electrode interfaces, and the strategies for building feasible SSLBs with different hybrid electrolyte combinations.

1. Introduction

Lithium-ion batteries (LIBs) are playing a more and more important role in our daily life. LIBs not only power our portable devices (e.g. cellphones, laptops and cameras), but also drive the transportation (e.g. electric vehicles (EVs), hybrid electric vehicles (HEVs)), and even serve as temporary storage systems for excess peak energy delivered by renewable energy sources, such as solar, wind, nuclear and hydro power. Since Sony launched the first commercial LIB with an intercalating $LiCoO_2$ (LCO) cathode in 1990s [1], LIBs have attracted increasing research attentions in recent 30 years. In order to meet the requirements for large-scale applications in EVs and grid energy storage system, a variety of high-energy-density cathode candidates such as Ni-rich lithium nickel manganese cobalt oxide cathode (NMC) [2,3], Li-rich NMC [4,5], lithium nickel cobalt aluminum oxide (NCA) [6,7], and alternative conversion-type battery systems of Li-sulfur (Li-S) and Li-air [8–12] have been developed and attracted substantial research attentions. However, the usage of liquid electrolytes in the commercial LIBs poses serious safety concerns such as fire and explosion. Most of those liquid electrolyte solvents have very low boiling point (below 300 °C) and flash point (below 150 °C) [13–15]. The thermal instability, volatility and flammability of organic liquid electrolytes are key problems that cause the safety issues of LIBs [13–16]. Li dendrite formation problem due to inhomogeneous charging of the anode is another safety concern that can cause cell short circuit in liquid-based LIBs [17–21].

Replacing liquid electrolytes with solid-state electrolytes (SSEs) provide a promising solution to tackle the safety issues. SSEs are thermally stable and basically nonflammable. The key functional properties of a SSE applied in solid-state lithium batteries (SSLBs) should include (i) high total (bulk and grain boundary) Li^+ ion conductivity over a wide temperature range, (ii) wide electrochemical window to couple with lithium metal anode and high-voltage cathode, (iii) chemically and mechanically compatible interfaces with anode and cathode, (iv) chemically stable in ambience environment, and (v) low interfacial resistance toward electrodes.

Even though SSEs have many attractive properties, especially in safety, an individual SSE having comprehensive functionalities has not yet been developed. Fig. 1 summaries the main drawbacks of each type of

* Corresponding author.
E-mail address: xsun@eng.uwo.ca (X. Sun).

https://doi.org/10.1016/j.ensm.2019.06.021
Received 16 March 2019; Received in revised form 30 May 2019; Accepted 14 June 2019
Available online 26 June 2019

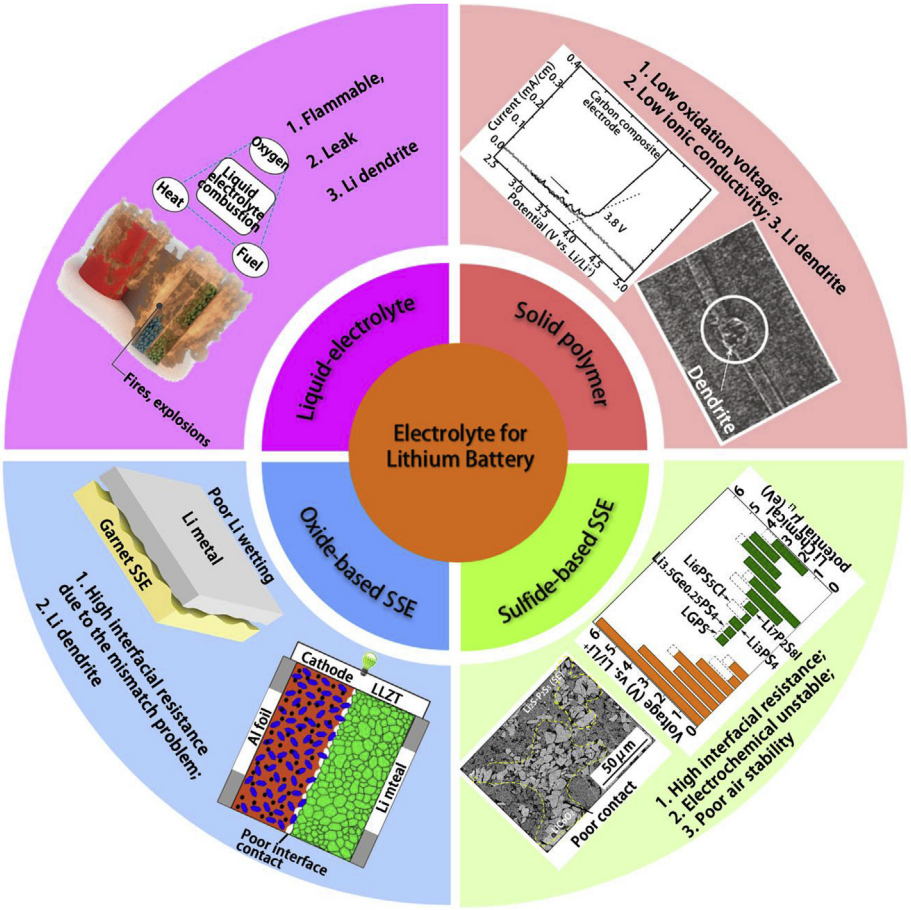

Fig. 1. Common electrolytes for lithium batteries and their main drawbacks [29,64–70]. Reproduced with permission [29], Copyright 2014, Springer Nature. Reproduced with permission [64,65], AAAS. Reproduced with permission [66], Copyright 2017, ECS. Reproduced with permission [67], Copyright 2016, Wiley. Reproduced with permission [68], Copyright © 2016 Hayashi, Sakuda and Tatsumisago. Reproduced with permission [69], Copyright 2001, Elsevier. Reproduced with permission [70], Copyright 2015, ACS. Further permissions related to the material excerpted should be directed to the original publisher.

electrolytes including liquid electrolyte, solid polymer electrolyte, oxide-based SSE, sulfide-based SSEs. The oxide- and sulfide-based SSEs are also classified as inorganic SSEs. Different SSEs encounter various challenges that hinder their practical applications. Firstly, most of SSEs including oxide-based SSE and the dry solid polymer electrolyte (SPE) have a relatively low ionic conductivity compared to the liquid-based counterpart at room temperature (RT). For example, PEO-based SPE (e.g. polyethylene oxide complexing with lithium salt) have an ionic conductivity around 10^{-7}-10^{-5} S/cm at RT. Most ceramic SSEs such as NASICON-type SSEs (e.g. $Li_{1+x}Al_xTi_{2-x}(PO_4)_3$ (LATP)) and $Li_{1+x}Al_xGe_{2-x}(PO_4)_3$ (LAGP)) [22,23]. garnet-type SSEs ($Li_7La_3Zr_2O_{12}$, (LLZO)) [24] and perovskite-type SSEs ($Li_{3x}La_{(2/3)-x}TiO_3$, (LLTO) [25] have an ionic conductivity around 10^{-5}-10^{-3} S/cm. Secondly, besides the low ionic conductivity problem, the high interfacial resistance between the SSEs and electrodes also restricts the practical applications of SSEs. Mismatch between the rigid SSEs and the solid-state electrodes is a common cause for the high interfacial resistance. Another reason for the high interfacial resistance is due to the formation of space charge layer (SCL) between sulfide-based SSEs and $LiCoO_2$ cathodes [26], or the formation of interphase materials original from the side reaction between SSEs and electrodes materials.

To build a comprehensive SSE, a new concept of hybrid electrolyte has been developed to rationally combine two or more types of Li^+ ion conductors. A hybrid electrolyte intends to compensate the advantage and disadvantage of each constituent. The most common hybrid electrolyte is composite electrolyte consisting of a soft polymer electrolyte and a rigid inorganic SSE. While the rigid inorganic SSE maintains relatively high ionic conductivity at RT, the soft and flexible SPE solves the mismatch and wettability problems on the interface with electrodes [27,28]. Meanwhile, the Li dendrite formation problem due to the mechanically poor SPE can be alleviated by the stiff ceramic SSE fillers [29]. Another types of hybrid electrolytes are multilayer structured hybrid electrolytes where a ceramic SSE layer serves as the major Li^+ ion conductor and separator with SPE outer layers to tailor the interface against electrodes. Or, instead of SPE, trace amount of liquid electrolyte is spread on the oxide SSE surface to ensure ionic conduction between the rigid oxide SSEs and electrodes. We refer this kind of configuration as liquid-oxide hybrid electrolyte. The design concepts and the advantages of hybrid electrolytes SSLBs are summaried in Fig. 2.

As increasing research efforts have been dedicated to developing hybrid electrolytes for advanced SSLBs, the progresses of hybrid electrolytes for lithium batteries have been reviewed with particular focuses of classifications, ionic conductivities, and applications in solid-state batteries [30,31]. Differently, this review aims to provide comprehensive perspectives from the broad context of the importance of hybrid electrolytes to subtle design concepts. We not only cover the introductory of classifications, synthesis methods, and ionic conductivity mechanism of the hybrid electrolyte, but also crystallize the strategies for enhancing the ionic conductivity, the understandings of the interfacial challenges for the electrolyte/electrolyte and electrolyte/electrode interfaces, and the strategies for building feasible SSLBs with different hybrid electrolyte combinations.

1.1. Solid-state electrolytes and challenges

Before introducing hybrid electrolytes, different types of SSEs including SPEs, oxide-based SSEs and sulfide-based SSEs will be systematically introduced and compared. In-depth details about ionic conductivities, interface properties, electrochemical/chemical properties, design mechanism and lithium ion transportation mechanism of SPEs, oxide-based SSEs and sulfide-based SSEs have been extensively reviewed [16,32–63], so the introduction to each individual SSE here mainly

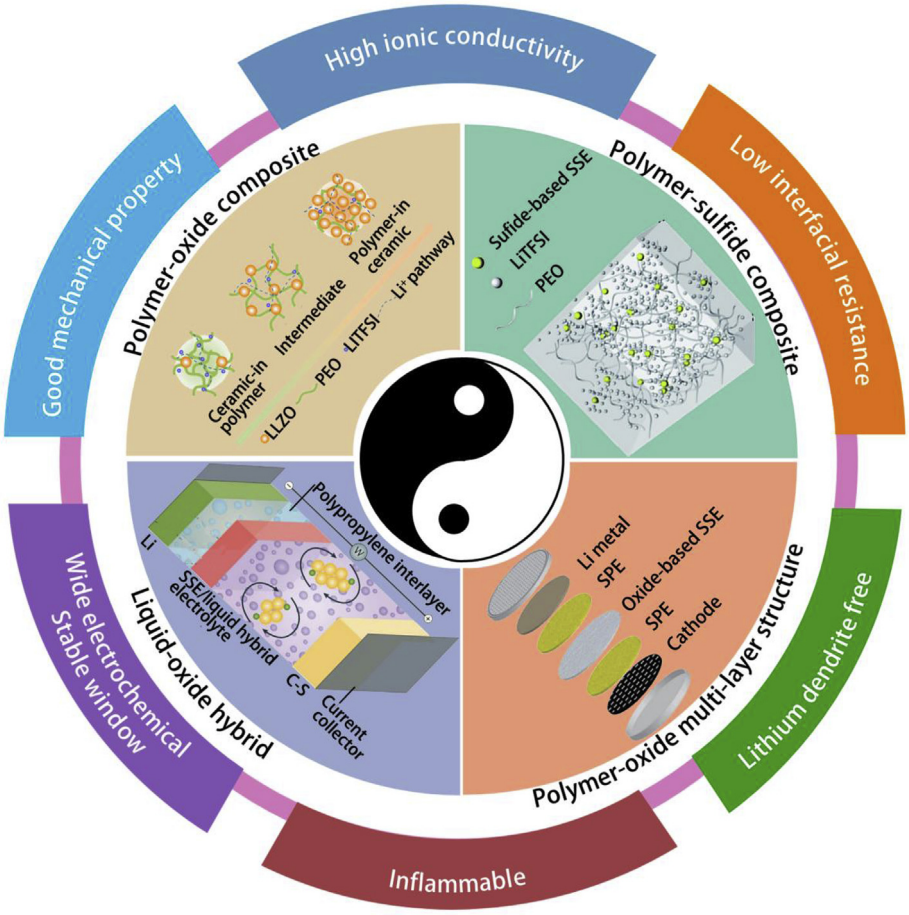

Fig. 2. Design concepts and the advantages of hybrid electrolytes for SSLBs [71–74]. Reproduced with permission [71], Copyright 2018, Elsevier. Reproduced with permission [72], Copyright 2017, RSC. Reproduced with permission [73], Copyright 2016, ACS. Reproduced with permission [74], Copyright 2017, Springer Nature.

focuses on their distinct characteristics and important parameters that are related to hybrid electrolyte designs.

1.1.1. Solid polymer electrolytes (SPEs)

In 1973, the discovery of ionic conductive complexes between polyethylene oxide (PEO) and alkali metal salts by Wright et al. [75] opened a new direction for SSE research. Generally speaking, a good SPE usually consists of a high dielectric host polymer complexed with a lithium salt with a low lattice energy (Fig. 3a shows the structure of a SPE with PEO complexing with $LiAsF_6$). Polymers with polar functional groups are chosen to facilitate the dissociation and transport of alkali ions; salts with high ionization ability are selected. Among all SPEs, PEO-based SPEs are most widely studied [76–84] due to their excellent salt-solvating ability and interfacial compatibility with electrodes. Moreover, SSLBs with a $LiFePO_4$ cathode, a Li metal anode and a polyether-based SPE show excellent cycling performance at 70 °C [84]. They have been commercialized in an electric car model, Bolloré Bluecar, to provide 30 KWh electricity with a driving range of 250 km. Other host polymer candidates including polyacrylonitrile (PAN) [85–87], poly(methylmethacrylate) (PMMA) [88,89], poly(vinylidenefluoride-co-hexafluoropropylene) (PVDF-HFP) [90,91] and poly(propylene carbonate) (PPC) [92,93], poly(ethylene carbonate) (PEC) [94] also receive increasing research interest lately for potential application in SSLBs.

However, the ionic conductivity of PEO-based SPEs is in the range of 10^{-7}-10^{-5} S/cm at RT (Fig. 3b) [76–78], which falls short to the requirement of SSLBs for operating at a wide temperature range. Moreover, due to the poor mechanical strength of the polymer matrix, SPEs suffer from Li dendrite formation problem [29]. Li dendrite growth at a Li/SPE/Li symmetrical cell had been observed using X-ray tomography technique (Fig. 3d–h) [29,95]. The results show that the defect of Li anode surface plays a key role in the nucleation of Li dendrites. N.S. Schauser et al. investigated the temperature influence on the Li dendrite formation in SPE. At a higher temperature (over 105 °C), significant dendrite growth was observed and caused failure of the cell, while under a lower temperature (lower than 90 °C), Li dendrite growth is prohibited [95]. These results were probably due to the lower mechanical strength of SPE under higher temperature that led to serious Li dendrite formation. Thus, to prevent growth of lithium dendrite, a high shear modulus is required for SPEs. As proposed by Monroe and J. Newman, if the shear modulus of SPE is higher than that of lithium metal, the dendrite growth can be inhibited [96–99].

Another challenge is the instability of SPEs at high voltages, which seriously restrict their applications in high-energy-density LIBs [69]. The instability of SPE under high voltage makes SPE/cathode interface a big challenge in high-energy-density LIBs system. PEO-based SPEs are known to be electrochemically stable under 3.8 V (vs. Li/Li^+) (Fig. 3c), so they are relatively stable towards $LiFePO_4$ cathode that has a charging plateau at about 3.4 V [84]. However, PEO-based SPEs fail to deliver good performance in SSLBs with a high voltage (>4 V) cathode such as $LiCoO_2$ [100]. To improve the stability of SPE at high voltage, engineering the SPE/cathode interface with a coating layer, such as Al_2O_3, Li_3PO_4 and poly(ethylcyanoacrylate), has been reported with improvement in cycling performance [100–102]. Therefore, the study of SSLBs with SPEs should focus on enhancing the mechanical properties for preventing Li dendrite formation and increasing electrochemical stability of SPEs for high-energy-density LIBs.

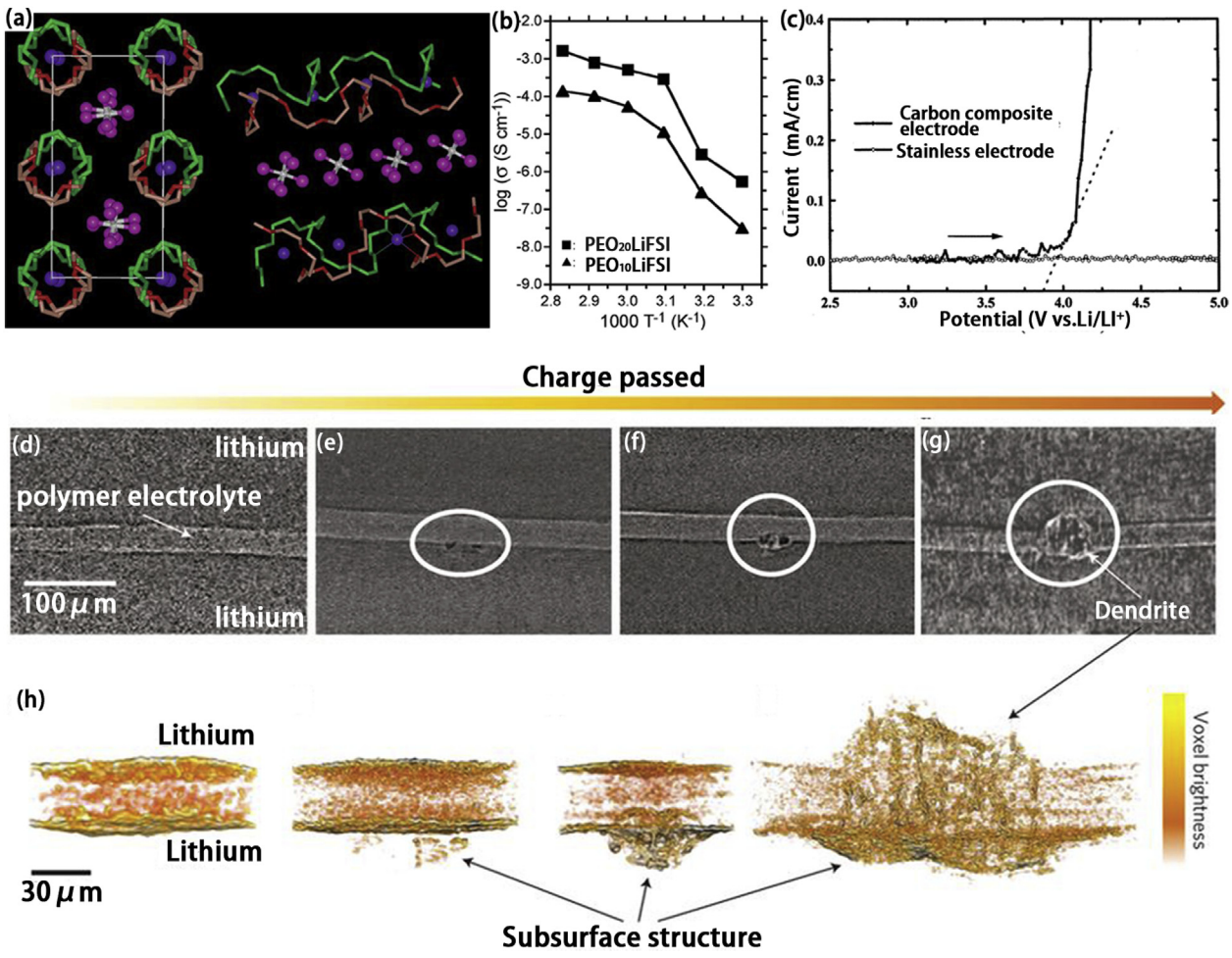

Fig. 3. (a) Structure of a crystalline PEO-based SPE consisting of PEO and $LiAsF_6$. Left, PEO chain axis is perpendicular to the page. Right, PEO chain axis is parallel to the page. Purple spheres, Li; white spheres, As; pink spheres, F; light green, carbon in PEO chain 1; dark green, oxygen in PEO chain 1. Light red, carbon in PEO chain 2; dark red, oxygen in PEO chain 2. Hydrogens are not shown [103]. Reproduced with permission [103], Copyright 2001, Springer Nature. (b) Temperature dependent ionic conductivity of PEO-based SPEs [104]. Reproduced with permission [104], Copyright 2014, RSC. (c) The electrochemical stable window of a PEO-based SPE is only 3.8 V [69]. Reproduced with permission [69], Copyright 2001, Elsevier. (d)–(g) X-ray tomography slices show the evolution of Li dendrite formation in SPE and their 3-dimensional (3D) reconstructions diagrams (h) [29]. Reproduced with permission [29], Copyright 2014, Springer Nature. (For interpretation of the references to color in this figure legend, the reader is referred to the Web version of this article.)

1.1.2. Oxide-based SSEs

NASICON-type, perovskite-type, and garnet-type SSEs are the most popular oxide-based SSEs and have demonstrated feasibilities in hybrid electrolytes for SSLBs. Their intrinsic advantages such high ionic conductivity and air stable properties make them attractable in the applications of hybrid electrolytes. Categorized by different structures, the oxide-based SSEs exhibit different ionic conductivities and chemical properties and face different challenges in the application of SSLBs. Representative examples will be discussed in this section.

NASICON-type SSEs, the name was first given to a sodium superionic conductor $NaM_2(PO_4)_3$ (M = Ge, Ti, Zr), having the crystalline NASICON framework consists of corner sharing PO_4 tetrahedra and MO_6 (M = Ge, Ti, Zr) octahedra forming a 3D network structure [105]. Na^+ ions are located on interstitial sites and transported along the c axis [106]. By replacing Na^+ with Li^+, NASICON-type SSEs become Li^+ ion conductors without the change of NASICON crystal structure (Fig. 4a). The currently most popular NASICON-type SSEs are $Li_{1+x}Al_xTi_{2-x}(PO_4)_3$ (LATP) and $Li_{1+x}Al_xGe_{2-x}(PO_4)_3$ (LAGP), which are obtained by partial Al substitution of Ti or Ge in $LiTi_2(PO_4)_3$ and $LiGe_2(PO_4)_3$, respectively. The highest ionic conductivity of NASICON-type SSEs reported to date at RT is in the range of 10^{-3} to 10^{-2} S/cm [106], which is almost comparable to that of liquid-based electrolytes. However, the rigid nature of NASICON-type SSEs makes them challenging to achieve good interface with electrodes. Another challenge is that the Ti-containing LATP can react with reductants such as lithium metal (Fig. 4j) and polysulfides, seriously restricting its application in high-energy-density SSLBs.

Garnet-type SSEs have a general chemical formula of $A_3B_2(XO_4)_3$ (A = Ca, Mg, Y, La et al. B = Al, Fe, Ga, Ge, Mn, Ni or V; X = Si, Ge, Al) where A, B, and X have eight, six, and four oxygen coordinated cation sites in a crystalline face-center-cubic structure [107]. The crystalline structure of cubic phase garnet-type SSE is showed in Fig. 4b. The studies of garnet-type SSEs cover Li_3-tpye $Li_3Ln_3Te_2O_{12}$ (Ln = Y, Pr, Nd, Sm-Lu) [108], Li_5-type $Li_5La_3M_2O_{12}$ (M = Nb, Ta) [109], Li_6-type $Li_6ALa_2M_2O_{12}$ (A = Mg, Ca, Sr, Ba) [110], and Li_7-type $Li_7La_3X_2O_{12}$ (X = Zr, Sn, Ta) [24]. The first three garnet SSEs have relatively low RT ionic conductivity (~10^{-5} S/cm), while $Li_7La_3Zr_2O_{12}$ (LLZO) possesses relatively high ionic conductivity (10^{-4}–10^{-3} S/cm). Therefore, research interests are mostly dedicated in LLZO and its derivatives with different elemental doping [111–113]. Garnet-type SSEs are also attractive for their wide electrochemical window and superior stability towards lithium metal anodes [67]. LLZO has two different phases, a lower ionic conductive tetragonal phase and a higher ionic conductive cubic phase. Cubic phase LLZO is more desirable for practical applications, but it usually requires very high sintering temperatures to obtain the cubic phase [24]. The

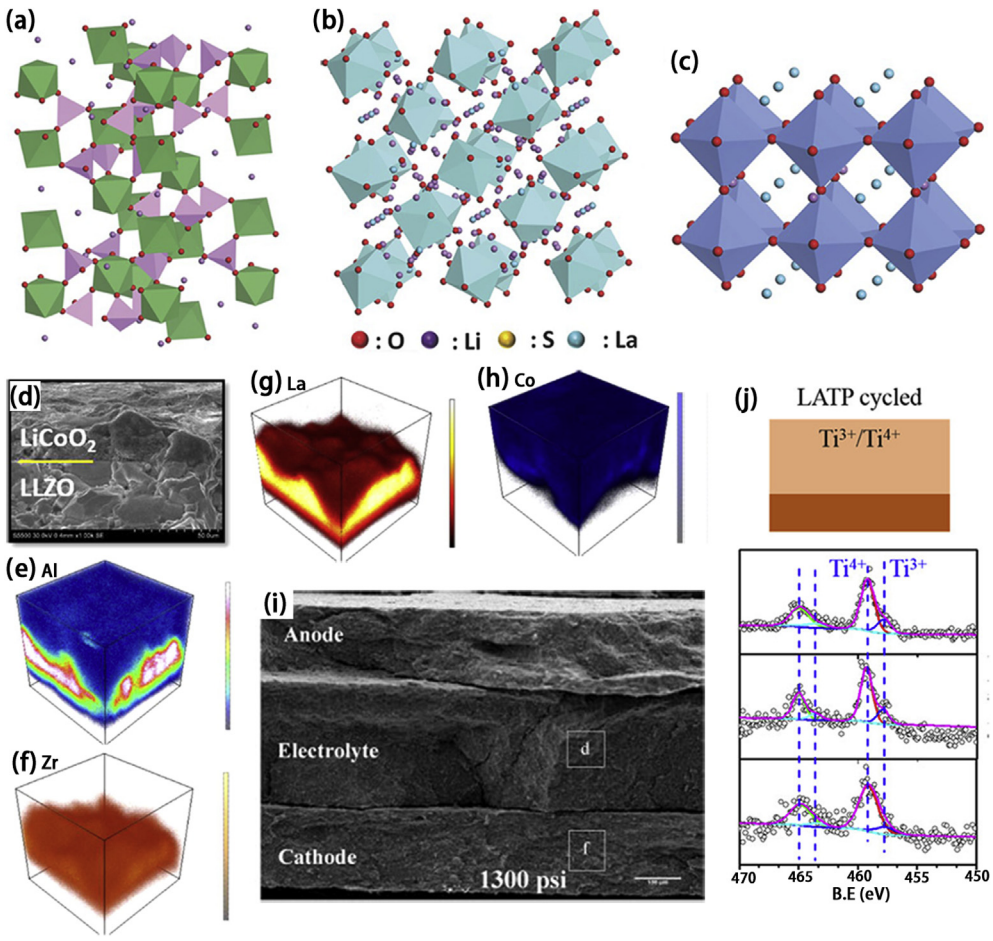

Fig. 4. The crystalline structures of (a) NASICON, (b) Garnet, and (c) Perovskite SSEs [139]. Reproduced with permission [139], Copyright 2018, Wiley. Time-of-flight secondary ion mass spectroscopy (TOF-SIMS) study of $LiCoO_2$/LLZO interface: (d) SEM image of a $LiCoO_2$/LLZO interface and elemental distributions of (e) Al^+, (f) Zr^+, (g) La^+, and (h) Co^+; color scales show the concentrations of each ion where the upper color represent higher concentrations [129]. Reproduced with permission [129], Copyright 2016, ACS. (i) Scanning electron microscopy (SEM) image showing the poor contact between NASICON SSE and Li_2MnO_4 [140]. Reproduced with permission [140], Copyright 2014, Elsevier. (j) X-ray photoelectron spectroscopy (XPS) study on the reduction of Ti^{4+} in LATP by lithium metal anode [138]. Reproduced with permission [138], Copyright 2018, ACS. (For interpretation of the references to color in this figure legend, the reader is referred to the Web version of this article.)

Li^+/H^+ exchange [114] upon exposure to moisture can cause Li_2CO_3 formation on the LLZO surface leading to additional problems such as poor lithium wettability and poor ionic conductivity. Even though LLZO is known to be high ionic conductivity and stable towards lithium metal anodes, Li dendrite problem [115,116] and interfacial mismatch issue due to the rigid properties remain challenging for garnet-type SSEs.

Perovskite-type SSEs with a structure of ABO_3 (A = Ca, Sr, La; B = Al, Ti) were first reported as an oxygen ion conductor [117]. After aliovalent substitution of both metal ions in A-sites with a formula of $Li_{3x}La_{2/3-x}TiO_3$, a Li^+ ion conductor is obtained with a high bulk ionic conductivity over 10^{-3} S/cm at RT [118]. Unfortunately, the high grain boundary resistance, high interfacial resistance, and poor compatibility of Ti^{4+} with lithium metal anode restrict their wide applications.

Overall, oxide-based SSEs have relatively high ionic conductivity and chemical stability at ambient environment. Oxide-based SSEs have the highest Young's modulus among all types of SSEs. The Young's moduli for LATP, garnet-type SSE LLZO, and perovskite-type SSE are 115 GPa [119], 150 GPa for [120], and 203 GPa [121], respectively. This rigid property could be beneficial for suppressing lithium dendrite if engineered properly but resulting in the mismatch problem towards electrodes. Fig. 4i shows the mismatch problem between NASICON SSE and electrodes where a big gap is present at the interface. More details about mechanical properties of the SSEs will be discussed and summarized in following content.

In terms of oxide-based SSE/electrode interface, several strategies have been reported to improve the interfacial contact and lower the interfacial resistance and they are summarized in Fig. 5. For example, melting lithium metal onto the oxide-based SSE surface instead of simply pressing a lithium metal foil to the SSE can achieve a matching interface. Molten lithium metal has high fluidity which can fill the gaps of the uneven SSE surface and enable intimate interfacial contact. However, garnet-type SSEs may have poor wettability to molten lithium, namely "lithiophobic" (Fig. 5a left). Thus, coatings including Al_2O_3, ZnO, Ge, etc. on SSEs can enable good lithium wettability, namely "lithiophilic" coatings (Fig. 5a right) [122–124]. For example, L. Hu's group [123] dramatically reduced the contact angle between molten lithium and a garnet-type SSE and reduced the RT interfacial resistance of from 1710 Ω/cm^2 to 1 Ω/cm^2 via a thin layer of Al_2O_3 coating on the garnet-type SSE by atomic layer deposition (ALD) (Fig. 5b). The lithium symmetric cell with Al_2O_3 coated garnet SSE presented excellent plating/stripping performance over 90 h with negligible increase of overpotential at a current density of 0.2 mA/cm^2.

However, this melting strategy is not suitable for engineering the cathode interface because of the high melting points of SSEs and cathode materials. Moreover, cathode is heterogeneous structure containing nano-size or micro-size active material particles, nano-size conductive carbon and polymer binder. The stiff and rough morphology of cathodes even make the mismatch problem more prominent. Alternatively, a feasible method is co-sintering oxide-based SSE and cathode materials together with a low-melting-point SSE as a sintering additive to promote the sintering process at a relatively low temperature (Fig. 5c). Ohta et al. developed a solid-state $LiCoO_2$ batteries with LLZO as the SSE and $LiBO_3$ as the sintering additive to lower the co-sintering temperature to 700 °C. This $LiCoO_2$ SSB delivered a discharge capacity of 85mAh/g in a voltage window of 3.0–4.05 V (vs. Li/Li^+) [125]. A similar study by C. Wang's group used $Li_{2.3}C_{0.7}B_{0.3}O_3$ as the sintering additive to construct an all ceramic SSLB with excellent cycling performance (Fig. 5d) [126]. Creating porous structure SSE to enlarge the contact area between SSE and electrode materials is another strategy to realize SSLB with oxide-based SSE(Fig. 5e–g) [127].

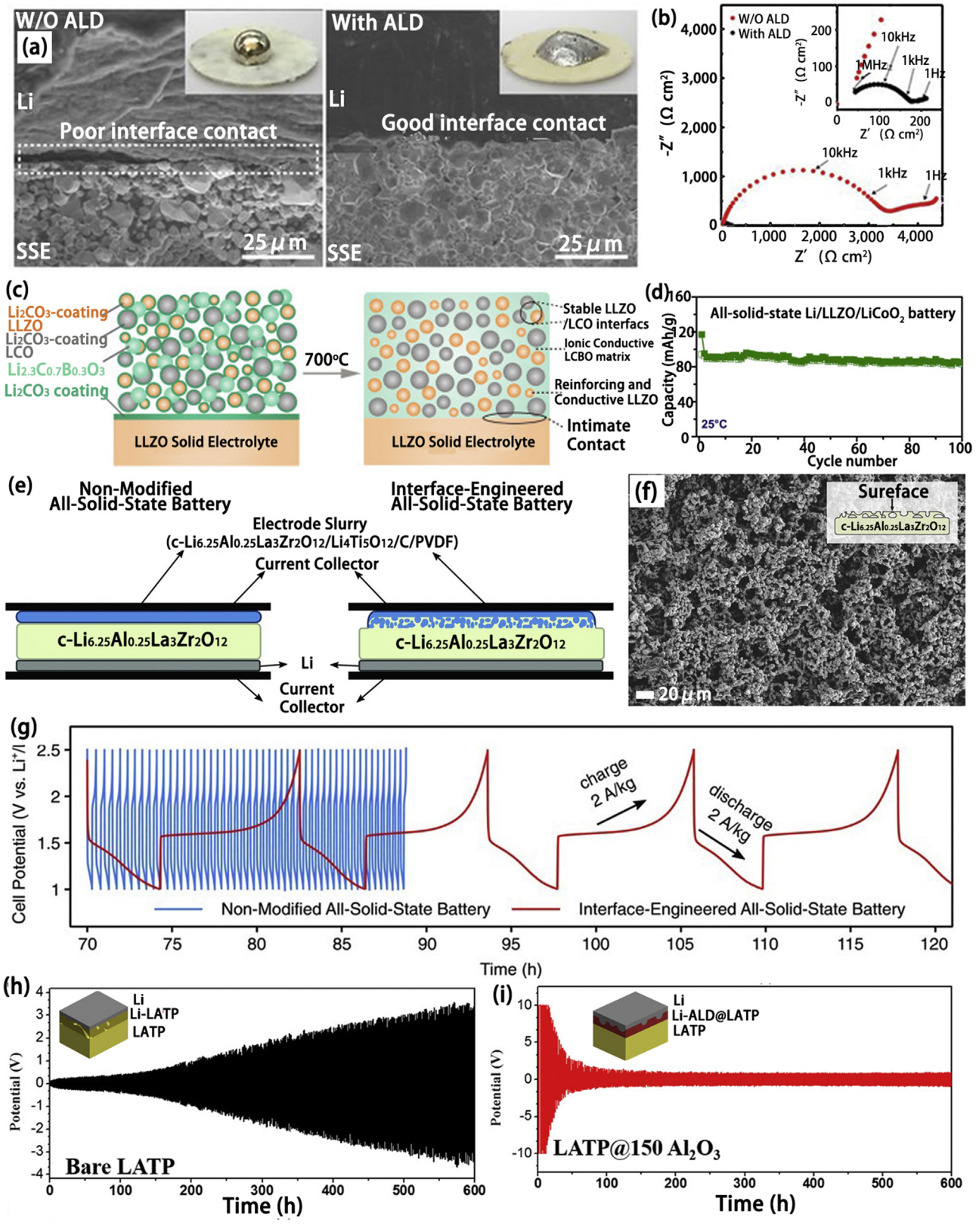

(caption on next page)

Fig. 5. Summary of strategies for building SSLBs with oxide-based SSEs. (a) SEM images of the garnet SSE/lithium metal interface without ALD Al_2O_3 coating (left) and with ALD Al_2O_3 coating (right). The insets are photos of melted lithium metal on top of the garnet SSE surfaces. An intimate contact between lithium metal and SSE was achieved with ALD Al_2O_3 coating. (b) Comparison of the impedances of symmetrical lithium cells with garnet SSEs with/without ALD Al_2O_3 coating. The inset is the enlarged EIS curve of ALD Al_2O_3 coating garnet SSE symmetrical cell where a very small impedance is presented [123]. Reproduced with permission [123], Copyright 2017, Springer Nature. (c) Schematic diagram shows the process of co-sintering to make a SSLB with oxide-based SSE. Left, mixture of LLZO particles, LCO particle, $Li_{2.3}C_{0.7}B_{0.3}O_3$ sintering additive on the top of LLZO SSE pellet. Right, co-sintering this pellet at 700 °C to obtain an intimate SSE/cathode interface. (d) Cycling performance at RT of the SSLB obtained from (c), lithium metal was used as anode [126]. Reproduced with permission [126], Copyright 2018, Elsevier. (e) Schematic diagrams show the structure of SSLBs with dense SSE (left) and porous structure SSE (right). (f) Surface SEM image of porous structure SSE pellet. (g) Comparison of SSLBs performances with dense SSE and porous structure SSE [127]. Reproduced with permission [127], Copyright 2016, Wiley. (h) Cycling performance of bare LATP/lithium symmetric cell at a current density of 0.01 mA/cm^2. A significant increase of overpotential is observed. (i) Cycling performance of ALD Al_2O_3 coating LATP/lithium symmetric cell at a current density of 0.01 mA/cm^2; The potential profile is quite stable with ALD coating [138]. Reproduced with permission [138], Copyright 2018, ACS.

Even though SSE/cathode interfacial mismatch problem can be partially addressed by the co-sintering method [125,128–130] or creating porous structure SSE to enlarge the contact area between SSE and electrode materials [127,131], the volume change of electrode materials during charge/discharge will still lead to loss of contact between SSEs and electrode materials due to the stiffness nature of SSEs [132–134].

The interphase problem due to side reactions or elemental diffusion at the interface between oxide-based SSE and cathode have been reported [129,135]. At the $LiCoO_2$/LLZO interface, Co undergoes mutual diffusion with Zr and La (Fig. 4d–h) forming an interphase with low ionic conductivity (i.e. high interfacial resistance). Another common problem is the incompatibility between Li anode and Ti-containing oxide-based SSEs. Ti^{4+} in LATP or LLTO can be easily reduced by the lithium metal anode (Fig. 4j) resulting in a phase change of the SSE which decreases ionic conductivity but increases electronic conductivity. This kind of highly electronic conductive interphase is particularly prone to exacerbate Li dendrite growth [136,137]. Our group has demonstrated a thin layer of Al_2O_3 coating on the LATP surface to prevent Ti^{4+} reduction in LATP, significantly enhancing the stability of LATP towards lithium metal anode (Fig. 5h and i) [138].

In summary, interfacial mismatch and side reactions between the oxide-based SSE and electrodes are the key challenges to the application of oxide-based SSEs and more research efforts are required. The strategies for these interfacial problems include (i) solidifying melting state lithium on SSE to ensure intimate contact, (ii) co-sintering active materials and SSE with a sintering additive, (iii) creating a porous structure SSE to increase the contact area between electrode materials and SSE, and (iv) using coating layer to prevent side reaction. It is believed that engineering the interface with a soft and high ionic conductive layer between SSE and electrodes may be a good strategy to tackle the challenges for SSLBs with oxide-based SSE.

1.1.3. Sulfide-based SSEs

Sulfide-based SSEs can be categorized by amorphous, crystalline, and glass-ceramic sulfide SSEs. The representative amorphous sulfide-based SSEs are $xLi_2S{\cdot}(1\text{-}x)P_2S_5$ and $xLi_2S{\cdot}(1\text{-}x)SiS_2$ systems. Both systems present a RT ionic conductivity over 10^{-4} S/cm [141,142]. Crystalline sulfide-based SSE Li_3PS_4 was first reported by Tachez et al. [143]. Later, Kanno's group reported a thio-LISICON type SSE produced by replacing O^{2-} of LISICON [$Li_{14}Zn(GeO_4)_4$] family with S^{2-} [144]. The replacement leads to a higher ionic conductivity at RT because S^{2-} has larger ionic radius, higher polarizability, and lower electronegativity than O^{2-}. The replacement of O^{2-} by S^{2-} lowers the binding of Li^+ in the crystal framework and enlarges the ion transport channel thus enhance the ionic conductivity [145]. Most of the reported crystalline sulfide-based SSEs have an ionic conductivity over 10^{-4} S/cm at RT (Fig. 6f) [145–148]. Glass-ceramic SSEs are prepared by crystallization of glass-state SSEs. Glass-ceramic SSE based on $xLi_2S\text{-}(1\text{-}x)P_2S_5$ have received tremendous research attentions especially after the discovery of $Li_{10}GeP_2S_{12}$ (LGPS) (Fig. 6a–c) families and their derivations such as $Li_{9.54}Si_{1.74}P_{1.44}S_{11.7}Cl_{0.3}$ (Fig. 6d and e) [146,149,150], which both exhibit ionic conductivities over 10^{-2} S/cm at RT.

The high RT ionic conductivity and relatively soft mechanical properties of sulfide-based SSEs make them promising candidates for the applications in SSLBs. SSLBs with a sulfide-based SSE can be fabricated by simply cold pressing without high temperature co-sintering. However, sulfide-based SSEs suffer from serious instability issues towards lithium metal anode and the conventional cathode materials, which significantly hinder their practical applications in SSLBs. The side reaction behaviors between electrodes and sulfide-based SSEs have received many research attentions [67,70,151–154]. The electrochemical stability window of different types of sulfide-based SSEs were evaluated by theoretical calculations (Fig. 6g for LGPS) and experimental characterizations [67,70,154,155], where they showed the sulfide-based SSEs have a narrow electrochemical stable window. In-situ XPS was performed to clarify the interfacial chemistry between sulfide-based SSE and lithium metal, which confirmed the decomposition products of Li_3P, Li_2S, and Li-Ge alloy at the interface [153]. The decomposed products have low ionic conductivities and thus introduce high interfacial resistance. To address this problem, alternative anodes like indium are commonly used in SSLBs [156]. An alternative strategy is interfacial engineering the lithium/SSE interface to stabilize the interface and lower the interfacial resistance [151,157–159]. C. Wang's Group applied LiF, LiI as a protecting layer on lithium metal anode in to stabilize lithium/sulfide-based SSE interface [158,159]. Our group first reported a molecule layer deposition (MLD) engineered lithium metal anode for stable contact with a sulfide-based SSE [151].

Considering the interface between sulfide-based SSEs and cathodes, the electrochemical instability problem and the formation of space-charge layer (SCL) seriously hinder the application of sulfide-based SSEs. The instability between sulfide-based SSEs and cathode materials such as $LiCoO_2$ were studied by the theoretical calculation and transmission electron microscopy (TEM) confirming the side-reaction products of Li_2S, CoS_3 and $Co(PO_3)_2$ at the interface that cause high interfacial resistance [152,160]. SCL is typically formed at the interface between sulfide-based SSEs and $LiCoO_2$ due to the chemical potential difference between them (Fig. 6h–j) [26]. The high resistance of SCL significantly lowers the capacity and rate performance of SSLBs. Interfacial engineering by an oxide material coating layer such as Al_2O_3, $Li_4Ti_5O_{12}$, and $LiNbO_3$, has been demonstrated as an effective way to inhibit the side-reactions and SCL formation [26,161,162].

Even though sulfide-based SSEs are relatively soft compared to oxide-based SSEs, sulfide-based SSEs still experience the mismatch problem. Their poor flexibility makes it difficult to buffer the volume change of the electrode materials during charge and discharge; the loss of intimate contact between SSE and cathode particles eventually deteriorates the performance of the SSLBs (Fig. 6k) [163]. Therefore, understanding the mechanical properties of SSEs and controlling the mechanical properties of SSEs to ensure good contact between SSEs and active materials are as important as preventing the SSE/electrode interfacial side-reaction for building a high performance SSLB.

1.1.4. The mechanical properties of SSEs

Different from the liquid electrolytes which have the fluidity to fill in pores and gaps to ensure intimate contacts with electrodes, the solid

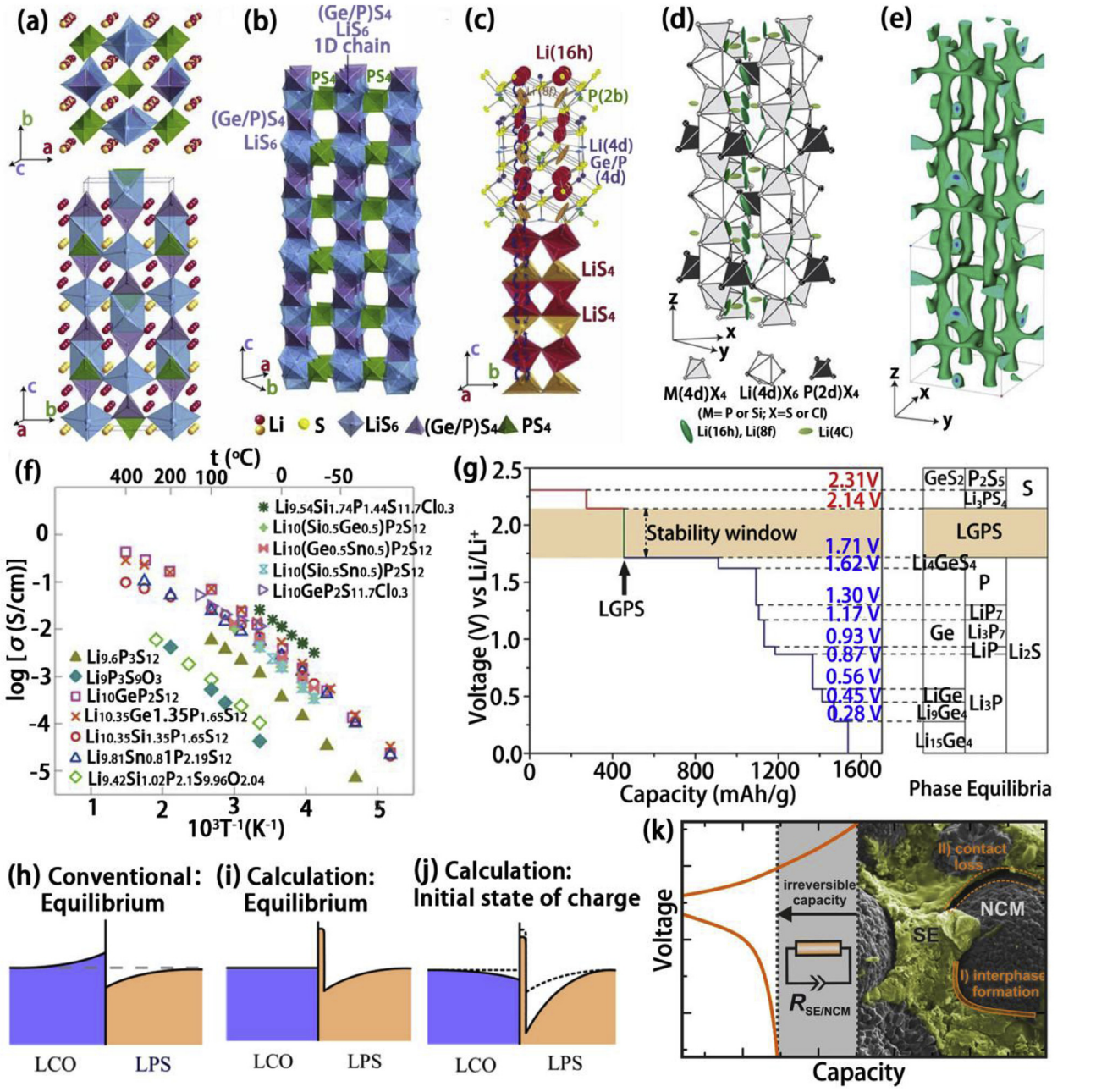

Fig. 6. (a) Crystal structure of LGPS sulfide-based SSE; (b) one dimensional view of LGPS framework; (c) Li^+ ion conduction pathways in LGPS; zigzag conduction pathways along the c-axis are indicated [146]. Reproduced with permission [146], Copyright 2011, Springer Nature. (d) Crystal structure of $Li_{9.54}Si_{1.74}P_{1.44}S_{11.7}Cl_{0.3}$; (e) nuclear distributions of Li atoms in $Li_{9.54}Si_{1.74}P_{1.44}S_{11.7}Cl_{0.3}$ at 25 °C [149]. (f) Comparison on ionic conductivities of the LGPS family, $Li_{9.6}P_3S_{12}$ and $Li_{9.54}Si_{1.74}P_{1.44}S_{11.7}Cl_{0.3}$ [149]. Reproduced with permission [149], Copyright 2016, Springer Nature. (g) The first principles calculation for the phase equilibria of LGPS during lithiation and delithiation process, where it shows the stable window of LGPS is 1.71–2.14 V [67]. Reproduced with permission [67], Copyright 2016, Wiley. The equilibrium Li concentrations predicted by the conventional model (h) and the calculation model (i). (j) The equilibrium Li concentrations predicted by calculation model at the initial stage of charging for the LCO/LPS interface [26]. Reproduced with permission [26], Copyright 2014, ACS. (k) Capacity lose at the initial charge/discharge cycle and the lose of interfacial contact between cathode particles and a sulfide-based SSE [163]. Reproduced with permission [163], Copyright 2017, ACS.

nature of SSEs could be a drawback in terms of physical compatibility with electrode materials under operating conditions. Especially, the volumetric evolutions of most active materials during charging and discharging cast extra difficulties in maintaining intimate contacts between the SSEs and the active materials. Commercial active materials such as $LiCoO_2$, $LiFePO_4$, $LiMn_2O_4$, and graphite usually experience big volumetric changes during charging and discharging, while next-generation active materials such as sulfur and silicon have even more significant volumetric changes of 80% and 400% respectively. Therefore, practical SSEs must be able to accommodate the resulting strain/stress without the mechanical degradation such as cracking or pulverizing. Understanding and improvements in SSE mechanical properties are progressing for SSLB applications [164–168]. Tables 1 and 2 summarize the general mechanical properties of inorganic SSEs (oxide- and sulfide-based SSEs) and polymer involved hybrid electrolytes, respectively. Interestingly, the mechanical properties of inorganic SSEs are highly related to their phase structures. Particularly, the relative Young's moduli are in an descending order from perovskite, garnet, NASICON, phosphaste, to thiophosphate

Table 1
The mechanical parameters of inorganic SSEs.

Inorganic SSEs	Phase	Grain size (μm)	Relative density (%)	Young's modulus (GPa)	Shear modulus (GPa)	Hardness (GPa)	Fracture toughness (MPa $m^{1/2}$)	Refs.
$Li_3Ti_2(PO_4)_3$ (calculated)	NASICON			143.7	57.6			[164]
$Li_{1.3}Al_{0.3}Ti_{1.7}(PO_4)_3$	NASICON	1.7 ± 0.7	96	115			1.1 ± 0.30	[119]
Li_3PO_4 (calculated)	phosphate			103.4	40.9			[164]
$Li_7La_3Zr_2O_{12}$ (calculated)	garnet			175.1	68.9			[164]
$Li_5La_3Nb_2O_{12}$ (calculated)	garnet			141.1	54.8			[164]
$Li_5La_3Ta_2O_{12}$ (calculated)	garnet			144.2	56.1			[164]
$Li_{6.24}La_3Zr_2Al_{0.24}O_{11.98}$	garnet	4.5–5	97	149.8 ± 0.4		6.3 ± 0.3		[171]
$Li_{6.24}La_3Zr_2Al_{0.24}O_{11.98}$	garnet	4.5–5	94	132.6 ± 0.2		5.2 ± 0.4		[171]
$Li_{6.19}La_3Zr_2Al_{0.27}O_{12}$	garnet	3.7 ± 1.8	98	140		9.1	0.97 ± 0.1	[172]
$Li_{6.19}La_3Zr_2Al_{0.27}O_{12}$	garnet	2.7 ± 1.7	85	135		9.1	2.37 ± 0.1	[172]
$Li_{6.17}La_3Zr_2Al_{0.28}O_{12}$	garnet	5–50	99	150.3 ± 2.2	59.8 ± 0.9			[120]
$Li_{6.28}La_3Zr_2Al_{0.24}O_{12}$	garnet	2–30					0.86–1.63	[173]
$Li_{6.5}La_3Ta_{0.5}Zr_2O_{12}$	garnet	1–10	99	153.8 ± 2.7	61.2 ± 1.1			[120]
$Li_{0.5}Ta_{0.5}TiO_3$ (calculated)	perovskite			262.5	104.0			[164]
$Li_{0.13}Ta_{0.63}TiO_3$ (calculated)	perovskite			233.9	91.2			[164]
$Li_{0.33}La_{0.57}TiO_3$	perovskite	0.8 ± 0.3	97	200 ± 3		9.2 ± 0.2	~1	[174]
$Li_{0.33}La_{0.55}TiO_3$	perovskite	2.42	99	222.6		7.18		[175]
$Li_{0.33}La_{0.567}TiO_3$	perovskite	13.0 ± 4.39	99	203		8.4 ± 0.48	1.24 ± 0.12	[121]
$Li_{0.33}La_{0.567}TiO_3$ - 2.5 %La	perovskite	4.08 ± 1.16	99	198		9.3 ± 1.1	1.08 ± 0.20	[121]
$Li_{0.33}La_{0.567}TiO_3$ + 2.5 % La	perovskite	1.41 ± 4.76	99	191		8.1 ± 0.75	1.22 ± 0.25	[121]
xLi_2S▪$(100-x)P_2S_5$ (hot press)				18–25				[176]
xLi_2S▪$(100-x)P_2S_5$ (cold press)				14–17				[176]
$70Li_2S$▪$30P_2S_5$				18.5 ± 0.9		1.9 ± 0.2	0.23 ± 0.04	[177]
$(100-y)(75Li_2S$▪$25P_2S_5)$▪$yLiI$				19–23	7.1–8.7			[170]
$70(50Li_2S$▪$50P_2S_5)$▪$30LiI$				17	6.3			[170]
$Li_{10}GeP_2S_{12}$ (calculated)	thiophosphate			37.19	14.35			[178]
$Li_{10}GeP_2S_{12}$ (calculated)	thiophosphate			21.7	7.9			[164]
$Li_{10}SiP_2S_{12}$ (calculated)	thiophosphate			24.8	9.2			
$Li_{10}SnP_2S_{12}$ (calculated)	thiophosphate			29.1	11.2			
Li_7P_3S11	thiophosphate			21.9	8.1			
Li_6PS_5Cl	thiophosphate			22.1	8.1			
Li_6PS_5Br	thiophosphate			25.3	9.3			
Li_6PS_5I	thiophosphate			30	11.3			
LIPON	thiophosphate			77		3.9–4.1		[179]
Li				5	4.25	10^{-3}		[120, 177]

Table 2
Mechanical properties of polymer and hybrid electrolytes.

Polymer electrolyte	Inorganic fillers size and percentage	Plasticizer and percentage	Temperature (°C)	Young's modulus (GPa)	Shear modulus (GPa)	Tensile strength (GPa)	Refs.
PEO			RT	$84.5 \pm 10.3 \times 10^{-3}$			[180]
PEO-$LiClO_4$			RT	$14.5 \pm 6.4 \times 10^{-3}$			[180]
PEO/(PEO-b-PE)-$LiClO_4$			RT	$114.2 \pm 9.3 \times 10^{-3}$			[180]
PEO-LITFSI			RT			1.7×10^{-3}	[181]
PEO-LITFSI			85	$\sim 10^{-6}$			[182]
PMMA-PVC-$LiCF_3SO_3$		dibutyl phthalate		1.18×10^{-6}			[183]
PVDF-HFP		1M $LIPF_6$ in EC/DMC (425%)		9.2×10^{-3}		6.5×10^{-3}	[184]
PVDF-HFP	Al_2O_3 30–50 nm (6%)	1M $LIPF_6$ in EC/DMC (459%)		18.5×10^{-3}		9.2×10^{-3}	[184]
PVDF-HFP	SiO_2 30–50 nm (6%)	1M $LIPF_6$ in EC/DMC (459%)		16.9×10^{-3}		10.3×10^{-3}	[184]
PVDF-HFP	$BaTiO_3$ 30–50 nm (6%)	1M $LIPF_6$ in EC/DMC (462%)		17.3×10^{-3}		12.5×10^{-3}	[184]
PVDF(80)-PEO(20)	LTAP (6%)			14.8×10^{-3}		9.3×10^{-3}	[185]
PFPE-LITFSI	$75Li_2S$▪$25P_2S_5$ (7%)				2.6×10^{-3}		[186]

structured inorganic SSEs, with the magnitude from 200 GPa to 20 GPa [164]. However, the Young's moduli of polymer-based electrolytes are lower by about 3 orders of magnitude compared to those of inorganic SSEs. Young's moduli is a parameter to describe the stiffness of a solid material. It defines the relation between the stress (force per unit area) and strain (proportional deformation) of the solid material which undergo a uniaxial deformation in the linear elasticity region. The higher the Young's moduli, the stiffer the material, the harder to be deformed.

Mechanical related interfacial properties are an important topic in SSLBs. C. Monroe and J. Newman suggested that the shear modulus of

SSEs should be at least twice higher than that of lithium metal to prevent lithium dendrite formation [99]. The shear modulus of lithium metal is 4.25 GPa, which means that SSEs with a shear modulus over 8.5 GPa can suppress lithium dendrite formation. Regarding mechanical suppression on lithium dendrites, most inorganic SSEs (oxide- and sulfide-based SSEs) are strong enough, but the polymer-based electrolytes and composite electrolytes cannot satisfy this parameter (Tables 1 and 2). Even though the shear modulus of polymer electrolytes are not given directly in Table 2, we can estimate them from the Young's modulus according to the following relationship [120].

$$G = E\frac{1}{2(1+\nu)} \quad (1)$$

where E is Young's modulus; G is shear's modulus; and ν is Poisson's ratio. For most homogeneous materials, ν is between 0 and 0.5, giving a smaller value of G than E. Thus, the shear modulus of polymer electrolytes is at the MPa level or below, which is 1000 times smaller than that of lithium metal.

However, in practice, the high-shear-modulus inorganic SSEs such as LLZO and Li_3PS_4 still suffer from lithium dendrite formation problem [123,136,137]. Possibly, the reason is that lithium dendrite grows around the grain boundary of inorganic SSEs where shear modulus is lower than that of the bulk materials (0.2–0.6 times of grain's shear modulus). If it is true, C. Monroe and J. Newman's proposal is still valid. However, lithium dendrite penetrating single crystal LLZO reported by T. Swamy et al. may overthrow this theory [169]. On the other hand, SPEs and hybrid electrolytes have low shear moduli actually demonstrated better compatibility with lithium anodes than the stiff inorganic SSEs because of the intimate contact with lithium anodes and uniform Li^+ ion flux across the interface. Therefore, not only the mechanical properties but also the interfacial Li^+ ion distributions are critical for inhibiting the lithium dendrite formation [73,123].

Maintaining good solid-solid contacts can become even more challenging when incorporating particle shaped active materials in SSLBs. Active material particles such as graphite, silicon, $LiCoO_2$, $LiFePO_4$, and sulfur experience volume changes of 13%, 400%, 2.6%, 7%, and 80% respectively. If the SSEs were to accommodate volumetric changes of active materials without mechanical degradation, SSEs should have low Young' modulus and low fracture toughness values. A detailed study between the battery performance and Young's modulus of sulfide-based SSEs was reported by M. Tatsumisago's group [170]. They found that lowering the Young's modulus of sulfide-based SSEs can enhance the performance of batteries. G. Bucci et al. suggested that a volumetric change over 7.5% (corresponding to 2.5% increase in the radius) for active particles will trigger the delamination between SSEs and active materials. If the elastic modulus of the SSE is lower than 25 GPa, the onset of delamination can be increase to 25% volumetric change of active particles, which is sufficient for accommodating $LiCoO_2$, $LiFePO_4$, and graphite [166,167]. In other words, sulfide-based SSEs and SPEs with Young's moduli below 25 GPa are suitable for SSLBs using commercial electrode materials such as $LiCoO_2$, $LiFePO_4$, and graphite etc. For the active materials with larger volumetric expansion such as sulfur and silicon, SPEs and hybrid electrolytes with an even lower Young's modulus are favorable.

Other SSEs such as nitride-based SSEs Li_3N, LiPON and $LiBH_4$ [194] are also received some research interests in SSLBs due to their intrinsic advantages. For example, Li_3N has an ionic conductivity over 10^{-4} S/cm at RT [195]. LiPON is widely used in thin film battery even though its ionic conductivity is only around 10^{-6} S/cm [196]. However, a detail discussion about these SSEs will not be covered in here because few of these SSEs are reported as a component of hybrid electrolytes.

The challenges and solutions for SSE/electrode interface is summarized in Table 3. There is no simple solution to address all the aforementioned issues in an individual SSE. Thus, hybrid electrolytes are proposed to combine the merits of two or more types of SSEs and show promising applications in SSLBs. According to the components and structure difference, the hybrid electrolytes can be classified into four types: polymer-oxide composite, polymer-sulfide composite, liquid-oxide, and polymer-oxide multilayer hybrid electrolytes (Fig. 2b). These hybrid electrolytes will be systematically discussed in the following sections.

2. Composite electrolytes

2.1. Synthesis of composite electrolytes

A hybrid electrolyte with inorganic fillers in SPE (ceramic in polymer) or SPE filled inorganic SSE (polymer in ceramic) is named composite electrolyte. When designing a composite electrolyte, the execution and fabrication method is very important. Before introducing the properties of the hybrid electrolytes and their application in SSLBs, we will start with their common synthesis methods. Fig. 7 schematically describes four common methods including solution casting, mechanochemical (hot press), infusion methods and 3D printing. Each method will be discussed in detail in the following sections.

Table 3
Summaries of the challenges and solutions for SSE/electrode interfaces.

SSEs	Interface issues toward Li anode	Solutions for SSE/Li interface	Interface issues toward cathode	Solutions for SSE/cathode interface
PEO SPE	1 Li dendrite formation [29];	1 inorganic fillers for enhancing mechanical strength and interface stability [187]; 2 rigid support for enhancing the mechanical strength [188,189]; 3 cross-linked polymer for enhancing the mechanical strength [190];	1 electrochemical oxidation of PEO at low voltage (<3.8 V) [69];	1 interface modification with metal oxide and polymer materials [100,101]; 2 SPE modification with a high voltage stable polymer electrolyte [191];
LLZO	1 poor wettability [123]; 2 high interfacial resistance;	1 interface engineering to achieve a lithiophilic LLZO/Li interface [123]; 2 Li_2CO_3 free LLZO surface for good lithium wettability [192];	1 poor interface contact [66]; 2 high interfacial resistance; 3 side reaction [135]; 4 volumatic expansion induced mechanical degradation [193];	1 co-sintering with low melting point SSE [129]; 2 interface coating to avoid side reaction [126]; 3 enlarging the SSE/electrode materials contact by porous SSE [127];
LATP	1 reduction of Ti^{4+} [138];	1 interface engineering LATP/Li to prevent the directly contact [138];	1 poor interface contact [140];	
Sulfide-based SSEs	1 side reaction [153]; 2 Li dendrite formation [136];	1 indium anode [156]; 2 interface modification to avoid side reaction [158];	1 poor contact [68]; 2 space charge layer (SCL) [26]; 2 side reaction [160]; 3 volumatic expansion induced mechanical degradation [163];	1 metal oxide coating to prevent SCL and side reaction [26,160]; 3 cycling battery at high pressure [132];

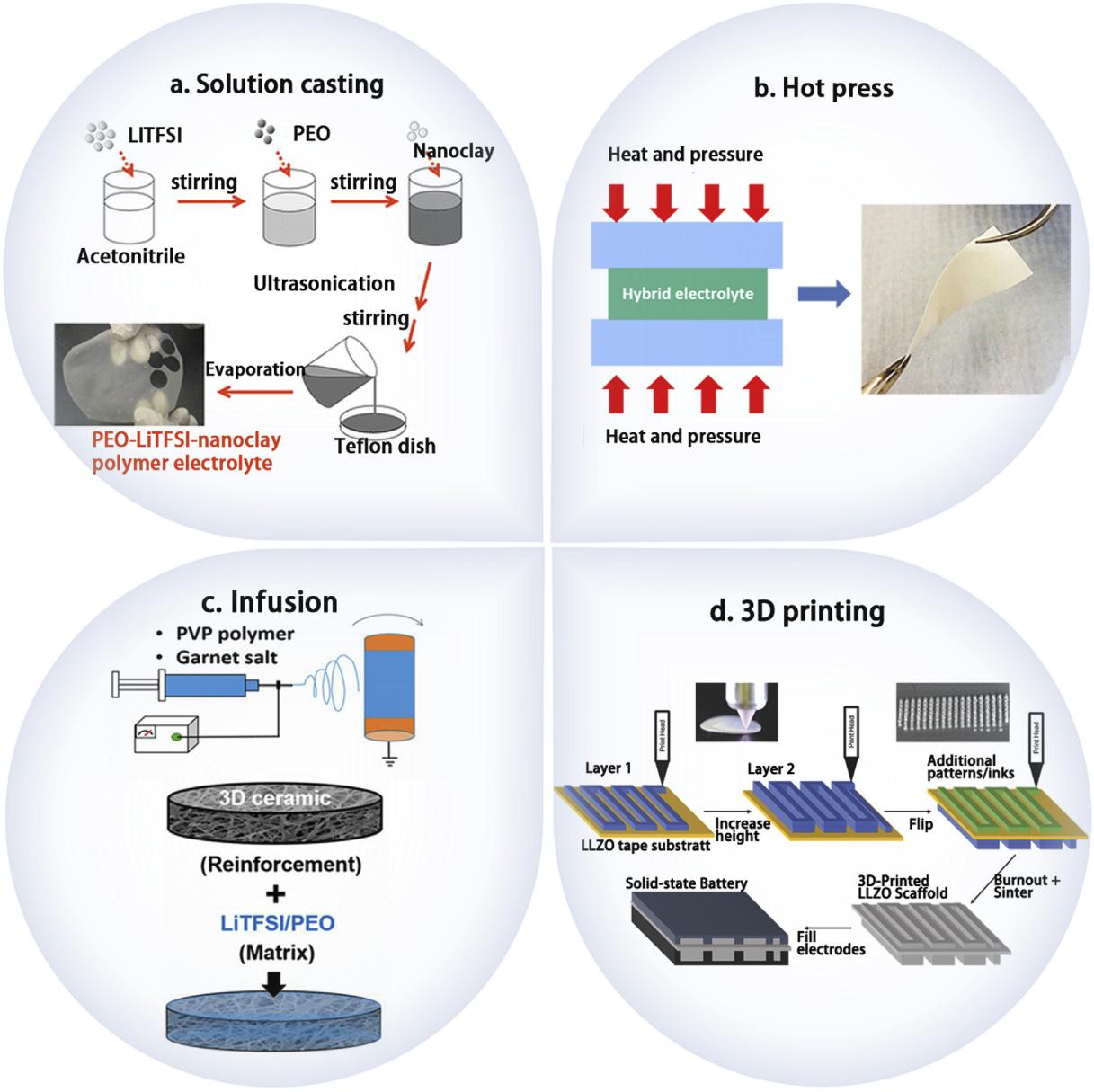

Fig. 7. Fabrication methods of composite hybrid electrolytes. (a) solution casting method, (b) hot press method (mechanochemical method), (c) infusion method and (d) 3D printing method [28,201–203]. Reproduced with permission [28]. Reproduced with permission [201], Copyright 2014, Springer Nature. Reproduced with permission [202], Copyright 2017, Elsevier. Reproduced with permission [203], Copyright 2018, Wiley.

2.1.1. *Solution casting method*

Among of the preparation methods, solution casting is one of the most popular method and scalable for practical application. Solution casting is a solidification process by evaporating the solvent of a SPE slurry in an inert mold of a desired shape or by doctor blade casting as thin film. This method is commonly used for preparing SPE, gel polymer electrolyte, and inorganic SSE fillers-containing composite electrolytes. The casting procedures of a composite electrolyte include three steps: (i) disperse designated polymer, salt and fillers in a solvent; (ii) cast the mixture into a mold or doctor blade on a substrate followed by evaporation of the solvent to solidify the electrolyte; (iii) detach the solidified electrolyte film from the mold or substrate. The solution casting method is facile, easily tunable for film thickness, low cost, and scalable.

Solvents used in the casting process must be carefully chosen. Desired solvents should be volatile and chemically inert to materials being dispersed. For casting a composite electrolyte with a PEO matrix, acetonitrile is the most common solvent because of its good solubility with PEO and low boiling point. More importantly, most ceramic SSEs are stable against acetonitrile solvent. Thus, acetonitrile is most commonly used to cast PEO-inorganic SSE composite electrolytes with good electrochemical performance. Water can be another good solvent in some cases, serving an essential role in the in-situ hydrolysis of titanium ethoxide or tetraethyl orthosilicate in PEO solution to make a composite electrolyte with in-situ formation of ultra-tiny TiO_2 or SiO_2 particles fillers to effectively enhance the ionic conductivity [197,198]. However, oxide-based SSEs such as LLZO can undergo Li^+/H^+ exchange in an moisture environment [199] and sulfide-based SSE is not stable against water, either [200]. Thus, the instability of oxide-based and sulfide-based SSEs in water limits its usage as a universal solvent.

2.1.2. *Mechanochemical method*

Composites of polymers and inorganic SSEs powders can be prepared mechanochemically, coupling mechanical and chemical processes. Ball milling is a typical example, in which locally high pressure and high

temperature is created to facilitate the complex between polymers and inorganic fillers. Mechanochemical methods can eliminate the use of solvents and corresponding drawbacks such as possible side reactions caused by solvents. Such a preparation method is particularly favorable to hybrid electrolytes involving solvent-sensitive components, such as sulfide-based SSEs. Ball milling in Ar atmosphere for preparation of PFPE(hydroxy-terminated perfluoropolyether polymer, with molecule structure of $HO–CH_2–CF_2O–(CF_2CF_2O)_x–(CF_2O)_y–CF_2–CH_2–OH$)-$75Li_2S$■$25P_2S_5$-lithium bis(trifluoromethanesulfonyl)imide (LITFSI), PEG(polyethylene glycol)-$70Li_2S$■$30P_2S_5$ and PEO-LLZO-LITFSI hybrid electrolytes have been studied [186,202,204]. Also, mechanochemical method is a powerful way to prepare hybrid electrolytes with components that are insoluble in any solvents. C. Liang's group reported a LLZO-βLi_3PS_4(LPS) hybrid electrolyte by ball milling LPS and LLZO followed by a pressing process to reduce grain boundary resistance and reshape the hybrid electrolyte. The highest ionic conductivity of the LLZO-LPS hybrid electrolyte can reach over 10^{-4} S/cm at RT [205]. After ball milling, hot pressing is common subsequent step for a mechanochemical process to ensure uniform thickness of a composite electrolyte film. The hot pressing process is involved in most of the preparation processes in the SPE-oxide composite electrolyte [202] and the fabrication of cathode-polymer composites electrode to reduce interfacial resistance between SSE and cathode electrode [206].

2.1.3. Infusion method

Hybrid electrolytes prepared by solution casting or a mechanochemical method often consist of a continuous SPE matrix with low ionic conductivity and dispersed inorganic SSEs particles with high ionic conductivity. The high ionic conductivity of inorganic SSEs cannot be fully utilized at a discrete condition. The preferential Li^+ ion conduction through the SPE rather than the inorganic SSEs significantly limits the RT ionic conductivity and feasibility of hybrid electrolyte. Alternatively, taking the advantage of the fluidity of a polymer solution, a composite electrolyte can be prepared by infusing a polymer solution into a porous inorganic SSEs framework and subsequent evaporation of solvent. In this case, the inorganic SSE component is continuous and accessible for fast Li^+ ion transport.

L. Hu's group fabricated a PEO-LLZO-LiTFSI hybrid electrolyte by repeated drop-casting (infusing) PEO/LITFSI solution into an electrospinned 3D LLZO nanofiber membrane [28]. Similarly, Y. Yang's group synthesized a PEO-LATP-$LiClO_4$ membrane by employing a vertically aligned interconnected template of LATP SSE filled with a PEO-LiClO_4-acetontrinile solution [207]. G. Yu and his co-workers developed a 3D nanostructured hydrogel-derived LLTO framework, which was used as a scaffold for fabricating PEO-LLTO-LiTFSI hybrid electrolyte [208]. Beneficial for the high ionic conductivity of continuous inorganic SSEs phase, these composite electrolytes delivered high ionic conductivities of close and even over 10^{-4} S/cm at RT.

2.1.4. 3D printing

Additive manufacturing (AM) alias 3D printing is emerging as a versatile technology for designing and fabricating complex electronic devices. For lithium batteries, many research efforts are dedicated to realize the 3D printing technique for creating electrodes with unique shapes [209–211], and preparing electrolytes to couple with unique shapes of electrodes [203,212–216]. Different from the casting method and hot press method where the electrolytes are produced as flat thin films, 3D printing derived electrolytes could be easily designed with novel structures such as porous, discrete lines, grid-like, vertical columns and others [203,213]. For example, using 3D printing method, D. W. McOwen et al. synthesized a novel structure of LLZO garnet type SSE. They created a stacked array LLZO SSE for implanting lithium anode. The as-prepared lithium symmetric cell with 3D printed LLZO SSE showed small LLZO/Li interface resistance and it can be cycled at a current density of 0.33 mA/cm^2 with the potential of 7.2 mV [203]. The high performance LLZO/Li symmetrical cell is possibly originated from the 3D lithium metal anode created by infusing melting Li into the 3D printed LLZO SSE flameworks, which can minimize the local current densities for stable lithium plating and stripping. Moreover, the 3D printed ceramic-polymer composite electrolyte reported by Aaron J. Blake et al. demonstrated better thermal stability compared to commercial Celgard separator and excellent LIB performance [212]. It is expected that 3D printing would perform important role in SSEs and SSLBs fabrications.

Although significant achievements have been obtained in 3D printing lithium batteries materials, there are still many challenges and difficulties that need to be overcome. Firstly, the most common used 3D printing method in electrode/electrolyte fabrication is the extrusion method. The extrusion type 3D printing is yet hard to achieve high resolution due to the limitation of extrusion head [214]. The large extrusion diameters make it hard to precisely control the microstructure of electrodes. Secondly, the ink/paste/slurry for the 3D printing must meet unique viscoelastic properties (high viscosity and shear-thinning behavior) to facilitate 3D printing [209], posting difficulty to prepare 3D printing ink/paste/slurry with SSEs and/or active materials. Thirdly, even though hybrid electrolyte combining SPE and inorganic SSE composite can be printable by 3D printing technique, the composite has low ionic conductivity at RT without plasticizer. To enhance its ionic conductivity, the elevated temperature over the glass transition temperature or plasticizer have to be applied. However, in these ways, the polymer will become gel state and the 3D printed hybrid electrolyte is hard to maintain its 3D structure. Therefore, applying high resolution and advanced 3D printing techniques in hybrid electrolyte fabrication and developing high ionic conductivity 3D printed hybrid electrolytes will be expected for 3D printed SSLBs.

2.2. Configurations of composite electrolytes

2.2.1. Insulating fillers in SPEs

Before wide development of the hybrid electrolyte concept, composite electrolytes with insulating fillers and a SPE matrix had received many research attentions. The insulating fillers in the composite electrolytes can improve the ionic conductivity to some extent. In early 1980s, α-Al_2O_3 was introduced to a SPE for the first time. The insulating fillers are shown to be able to improve the ionic conductivity by almost two orders of magnitude to 10^{-5} S/cm level at RT [217,218]. Thereafter, other different metal oxides such as TiO_2 [218–220], ZrO_2 [221,222], and SiO_2 [221,223,224] have been widely studied in the composite electrolytes. Besides metal oxides fillers, metal organic framework (MOF) with a coordination network composed of central metal ions and organic ligands, exhibiting properties of both inorganic and organic materials, are proposed as unique fillers. In comparison with the traditional inorganic fillers, MOFs not only possess some similar properties to metal oxide fillers such as high thermal stability, large surface area, and abundant Lewis-acid sites, but also have easily modified organic functional groups for improving the ionic conductivity and interfacial compatibility as well [187,225]. Based on the above advantages, C. Yuan et al., dispersed the MOF-5 nanoparticles into a PEO electrolyte. As a result, improved interfacial stability and a ionic conductivity of 3.16×10^{-5} S cm^{-1} at 25 °C were obtained [226]. Following up, several different kinds of MOFs such as Al(BTC) and MIL-53(Al) with similar roles were proposed to improve ionic conductivity [227,228]. In order to compensate the decreased ionic conductivity resulted from the aggregation of high surface energy of MOFs fillers, Z. Wang et al., linked the MOF nanoparticles to the flexible polymer chains by one-pot UV photopolymerization method. Benefitting from the uniformly dispersed MOF fillers via chemical bonding, a ionic conductivity of 4.31×10^{-5} S cm^{-1} at 30 °C was achieved [225]. Despite the improved ionic conductivity, mechanical properties and interfacial compatibility by adding these insulating fillers, the relative low ionic conductivity of 10^{-5} S cm^{-1} level at RT still cannot meet the practical demands for SSLBs.

2.2.2. Polymer-oxide SSE composite electrolyte

Considering aforementioned inorganic fillers are ionic insulator, which significantly limits further improvements of the ionic conductivity. A composite electrolyte with oxide-based SSEs mixing with SPE is discussed in this part. Combination of a SPE and an oxide-based SSE can possibly ensure mechanical flexibility, high ionic conductivity, good wettability to electrodes, good mechanical properties, dendrite free, and enhanced electrochemical stable window at the same time. The composite electrolyte can be classified as 'ceramic in polymer' and 'polymer in ceramic' according to the contents of the ceramic fillers (Fig. 8a and b).

Many recent studies focus on enhancing the ionic conductivity of SPEs by adding oxide-based SSE fillers. NASICON SSEs, including LATP and LAGP, have been widely studied as fillers [207,229–232]. The inorganic SSE fillers can not only reduce the crystalline of polymer matrix but also possibly provide extra ion transporting pathway. Y. Wang et al. systematically studied the effect of the incorporation of LATP fillers in a PEO-LATP hybrid electrolyte. They found that increasing the LATP content can decrease the melting temperature (T_m) of the PEO complex. Scanning electron microscopy (SEM) analysis showed decreased size of the PEO spherulites after addition of LATP fillers. An ionic conductivity of 1.167×10^{-3} S/cm at 60 °C was achieved with 15 wt.% LATP fillers at a EO/Li^+ ratio of 8 [230].

Since LATP suffers from Ti^{4+} reduction problem in contact with lithium metal anode, LAGP of the same structure but without Ti^{4+} also received many research attentions in composite electrolytes. Y. Zhao et al. had studied the influence of size and concentration of LAGP on the ionic conductivity of the PEO-LAGP-LiTFSI hybrid electrolyte. With different sizes of LAGP fillers, the hybrid electrolyte achieved optimal ionic conductivities with 15–20 wt.% of LAGP. For example, the ionic conductivity of PEO-LAGP-LITFSI was optimized to 6.76×10^{-4} S/cm at 60 °C with 20 wt.% nano-sized LAGP [233].

Enhanced ionic conductivity with perovskite-type SSE fillers in SPE matrix was also observed [234]. Y. Cui's group synthesized a nanowire shape of LLTO and incorporate it into PAN-$LiClO_4$ SPE and they found that with 15 wt.% nanowire LLTO fillers, the hybrid electrolyte PAN--LLTO-$LiClO_4$ exhibited a RT ionic conductivity of 2.4×10^{-4} S/cm.

Similar to other oxide-based SSEs, the garnet-type SSE LLZO has high ionic conductivity at RT, good electrochemical chemical and thermal stability. Unlike the LATP containing an unstable Ti^{4+} constituent, LLZO possesses superior electrochemical stability towards lithium metal anode [154,235]. Consequently, LLZO fillers are expected to not only improve the ionic conductivity but also further improve the stability of hybrid electrolyte at the interface with lithium metal anode [236]. The reported data shows that SPE-LLZO hybrid electrolytes with different polymer-to-filler ratio had a wide range of ionic conductivities from 10^{-6} to 10^{-4} S/cm at RT. While a RT ionic conductivity of 10^{-6} S/cm order of PEO-LITFSI SPE filled in LLZO (70 wt.%) was reported by M. Keller et al. [202], a RT ionic conductivity of 10^{-4} S/cm of PEO-LLZO hybrid electrolyte was reported by L. Hu' group [28] and J. Zhang et al. [237]. In the latter two cases, the reasons for the higher ionic conductivities are probably because of the usage of the 3D LLZO flamework and ultra-small (~40 nm) size LLZO as the fillers.

In addition to the wide application of PEO-based SPEs in composite electrolytes, polymer electrolytes based on other polymers such as polyvinylidene fluoride (PVDF), PVDF-HFP, and polyethylene carbonate (PEC) also received many research attentions for constructing composite electrolytes due to their unique properties such as high mechanical strength and high lithium transference number [93,238–242]. However, additional solvent, liquid electrolyte, or combination with other SSEs are required to achieve feasible battery performance in these systems. The PVDF-LLZO hybrid electrolyte reported by X. Zhang et al. exhibited a high ionic conductivity of 5×10^{-4} S/cm at 25 °C, but residual DMF solvent remaining from the preparation process was found in the hybrid electrolyte according to their thermogravimetric analysis (TGA) results. The DMF content could have played an important role in the high ionic conductivity and battery performance. $LiCoO_2$ batteries with this PVDF-LLZO hybrid electrolyte exhibited excellent cycling performance and rate performance, delivering a discharge capacity of 130 mAh/g at 4C rate, which is comparable to that of liquid electrolyte system [239]. C. Sun's group reported a PVDF-HFP-LLZO hybrid electrolyte with RT ionic conductivity of 1.23×10^{-6} S/cm, which was increased to 1.1×10^{-4} S/cm with the addition of 20 μL liquid electrolyte [242]. The $LiFePO_4$ battery with the PVDF-HFP-LLZO-liquid hybrid electrolyte presented excellent electrochemical performance at RT. L. Fan's group reported a PEC-LLZO hybrid electrolyte prepared by solution casting method, which had an ionic conductivity of 5.24×10^{-5} S/cm at 55 °C. This PEC-LLZO hybrid electrolyte presented much better thermal stability compared to commercial Celgard separator, and rendered a stable

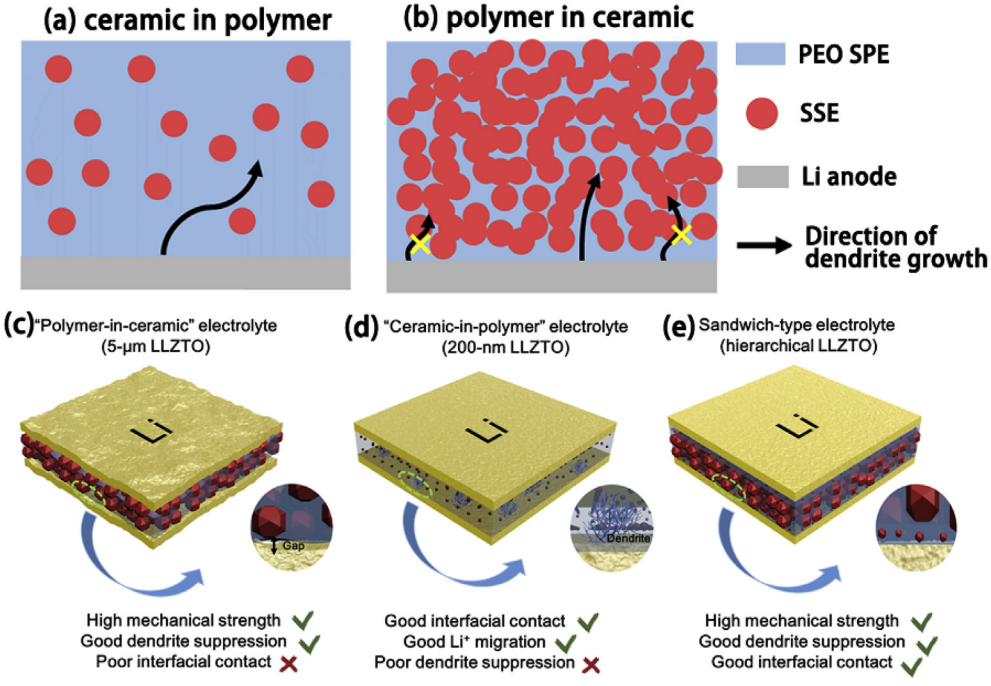

Fig. 8. The composite electrolytes of (a) ceramic in polymer and (b) polymer in ceramic. Lithium dendrite growth mechanism of (c) 'polymer in ceramic' with SPE filled in 5 μm size of LLZTO garnet SSE, (d) 'ceramic in polymer' with 200 nm size of LLZTO garnet SSE filled in SPE and (e) sandwich type composite electrolyte with 'ceramic in polymer' composite electrolyte at the Li/'polymer in ceramic' composite electrolyte interface [243]. Reproduced with permission [243], Copyright 2019, Wiley.

flexible SSLB at elevated temperature [238].

'Polymer in ceramic' composite electrolyte has high mechanical strength which is good at dendrite suppression. However, poor interfacial contact with electrode results in high interfacial resistance. 'Ceramic in polymer' composite electrolyte has better interfacial contact with electrodes, but its strength is not enough for dendrite suppression. The design using 'polymer in ceramic' composite electrolyte as the main ionic conductor and separator, 'ceramic in polymer' composite electrolyte as the interface to ensure intimate contact with lithium anode can render a long cycling performance, dendrite free SSLB (Fig. 8c–e) [243].

2.2.3. Polymer-sulfide composite electrolytes

Sulfide-based SSEs have much higher ionic conductivities at RT than oxide-based SSEs, some of which are even comparable to liquid electrolytes [146]. Therefore, it is attractive to combine sulfide-based SSEs with SPEs to achieve a decent ionic conductivity and mechanical property. X. Xu's group reported an improved ionic conductivity, enlarged electrochemical window, and stabilized electrolyte/Li interface hybrid electrolyte consisting of LGPS and PEO-LITFSI SPE [244]. In addition, the succinonitrile doping further increased the RT ionic conductivity of this hybrid electrolyte [244]. Another type of sulfide-based SSE containing Li_2S, P_2S_5 and P_2O_5, Li_3PS_4 have also been reported to complex with PEO-based SPE [72,245]. Similar to the insulating fillers and oxide-based SSE filler, the enhancement in the ionic conductivity and interfacial stability toward lithium metal anode was also achieved after adding sulfide-based SSEs into SPE.

To address the instability of sulfide-based SSEs in air and to enhance its flexibility, integrating SPEs into a sulfide-based SSE matrix is a strategy ('polymer in ceramic'). Sulfide-based SSEs have a Young's modulus in the range of 14–37 GPa (Table 1). Although the values are lower than that of oxide-based SSEs (~150 GPa) [176,246], the sulfide-based SSEs are still rigid and brittle resulting in high grain boundary resistance and high interfacial resistance towards electrodes. The rigid property cannot accommodate the volume change of electrodes during charge/discharge process. To address these problems, a SPE, whose elastic modulus is around 20 MPa, three orders magnitudes lower than that of sulfide-based SSE [247], is introduced to improve flexibility and enhance the ambient stability of the sulfide-based SSE. However, the incorporation of a low ionic conductive SPE into a sulfide-based SSE matrix will sacrifice the high ionic conductivity. For example, incorporation of 1 wt.% - 5 wt.% comb shaped SPE (poly(oxyethylene)s with tri(oxyethylene)s as side chains complexing with $LiClO_4$. This polymer has the molecule structure of $-(CH_2CH_2O)_l-(CH_2CHO-(CH_2O(CH_2CH_2O)_3CH_3))_m)_p-$, $l = 81$, $m = 19$.) into $95(0.6Li_2S{\cdot}0.4SiS_2){\cdot}5Li_4SiO_4$ (mol%) sulfide-based SSE resulted in an ionic conductivity of $\sim 10^{-5}$ S/cm at 60 °C, which is almost 10 times lower than that of the bulk sulfide-based SSE despite enhancing the flexibility of the SSE [248]. Thus, SPEs with high ionic conductivities are preferred. PFPE random copolymers-based SPE with an ionic conductivity over 10^{-4} S/cm at RT is favorable [249]. I. Villaluenga et al. integrated 23 wt.% of PFPE-LITFSI SPE into a sulfide-based SSE, $75Li_2S{\cdot}25P_2S_5$, matrix to fill up the gaps in the sulfide-based SSE pellets obtained from the cold press process. Significantly faster ion transport and lower grain boundary resistance were achieved in this hybrid electrolyte by the compact packing. They also developed a method to calculate the ionic conductivity σ_{calc} of the hybrid electrolyte by the following equation (Eq. (2)) (ignoring any tortuosity):

$$\sigma_{calc} = \varphi_{sulfide} * \sigma_{sulfide} + \varphi_{PFPE} * \sigma_{PFPE} \quad (2)$$

where φ_{sulfide} and φ_{PFPE} are the volume fractions of the sulfide-based SSE and PFPE-LITFSI SPE; $\sigma_{sulfide}$ and σ_{PFPE} are the corresponding ionic conductivities. The calculated values were in good consistence with the experimental values. The as-prepared hybrid electrolyte achieved an ionic conductivity over 10^{-4} S/cm at 30 °C [186].

In a short summary of the as-mentioned SSEs, SPE-oxide and SPE-sulfide composite hybrid electrolytes, the ionic conductivities of each individual SSE and composite hybrid electrolytes are compared in Fig. 9 below. From the chart, it is clear that the reported hybrid electrolytes have comparable ionic conductivities to the individual SSEs, not to mention other comprehensive advantages.

2.3. Strategies to improve ionic conductivity of hybrid electrolytes

In the past two decades, many efforts have been dedicated to study the mechanism of insulating fillers (e.g. Al_2O_3, TiO_2, SiO_2) in improving the ionic conductivity of the composite electrolytes. The improvements due to insulating ceramic fillers were proposed by following mechanisms: (i) the fillers physically interrupt and suppress the crystalline of polymer; (ii) Lewis acid-base type surface interactions between the filler surface and polymer chains kinetically inhibit the crystallization of polymer chains; (iii) Lewis acid-base interactions at the interface between fillers surface and SPE provide preferential pathways for Li^+ ion conduction; (iv) Lewis acid-base type surface interactions with the lithium salt facilitate the dissociation of the salt [147,276–280].

In addition to the above mentioned filler effects, the inorganic SSE filler bulk can also serve as extra Li^+ ion conduction channels, showing advantages over the insulating fillers [202,281]. Therefore, SSEs fillers are preferred when designing a high ionic conductive hybrid electrolyte. In this chapter, focusing on the ionic conductivity enhancement for hybrid electrolytes, effects of size, concentration, and shape of the SSE fillers as well as plasticizer effects will be discussed.

2.3.1. Size and concentration of fillers

For insulating fillers such as TiO_2, Al_2O_3 and SiO_2, smaller size is preferred. Especially, nano-sized fillers with high specific surface areas are able to provide strong interaction with the polymer chains and lithium salts. Ceramic fillers interrupt the long-range order of polymer chains and thus increase the percentage of amorphous phase. The effect is more significant when the size of fillers is close to the chain length of the polymer [282]. M. Dissanayake et al. had systematically studied the effects of Al_2O_3 filler size and concentration on conductivities in a PEO--$LiCF_3SO_3$ (LiTf) SPE [276]. They found that the smaller size of the fillers led to a higher ionic conductivity. The optimal ionic conductivity achieved with 5.8-nm size Al_2O_3 fillers was one order of magnitude higher than that with 10-μm size fillers. They believed that the smaller sized Al_2O_3 fillers have higher surface areas which are beneficial to the favorable surface interactions.

The effects of size and concentration of LLZO SSE fillers in a PEO polymer matrix was systematically studied by J. Zhang et al. [237]. In the study, PEO-LLZO hybrid electrolytes were prepared without any lithium salts. They believed that Li^+ near the LLZO particle surface can be influenced by the PEO polymer. In consequence, lithium vacancies on LLZO grain surface are created. The surface Li vacancies of LLZO provide sites for Li^+ transfer. As a result, both high ionic conductivity of LLZO particle and the surface vacancies contributed to the overall conductivity enhancement of the hybrid electrolyte. The percolation effect was considered to play an important role in improving ionic conductivity. Fig. 10a shows the ionic conductivities of PEO-LLZO hybrid electrolytes with different sizes of LLZO fillers and different concentrations. With the size of 40 nm, 400 nm and 10 μm LLZO fillers, the conductivities were optimized at 12.7, 15.1, and 21.1 vol.%, respectively. The highest ionic conductivity of PEO-LLZO composite electrolyte at 30 °C can be over 10^{-4} S/cm with 12.7 vol.% 40 nm LLZO fillers. Y. Zhao et al. also studied the effects of LAGP fillers size and concentration effect on ionic conductivity for PEO-LAGP-LITFSI composite electrolyte [233]. With different sizes of LAGP fillers, the conductivities were optimized with 15–20 wt.% LAGP fillers. For example, with 20 wt.% nano-size LAGP fillers, the hybrid electrolytes exhibited the highest ionic conductivity of 6.76×10^{-4} S/cm at 60 °C.

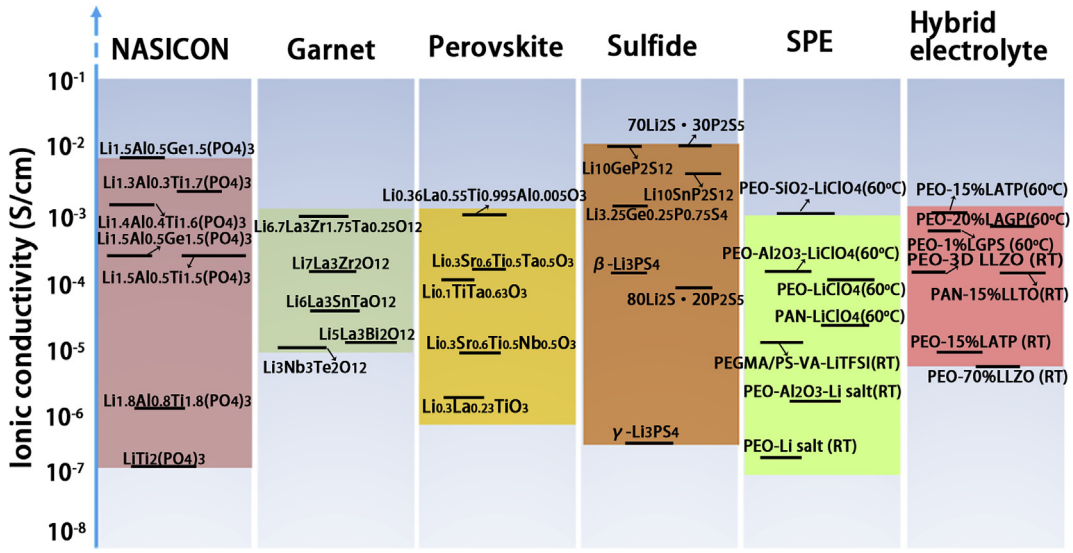

Fig. 9. Comparison on ionic conductivities of different types of SSEs including NASICON-type [106,230,250–256], garnet-type [24,108,257–260], perovskite-type [261–266], sulfide-based SSEs [36,143,145,146,267–271], SPE [75,83,234,272,273], and hybrid electrolytes with composite structure [28,202,206,207,230,232,233,236,274,275]. Hybrid electrolytes show comparable ionic conductivities to other individual SSEs.

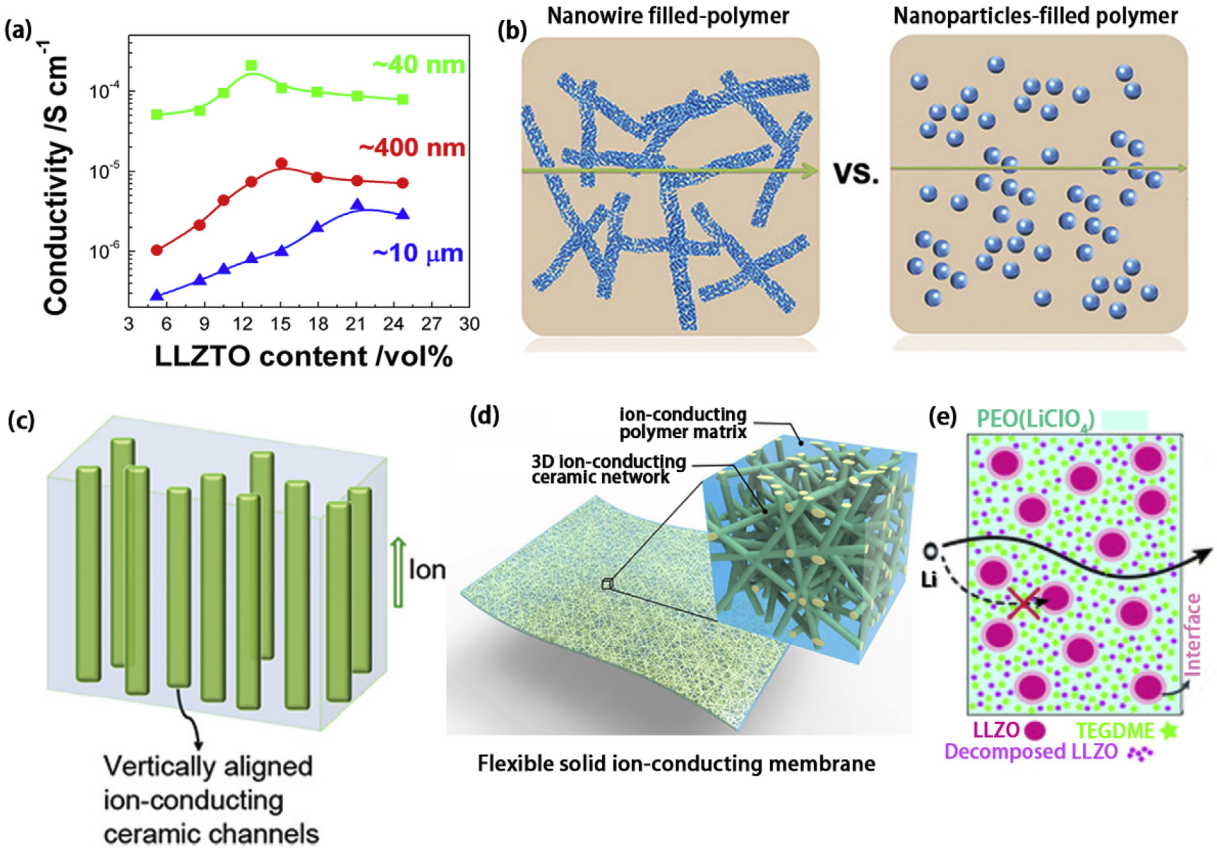

Fig. 10. Strategies for designing a high ionic conductivity hybrid electrolyte. (a) Size and concentration effects on the ionic conductivity of PEO-LLZO hybrid electrolytes [237]. Reproduced with permission [237], Copyright 2016, Elsevier. (b) Comparison of the Li^+ ion transport pathways in hybrid electrolytes with nanowire or particle LLTO fillers [234]. Reproduced with permission [234], Copyright 2015, ACS. (c) Vertically aligned Li^+ ion transporting channels to enhance the ionic conductivity [207]. Reproduced with permission [207], Copyright 2017, ACS. (d) Creating a 3D ionic conducting ceramic network for enhancing the ionic conductivity of a hybrid electrolyte [28]. Reproduced with permission [28]. (e) Plasticizer additives to increase the RT ionic conductivity of a hybrid electrolyte [291]. Reproduced with permission [291], Copyright 2017, RSC.

2.3.2. *Shape of fillers*

Depending on the Li^+ ion conduction mechanism, the shape of SSE fillers can be an important factor effecting the ionic conductivity of composite electrolytes. For insulating ceramic fillers, the conductivity improvement mainly relies on the interactions of their surface groups with the surrounding polymer chains and lithium salts. As long as the

insulating fillers have high surface area allowing effective surface interactions, a particular shape of insulating fillers is not of importance. Particle shape of insulting fillers are most commonly used in this case due to the variety of metal oxides such as nano-size Al_2O_3, SiO_2, and TiO_2 particles with different surface groups are commercially available [76,197,273,283,284]. Differently, besides surface interactions between fillers and polymer and lithium salts, ionic conducting SSE fillers can provide additional Li^+ ion pathways within the fillers, hence particular interconnecting structures can be designed to maximize ionic conductivity and minimize the grain boundary. In addition to commercial and home-made nano-size SSEs particles [233], novel shapes of nanowire (random or vertical aligned) and 3D network structures have been rationally designed and synthesized for hybrid electrolytes [28,207,234].

One dimensional LLTO nanowire fillers can be prepared by electrospinning polyvinylpyrrolidone polymer fiber that contain Li, La, and Ti salts and subsequent calcination at 600–900 °C in air for 2 h [234]. The nanowire fillers were applied in PAN-$LiClO_4$ based hybrid electrolyte in comparison with LLTO nanoparticle fillers. As schematically shown in Fig. 10b, the interconnecting nanowires provide a network for fast Li^+ ion conduction, while the Li^+ ion pathway is intermittent through the discrete particles. The nanowire LLTO fillers enabled significantly higher ionic conductivity than nanoparticle LLTO fillers with the same concentration. With 15 wt.% LLTO nanowire fillers, an ionic conductivity over 10^{-4} S/cm was achieved at 20 °C.

Simply mixing the inorganic SSE particles and SPE, where the SPE is a continuous phase and the inorganic SSE is a dispersed phase, is the most common method to prepare composite electrolyte. However, the Li^+ ion can only transfer within SPE rather than from high conductive inorganic SSE particle to another, which significantly decreased the capability of SSE fillers. In this consideration, 3D continues inorganic conductive frameworks were developed for shortening the Li^+ ion transport pathway and further enhance the ionic conductivity. A vertically aligned LATP fabricated via an ice-template method filling with PEO-based SPE had been reported by Y. Yang's group (Fig. 10c). The vertical structure of LATP is expected to provide a fast-ionic conductive channel in the composite electrolyte, thus, the result showed that a high ionic conductivity of 5.2×10^{-5} S/cm at RT was achieved [207]. L. Hu's group developed a 3D Li^+ ion conducting network with garnet-type SSE LLZO to provide continuous channels for Li^+ ion conduction in a PEO matrix (Fig. 10d) [28,285]. The RT ionic conductivity of this composite electrolyte was up to 2.5×10^{-4} S/cm, which was among the highest reported ionic conductivity for polymer-oxide hybrid electrolyte [28]. As a proof of concept, a continuous Li^+ ion conducting network can effectively improve the RT ionic conductivity of polymer-oxide hybrid electrolytes.

2.3.3. Adding plasticizers

Besides tuning the design and properties of fillers, composite electrolytes can be tailored for higher ionic conductivity by adding plasticizers. Plasticizers can be low-molar-mass organics, organic solvents or ionic liquids (ILs). The working principle of plasticizers is to increase the content of amorphous phase of the SPE and improve segmental motion; at the same time, plasticizers promote the dissociation of lithium salt and thus increase the number of effective charge carries [286–288]. Succinonitrile (SN) is a good example of a plasticizer which remains a plastic crystal under RT. Importantly, composites of SN and lithium salts have very high RT ionic conductivity (in the order of 10^{-4} S/cm) [289]. Study shows that incorporating just a small amount of SN (9 wt.%) into a PEO-LAGP-$LiClO_4$ hybrid electrolyte can significantly improve the RT ionic conductivity from 3.0×10^{-5} to 1.1×10^{-4} S/cm. Using this hybrid electrolyte, SSLB with a $LiFePO_4$ cathode delivered satisfying discharge capacity at 0.2 C and 0.5 C under 25 °C [232].

Using liquid electrolytes as plasticizers is also a very popular method to enhance the ionic conductivity and ensure complete wetting of electrodes for RT SSLBs functionality [231]. Hybrid electrolytes of P(VdF-co-HFP)-LAGP-carbonate liquid electrolyte and P(VdF-co-HFP)-LLTO- carbonate liquid electrolyte had been reported by Seul-Ki Kim et al. and Hang T. T. Le et al. respectively. Both hybrid electrolytes presented good electrochemical performance in RT SSLBs [231,290].

In summary, the influences of the size, concentration, and the shape of the SSEs fillers in composite hybrid electrolyte are critical for the enhancement of the ionic conductivity of hybrid electrolytes. Small size and interconnected shape of SSEs fillers are favorable. The present of plasticizers in composite electrolytes can also enhance the ionic conductivity because it can lower the crystalline of SPE and promote the dissociation of lithium salt.

2.4. Li^+ ion conduction in hybrid electrolytes

Understanding the Li^+ ion transporting pathways or conduction mechanisms within hybrid electrolytes is very important for the development of hybrid electrolytes. In the past several decades, many efforts have been dedicated to study the Li^+ ion conduction mechanism in SPE, oxide-based SSEs and sulfide-based SSEs [76,103,113,278,292–294]. Understanding the Li^+ ion conduction mechanism can provide researchers the guidelines for designing a high ionic conductivity SSE.

While liquid electrolytes dissolve lithium salts in solvents and the diffusion of solvated ions provide the ionic conductivity, SPE complex designated salts in a polymer matrix and the diffusion of ions does not play the key role in the ionic conductivity of SPE. To facilitate the dissociation of Li^+ ions, the lithium salts used in SPEs usually have low lattice energy. The dielectric constant of the host polymer should be relatively high to avoid conduction of electrons [32]. The Li^+ ions from salts are coordinated with the function groups on the polymer chains (e.g. -O- in PEO, -CN in polyacrylonitrilde, -NR in polyamide, etc.). The polymer chains undergo continuous local segmental motions and create free volumes. Li^+ ions migrate from one coordination site to another or hop from one chain to another via the free volumes by the segmental motions [32]. Under such Li^+ ion transfer mechanism, the segmental motions of polymer chains and the number of mobile Li^+ ions in the polymer matrix are the critical factors determining the ionic conductivity of a SPE. The polymer segmental motions significantly depend on temperature, so does the ionic conductivity. The temperature dependent ionic conductivity can be described by the Vogel-Tamman-Fulcher (VTF) relation and the Arrhenius-type relation.

VTF-type relation is expressed as:

$$\sigma = \sigma_0 T^{-\frac{1}{2}} exp\left(-\frac{B}{T - T_o}\right) \quad (3)$$

where σ_0 is the pre-exponential factor; B is the pseudo-activation energy for the conductivity; and T_o is the equilibrium glass transition temperature (T_g) ($T_o \approx T_g$ - 50K). For SPEs, a nonlinear relationship between ionic conductivity σ and $1/T$ typically means that the Li^+ ion hopping motion is coupled with relaxation/breathing and/or segmental motion of polymer chains [32,295].

Arrhenius-type relation is expressed as:

$$\sigma = \sigma_o exp\left(-\frac{E_a}{KT}\right) \quad (4)$$

where E_a is the activation energy which can be extracted from the gradient of log σ versus $1/T$ plot. Arrhenius-type behavior descripts the ion hopping decoupled from long-range motions of the matrix (e.g. amorphous phase and glass phases polymer below the glass transition temperature, inorganic ceramic SSEs, etc) [295].

Oxide-based or sulfide-based SSEs as fillers in a composite electrolyte are expected to deliver higher ionic conductivities than insulating fillers, because not only the polymer matrix but also the fillers have the ability to conduct Li^+ ions. Even though many composite electrolytes such as PEO-LLZO, PEO-LATP, PAN-LLTO etc [28,71,207,234,296]. have been reported with improved ionic conductivity compared to that of bare SPE, the underlining Li^+ ion conduction mechanism in hybrid electrolytes was

less discussed. Lack of direct characterization techniques on Li^+ ion behaviors makes it particularly challenging for mechanism studies. Characterization techniques, such as Infrared (IR) and Raman spectroscopies, have been used to measure the change of salt anions to obtain hints of Li^+ ions dissociation. For example, the lithium salt, $LiClO_4$, exhibits multiple IR characteristic peaks (624, 635 and 664 cm^{-1}) depending on the status of the salt. IR spectra of PAN-Al_2O_3-$LiClO_4$ composite electrolytes with difference concentration of Al_2O_3 fillers was studied by Z. Wang et al. They found that Al_2O_3 fillers interacted with the ClO_4^- anions and correspondingly increased the effective number of free Li^+ ions, thus enhanced the ionic conductivity of the SPE [278]. However, IR and Raman characterization cannot give direct information about Li^+ ions within the SSE.

Development of direct probing techniques to characterize Li^+ ions pathway in SSEs is particular important for understanding the Li^+ ion conduction mechanism. Recently, nuclear magnetic resonance spectroscopy (NMR) was proposed as a powerful tool to study the Li^+ ion transfer mechanism in SSEs [113,281,291]. Y. Hu's group first reported the combination of selective isotope labeling and solid-state Li NMR to precisely identify the lithium sites and probe the Li^+ ion pathway within a PEO-LLZO-$LiClO_4$ hybrid electrolyte [281]. Fig. 11a schematically shows the possible Li environments within a PEO-LLZO-$LiClO_4$ hybrid electrolyte, including the Li in PEO-$LiClO_4$ polymer matrix, the LLZO grain, and the PEO/LLZO interface. Corresponding high-resolution ^6Li NMR spectrum of PEO-$LiClO_4$ SPE, pure phase LLZO, and PEO-LLZO-$LiClO_4$ hybrid electrolyte are presented in Fig. 11b. On the spectrum of the hybrid electrolyte, the shoulder at 1.4 ppm indicates the Li at the PEO/LLZO interface. The Li^+ ion pathways were probed in a lithium symmetric cell with ^6Li metal as electrodes (Fig. 11c). Upon cycling, ^6Li from one electrode moved across the hybrid electrolyte to the other electrode, replacing ^7Li in the hybrid electrolyte, depicting a diffusion pathway of the $^6Li^+$ ions. By comparing the ^6Li amount in the different parts of the hybrid electrolyte before and after cycling, the Li^+ ions pathway can be disclosed. The results showed that there was a significantly increase in the peak of LLZO grains (increased by 39%), slight increase in the peak of PEO/LLZO interface (6%), and unchanged peak of PEO-$LiClO_4$ SPE (Fig. 11d), which suggested a preferred Li^+ ions pathway through the LLZO phase rather than the SPE. Furthermore, the Li^+ ions conduction mechanism in the PEO-LLZO-$LiClO_4$ hybrid system with addition of a plasticizer, tetraethylene glycol dimethyl ether (TEGDME) was also studied (Fig. 11e). Li environments in the PEO-TEGDME-LLZO-$LiClO_4$ hybrid are similar to those in PEO-LLZO-$LiClO_4$ hybrid electrolyte. However, with the TEGDME additive, LLZO is partially decomposed and dissolved into TEGDME. Then, a completely different Li^+ ion pathway was found. Li^+ ion transport favored the liquid TEGDME-associated phases over the LLZO or the PEO/LLZO interface (Fig. 11g) [291].

In PEO-LLZO-$LiClO_4$ hybrid electrolyte without TEGDME, Li^+ ions prefer the path through the LLZO phase which has a RT ionic conductivity of 10^{-4} S/cm, 3 orders higher than PEO-$LiClO_4$ SPE (~10^{-7} S/cm). However, in the presence of TEGDME, Li^+ ions prefer pathways via the liquid TEGDME-associated phase which possesses an even higher ionic conductivity than the LLZO phase and PEO-$LiClO_4$ SPE. From these two studies, a conclusion is that Li^+ ions would choose a low resistant pathway within a hybrid electrolyte. Therefore, a composite electrolyte with high ionic conductive components are critical for improving of the total ionic conductivity.

In summary, NMR is a powerful tool to study the Li^+ ion transport mechanism in hybrid electrolytes. A preferential pathway of Li^+ ion through the component of highest ionic conductivity (e.g. the oxide-based SSE phase in SPE-oxide composite electrolyte and the liquid-associated phases in the presence of a plasticizer) is revealed. This should be the reason why SPE-oxide composite electrolytes using SSE

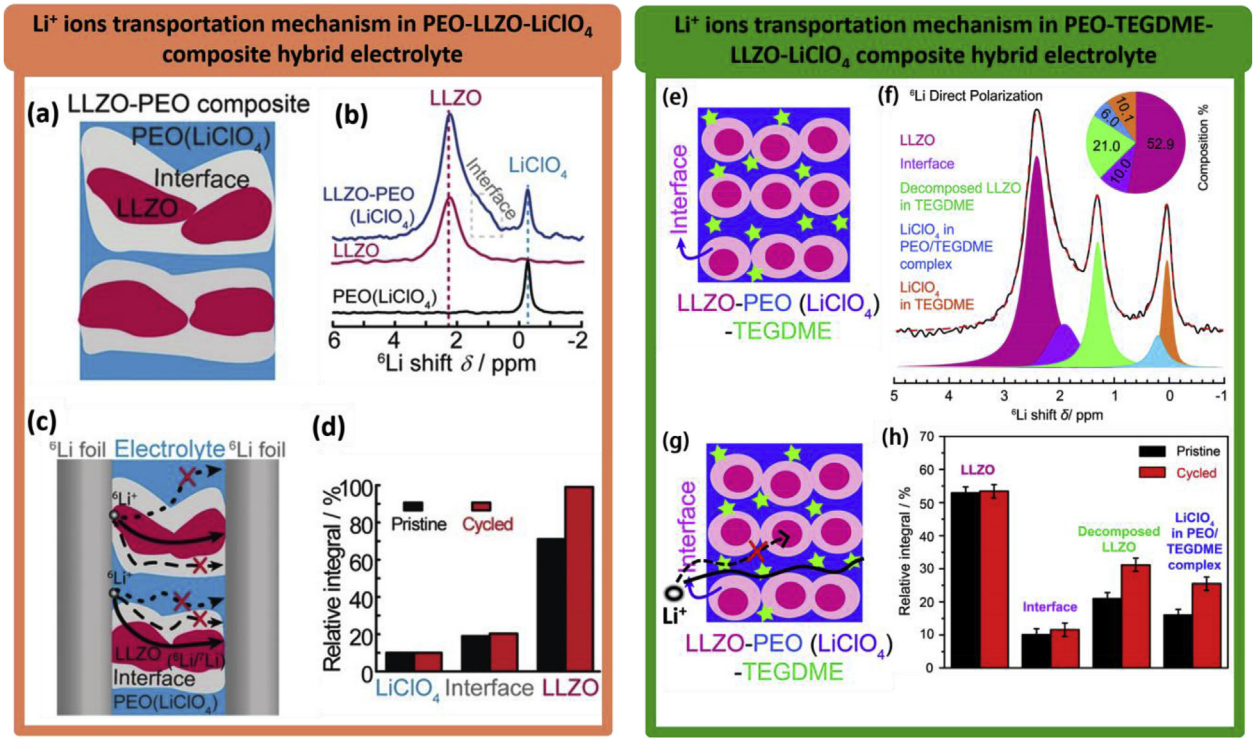

Fig. 11. (a) Schematic diagram of Li environment within the PEO-LLZO-$LiClO_4$ composite electrolyte including PEO-$LiClO_4$ SPE matrix, LLZO, and PEO/LLZO interface; (b) high-resolution ^6Li NMR spectra of PEO-$LiClO_4$, LLZO and PEO-LLZO-$LiClO_4$ hybrid electrolyte; (c) schematic diagram of ^6Li pathways in a symmetric cell with PEO-LLZO-$LiClO_4$ hybrid electrolyte; (d) quantitative analysis of ^6Li amount in PEO-$LiClO_4$, PEO/LLZO interface, and LLZO in the PEO-LLZO-$LiClO_4$ composite electrolyte before and after cycling [281]. Reproduced with permission [281], Copyright 2016, Wiley. (e) Schematic diagram of Li environment within the PEO--TEGDME-LLZO-$LiClO_4$ composite electrolyte. (f) High-resolution ^6Li NMR spectra of PEO-TEGDME-LLZO-$LiClO_4$ and the concentration of Li in each component; (g) proposed Li^+ ion transport pathway within the composite electrolyte; (h) quantitative analysis of ^6Li amount in LLZO, interface, decomposed LLZO and PEO--TEGDME-$LiClO_4$ in the PEO-TEGDME-LLZO-$LiClO_4$ composite electrolyte before and after cycling [291]. Reproduced with permission [291], Copyright 2017, RSC.

nanowire fillers or 3D SSE network fillers showed higher ionic conductivities than that of discrete nano-particles fillers. With continue Li^+ ion pathway in the SSE nanowires or 3D SSE network fillers, the Li^+ ion can transport across fewer boundaries than that with discrete nano-particles fillers. Since Li^+ ion transportation is favorable in the high ionic conductivity phase, creating a 3D ionic network by a very high ionic conductivity SSE such as sulfide-based SSE as the framework to make SPE-inorganic hybrid electrolyte is expected to have an even higher ionic conductivity at RT.

3. Addressing the interfacial issues by hybrid electrolytes

The biggest challenge in building a high-performance SSLB is the high interfacial resistance between SSEs and electrodes. The stiff nature of ceramic SSEs causes poor contact with electrodes and hence high interfacial resistance. Efforts to reduce interfacial resistance by interfacial engineering have received increasing attentions in recent years. The SSE/anode and SSE/cathode interfaces emphasize different interfacial problems that require differently tailored solutions, which have been discussed in previous chapters. As another solution to address the interfacial issues, hybrid electrolytes, configured with a stiff inorganic SSE and a rationally engineered interfacial with SPE or liquid electrolyte, will be discussed in chapter.

3.1. Solid-state batteries with composite cathodes and composite electrolytes

SSLBs created by all-composite method have been widely studied and reported to be able to alleviate the mismatch problem. All-composite method utilizes a certain amount of SPE to fabricate composite electrodes and composite electrolytes by hot pressing to achieve an intimate SSE/electrode interface. R. Chen et al. demonstrated this kind of all-composite SSLBs consisting of a composite electrolyte with 40 wt.% PEO-LITFSI SPE filled in 60 wt.% LLZO, composite $LiFePO_4$ cathodes with different contents of SPE (10–30 wt.%), and a lithium metal as the anode. After hot pressing, the hybrid electrolyte/cathode interface was seamless and free of pores. The cell with 15 wt.% SPE composite cathode delivered the highest discharge capacity of 152 mAh/g with an overall resistance of 1300 Ω at 60 °C (Fig. 12b and c) [206]. A similar work by Y. He's group used a LLZO nanowire fillers filled SPE to construct a composite electrolyte that has an ionic conductivity of 2.39×10^{-4} S/cm at RT and 1.53×10^{-3} S/cm at 60 °C (Fig. 12d). By integrating SPE with $LiFePO_4$, the composite cathode shows an intimate contact to the hybrid electrolyte. The SSLB can deliver a discharge capacity of 158.8 mAh/g at 0.5 C at 60 °C and 158.7 mAh/g at 0.1C at 45 °C (Fig. 12e) [297]. Another work done by H. Wang's group who demonstrated a tape casting method to infuse PEO SPE into the porous cathode to ensure intimate contact with the SSE. The resulting $LiFePO_4$ SSLB showed improved electrochemical performance compared to the conventional $LiFePO_4$ SSLB (Fig. 12a) [298].

The lithium dendrite formation problem is detrimental to SPE. It is proposed that a SPE with the higher shear modulus than that of lithium metal can suppress dendrite growth [96,190]. Thus, the lithium dendrite formation problem can be reasonably addressed by integrating a rigid oxide-based SSE into the SPE matrix, forming composite electrolyte with enhanced mechanical strength. Therefore, lithium symmetrical cells with composite electrolyte present excellent lithium plating/stripping cycling performance without lithium dendrite formation compared to the bare SPE (Fig. 12f) [28,73,237,297].

Another challenge of SPE is the low oxidation window. Composite electrolytes with inorganic SSE fillers in SPE matrix show an obviously enlarged electrochemical stability window. The higher the filler concentration, the wider the electrochemical window has been observed [236,237,274]. This can explain why the NMC622 SSLB with a PEO-LLZO-$LiClO_4$ composite electrolyte can deliver a higher capacity than that with a pure PEO-$LiClO_4$ SPE [236].

3.2. Liquid-oxide multilayer hybrid electrolytes

To address the high interfacial resistance problem in oxide-based SSEs, different strategies have been developed to tailor the interface between oxide-based SSEs and electrodes. Significant progresses have been achieved in reducing the interfacial resistance between lithium anode and oxide-based SSE by solidifying molten lithium on oxide-based SSE surface. A negligible Li/SSE interface resistance can be achieved by this method [122–124].

However, unlike lithium metal with a low melting point of 180 °C, cathodes with a high melting point above 1000 °C are difficult to adopt the melting method for cathode/SSE interface building. Moreover, cathodes are usually in forms of miron-sized or nano-sized particles with pores and gaps [299,300]. The complicated surface morphology introduces extra challenges for a matching interface. Thus, using liquid electrolytes to compensate the gaps between the oxide-based SSE and the cathode as well as the gaps between the cathode particles is still a common practice to enable SSLBs working effectively [2,301,302].

Our group comprehensively studied the amount of liquid electrolyte in addressing the cathode and LATP SSE interface (Fig. 13a–c) [303]. The results showed that adding as little as 2 μL of liquid electrolyte at the $LiFePO_4$ cathode/LATP interface can enable the battery operation at RT with a discharge capacity of 125 mAh/g at 1 C and 98 mAh/g at 4 C. Interestingly, excess liquid electrolyte showed no further contribution to the electrochemical performance enhancement. Such small amount of liquid electrolyte will be completely absorbed by the electrode and free of leakage concerns.

Liquid-oxide hybrid electrolytes are also widely studied in Li-S batteries. Oxide-based SSEs in this kind of Li-S batteries not only can inhibit the polysulfide from shuttling due to the dense structure but also capable of suppressing lithium dendrite growth. Even though many previous works focus on achieving an all-solid-state Li-S battery (ASSLSB) and avoid using liquid solvent, the reported performance ASSLSBs are far away from satisfaction [304–308]. The reasons behind are probably due to the poor ionic and electronic conductivities of sulfur cathode, the high interfacial resistance, and slow solid-solid reactions. Employing a small amount of liquid electrolyte (i.e. liquid-oxide hybrid electrolyte) to modify the SSE/cathode interface could be critical for Li-S batteries. The presence of desirable solvents can enable the formation of polysulfides, significantly improving the electrochemical kinetics via solid-liquid transfer reactions. Y. Xia's group applied a liquid-LATP hybrid electrolyte in a Li-S battery and showed greatly enhanced cycle life without sacrificing capacity or inducing polysulfide shuttling (Fig. 13d–f) [301]. Similar studies using liquid-oxide hybrid electrolytes in Li-S batteries are also reported by other groups [302,309–312]. In Li-S batteries with a liquid-oxide hybrid electrolyte, the inorganic oxide-based SSE not only functions as a separator to prevent the short-circuit of the battery but also services as a shield to inhibit the migration of polysulfides, so the self-discharge problem is eliminated. Excellent cycling performance and a Coulombic efficiency of almost 100% could be achieved. The liquid electrolyte in the cathode can not only provide a medium for the sulfur-polysulfide-sulfide redox reactions within the cathode but also reduce the SSE/electrode interfacial Li^+ ion transport resistance.

Solid-state Li-air batteries are also benefited from the usage of liquid-oxide hybrid electrolytes. Due to the existence of oxide ceramic SSE, the liquid electrolyte in anode side (anolyte) and cathode side (catholyte) can be different in one single cell, which means a hybrid electrolyte with three different electrolytes can be realized in a single cell. Organic electrolytes are not favorable as catholyte in Li-air battery because they are neither stable in air nor compatible to the discharge products. Blockage of the cathode will occur once the insoluble discharge products are produced. Nevertheless, these problems can be addressed by using an aqueous-based catholyte. On the other hand, aqueous-based electrolyte is not suitable as anolyte due to the aggressive reaction between lithium metal and water, while organic electrolyte is a good anolyte candidate. The application of liquid-oxide hybrid electrolyte makes it possible to

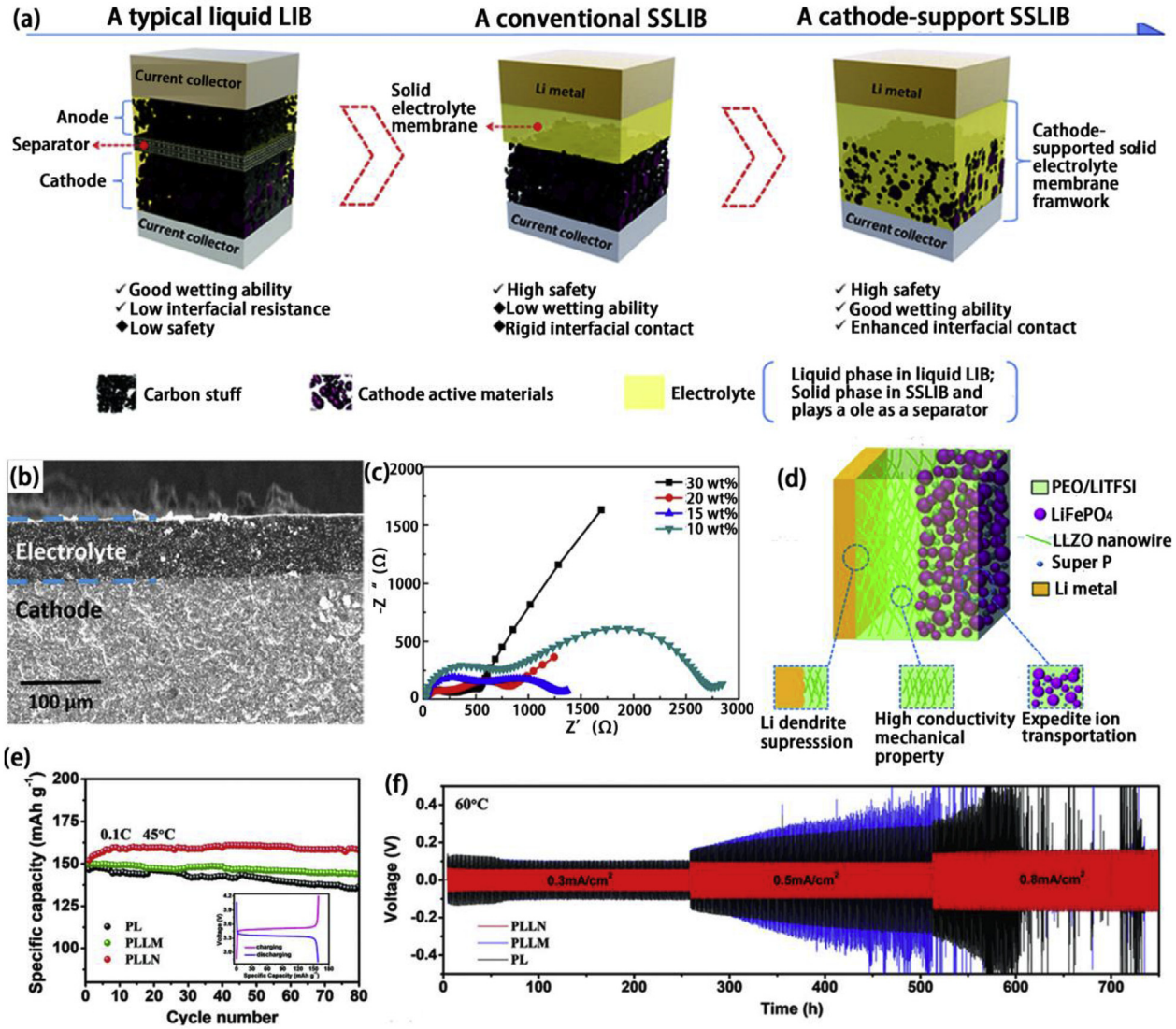

Fig. 12. (a) Comparison of the liquid electrolyte-based LIB, SSLB with conventional cathode and SSLB with composite cathode [298]. Reproduced with permission [298], Copyright 2019, RSC. (b) Cross-sectional SEM image of composite cathode/composite electrolyte interface; (c) EIS of the all-composite SSLBs with different contents of SPE in the composite cathode [206]. Reproduced with permission [206], Copyright 2017, ACS. (d) A schematic diagram of the all-composite SSLB with nano-wire LLZO fillers in the SPE and a SPE-$LiFePO_4$ composite cathode. The nano-wire LLZO filled SPE can help to prevent dendrite formation, while the SPE in cathode address the mismatch problem and Li^+ ion conduction in cathode; (e) the cycling performance of SSLBs with different composite electrolytes; (f) voltage-time profiles of lithium symmetric cells with bare-SPE (PL), composite electrolyte with LLZO nanoparticles fillers (PLLM), and composite electrolyte with LLZO nano-wire fillers (PLLN) [297]. Reproduced with permission [297], Copyright 2019, Wiley.

fabricate a Li-air battery with organic-based anolyte and aqueous-based catholyte with a separator of oxide-based SSE. H. Zhou et al. demonstrated this concept in Li-air battery by using 1M $LiClO_4$ in ethylene carbonate/dimethyl carbonate as anolyte and 1M KOH + 1M $LiNO_3$ alkaline solution as the catholyte and a NASICON based SSE as the ceramic separator. Stable charge/discharge voltage for 10 cycles is demonstrated (Fig. 13g–i) [313].

The liquid electrolyte and oxide-based SSE interfacial properties have been studied by J. Janek et al. [314]. Liquid electrolyte and LAGP interfacial properties were studied by impedance analysis and XPS. In the lithium battery with a liquid-oxide hybrid electrolyte, Li^+ ions need to cross 3 types of boundaries including electrode/liquid electrolyte boundary, liquid electrolyte/SSE boundary (R_{ls}), grain boundary within SSE (Fig. 14a). The study showed that the R_{ls} plays a determining role in the energy density loss of the lithium battery when the SSE thickness below 100 μm (Fig. 14b). The formation of liquid electrolyte/SSE interface undergoes 3 stages, wetting, formation, and stabilization. At the wetting stage, the magnitude of R_{ls} decreases because the liquid electrolyte fills the surface cavities of the SSE, which implies an increase in contact area and thus a reduction of the cell resistance. Subsequently, the liquid electrolyte/SSE interface was formed and stabilized. Notably, they found that the water contamination in the liquid electrolyte significantly influenced the value of R_{ls}. Higher water concentration in the liquid electrolyte led to a higher interfacial resistance (Fig. 14c). XPS studies revealed that the decomposition of lithium salt or SSE contributed to the formation of LAGP-liquid electrolyte interphase (Fig. 14d–k). Similar XPS results were reported in LATP-liquid electrolyte interface by our group [303].

In summary, liquid-oxide hybrid electrolytes can not only address the interface challenge in SSLBs with oxide-based SSEs, but also work as a barrier to prevent shuttles of unfavorable redox species between electrodes. Therefore, liquid-oxide hybrid electrolytes are highly desirable for Li-S and Li-air battery systems. However, the stability between oxide-based SSEs and liquid electrolytes should still be taken into consideration

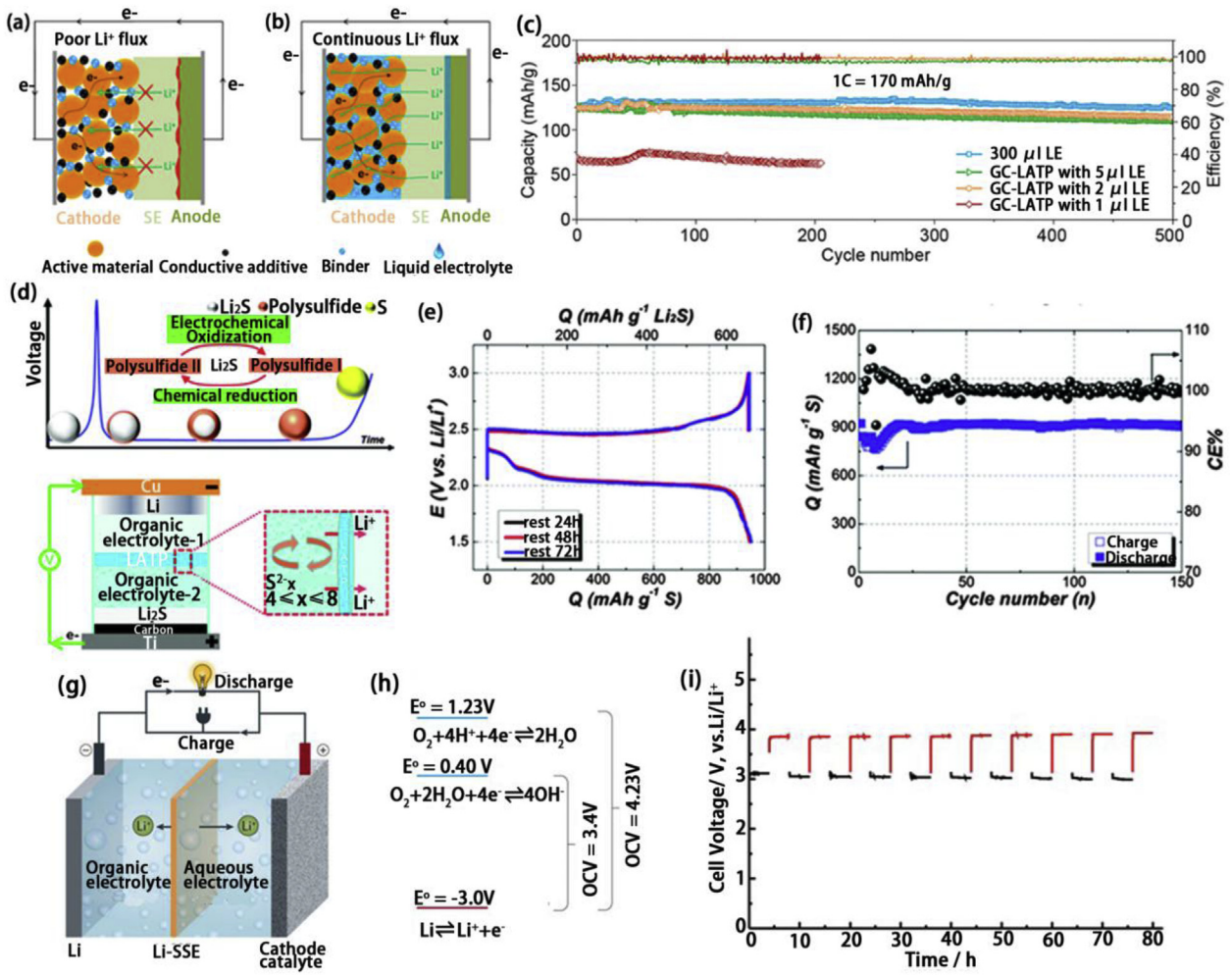

Fig. 13. (a) Configurations showing the poor contact between oxide-based SSE and cathode, anode electrodes. (b) After adding small amount of liquid electrolyte, the interface is well wetted, realizing a unformal Li^+ flux. (c) Comparison on the performance of the $LiFePO_4$ LIBs with different amounts of liquid-based electrolyte in the LATP/electrode [303]. Reproduced with permission [303], Copyright 2018, Elsevier. (d) Schematic illustration of the activation process of the Li_2S cathode over initial charge and the configuration of Li-S battery with liquid-LATP hybrid electrolyte; polysulfide shuttling effects are prevented by the LATP. Corresponding charge/-discharge profiles of Li-S battery after resting at different resting times are showed in (e). (f) The cycling performance of Li-S battery with liquid-LATP hybrid electrolyte [301]. Reproduced with permission [301], Copyright 2015, RSC. (g) Configuration of a Li-air battery with organic anolyte, aqueous catholyte, and an oxide-based SSE interlayer. (h) The anodic and cathodic reactions in Li-air battery with the liquid-oxide hybrid electrolyte, as well as the open-circuit voltages (OCVs) of the cell [74]. Reproduced with permission [74], Copyright 2017, Springer Nature. (i) The performance of a Li-air battery with the liquid-oxide hybrid electrolyte [313]. Reproduced with permission [313], Copyright 2010, Wiley.

during SSLBs designs.

3.3. SPE-oxide multilayer hybrid electrolytes

The existent of liquid electrolyte still poses potential of safety issues such leakage and fire. To totally avoid the usage of liquid electrolytes, flexible SPEs can be another solution to tailor the ceramic SSE/electrode interface. The general configuration of a SPE-oxide multilayer hybrid electrolyte is laminated as SPE/oxide or SPE/oxide/SPE sandwich structures (Fig. 15a) [73,315–319]. Considering the total cell resistance and volumetric energy density, the thickness of multilayer electrolyte should be as thin as possible.

J. B. Goodenough et al. have studied the electrochemical properties of SPE-oxide sandwich hybrid electrolytes. Fig. 15b and c propose the electric potential profiles across a sandwich hybrid electrolyte and a single SPE in a $LiFePO_4$ cell. Due to redistribution of charge carriers in different conductors (including anode, SPE, oxide-based SSE, and cathode), an electric double layer was created at the interface between two conductors, causing an electric field (i.e. potential difference) at the interface. In a single SPE cell, a strong electric field generated at the anode/SPE interface can reduce the lowest unoccupied molecular orbital energy of the SPE related to the Fermi energy of lithium, and thus facilitates the decomposition of the SPE [73]. In contrast, the overall electric field across the sandwich electrolyte is interrupted by the oxide-based SSE interlayer (Fig. 15b). The oxide-based SSE can block the passage of the salt anions and increased the Li^+ ion transference number, t_{Li^+}. Reduced electric field at the anode/SPE interface helps to stabilize the SPE. The intimate contact between lithium anode and SPE also provides an unformal Li^+ ion flux that mitigates lithium dendrite formation. As a result, all solid-state $LiFePO_4$ batteries with a SPE/LATP/SPE hybrid electrolyte showed significantly improved cycling performance compared to the single layer SPE-based $LiFePO_4$ batteries (Fig. 15d) [73].

Sandwich hybrid electrolytes can be also used for tackling the interface incompatibility between electrodes and SSEs by avoiding the directly contact. By placing a layer of plastic crystal electrolyte (PCE) between lithium metal anode and LGPS sulfide-based SSE, the capacity of $LiFePO_4$ battery is significantly enhanced (Fig. 15e and f). P K-edge and S K-edge X-ray absorption spectroscopy (XAS) results indicate that the reduction of phosphorus by lithium was happened in unprotected Li/LGPS interface while the reduction is prevented in PCE protected Li/

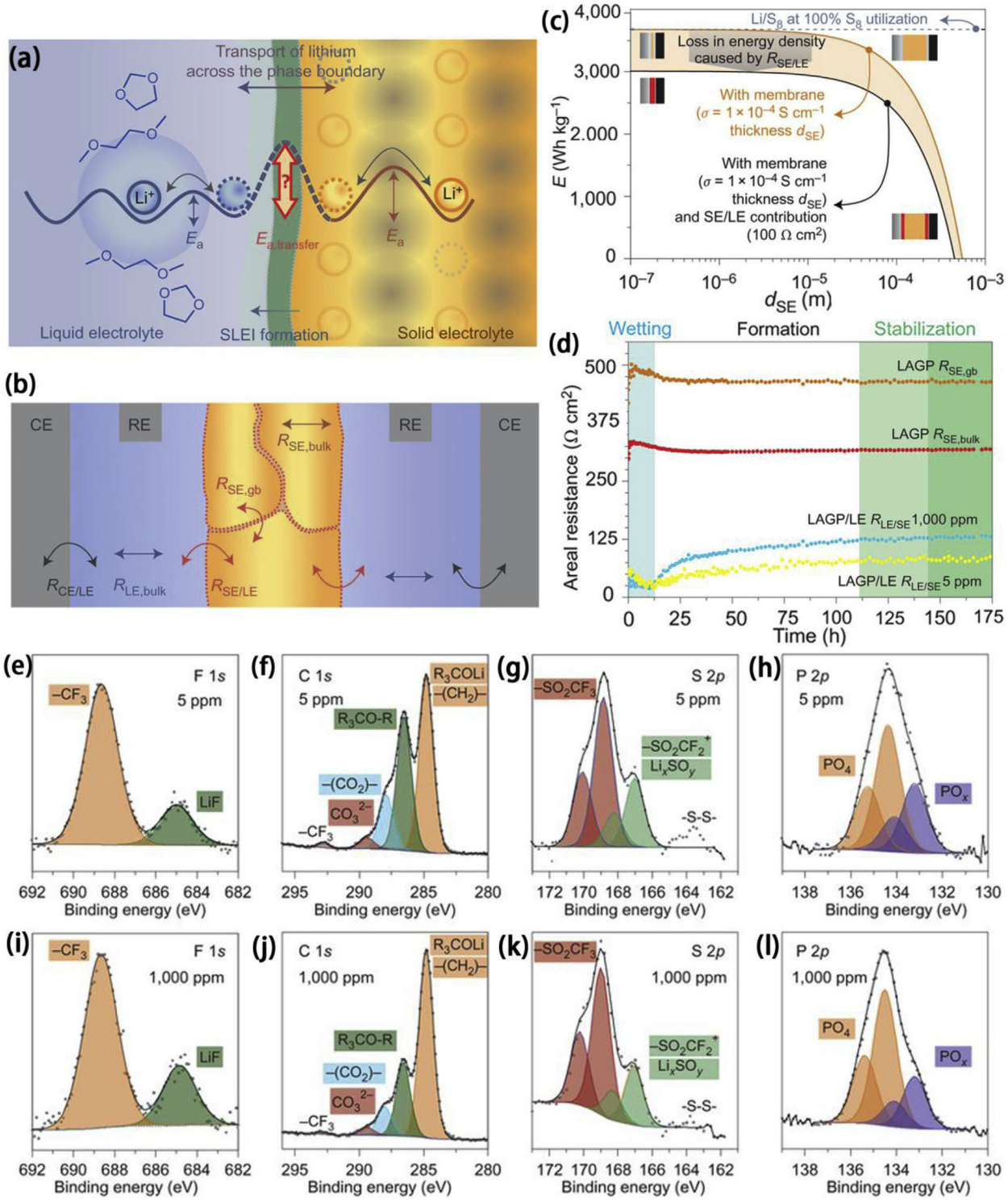

Fig. 14. (a), (b) Schematic diagram showing the interfaces within a lithium battery with liquid-oxide hybrid electrolyte. (c) Energy density loss of a lithium battery with liquid-oxide hybrid electrolyte due to the overpotentials from oxide-based SSE resistance and liquid/SSE interfacial resistance. (d) Evolutions of interfacial resistance in lithium battery with liquid-oxide hybrid electrolyte. (e–l) XPS studies of liquid/SSE interphase after time-dependent EIS experiments with water contents of 5 ppm (upper row) and of 1,000 ppm (lower row) [314]. Reproduced with permission [314], Copyright 2016, Springer Nature.

LGPS interface (Fig. 15g and h) [320].

Additionally, blocking ions or molecules by a ceramic SSE interlayer can tackle the crossover problem in various lithium battery systems. In solid-state Li-S battery with SPE, SPE have the ability to complex with lithium polysulfide so the polysulfide crossover problem still exist [82]. This problem is absent in the Li-S battery with SPE-oxide sandwich hybrid electrolyte due to the blocking effect of the oxide-based SSE interlayer. Sandwich hybrid electrolytes with a LATP or LAGP interlayer have been widely studied for preventing the polysulfide shuttling effects in ASSLSBs [317,318,321]. However, LATP is actually not stable towards polysulfide species. Our group applied the atomic layer deposition (ALD) technique to protect LATP SSE from being reduced by the polysulfide in

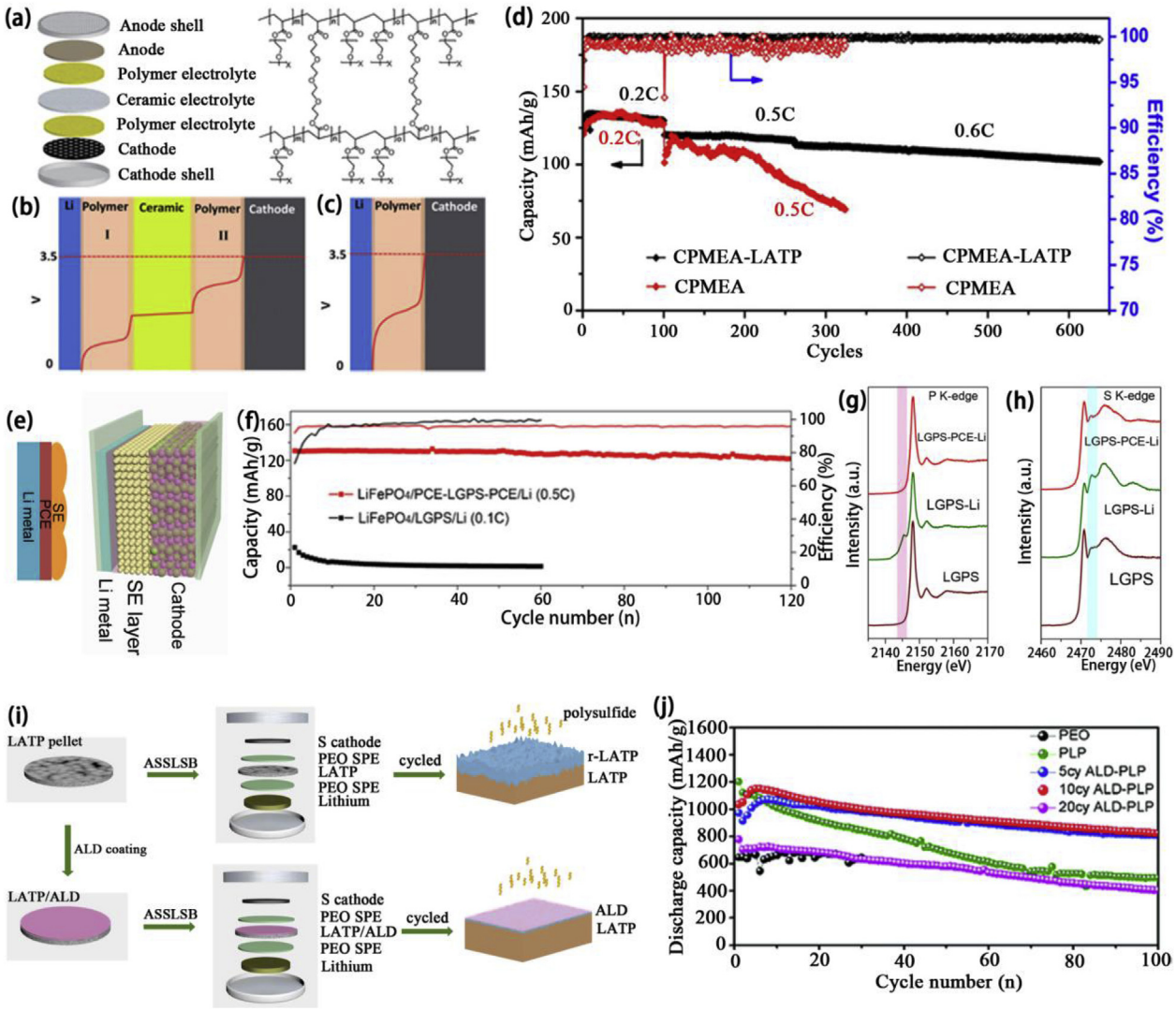

Fig. 15. (a) The configuration of a SSLB with a SPE-oxide sandwich hybrid electrolyte and the molecule structure of the SPE. Electric potential profile across (b) a SPE-oxide sandwich electrolyte and (c) a single SPE; (d) Comparison of the performances of the SSLBs with single layer SPE and SPE-oxide sandwich electrolyte at 0.2 C, 0.5 C and 0.6 C [73]. Reproduced with permission [73], Copyright 2016, ACS. (e) Configuration of a Li-LiFePO4 battery with LGPS SSE and plastic crystal electrolyte (PCE) in the Li/LGPS interface and its corresponding long cycling performance at 0.5 C (f). Comparison of P K-edge (g) S K-edge (h) of pristine LGPS (wine), LGPS after cycling (green) and LGPS with PCE protecting after cycling (red) [320]. Reproduced with permission [320], Copyright 2019, Wiley. (i) Configuration of ASSLSBs with SPE-oxide sandwich hybrid electrolyte with or without ALD protection; (j) Corresponding long cycling performance of ASSLSBs with different thicknesses of ALD protection [318]. Reproduced with permission [318], Copyright 2018, RSC. (For interpretation of the references to color in this figure legend, the reader is referred to the Web version of this article.)

the ASSLSBs with SPE-LATP sandwich hybrid electrolyte. Results showed that as thinner as 10 cycles of ALD Al_2O_3 coating can significantly enhance the performance of ASSLSBs because the reduction of LATP was inhibited (Fig. 15i and j) [318].

However, in SPE-oxide sandwich-type hybrid electrolyte system, although unfavorable interphase formation between SPEs and oxide-based SSEs have not yet been reported, the Li^+ ion transport still need to cross a SPE/oxide interface. Studies show that different types of oxide-based SSE showed different interfacial properties towards SPE. Takeshi Abe et al. first studied the PEO/LLTO interface and reported a significant larger resistance of the PEO/LLTO interface than that of the bulk LLTO or PEO-based SPE. The PEO/LLTO interfacial resistance was at the $10^3\ \Omega$ level, almost 10 times higher than that of bulk LLTO and 100 times higher than that of bulk PEO SPE [322]. However, in terms of a NASICON-type SSE, W. E. Tenhaeff et al. demonstrated a relatively small resistance between PEO-based SPE and NISICON-type glass ceramic electrolyte interface compared to the overall resistance of this multi-layer hybrid electrolyte. The resistance value was stable upon temperature variations [323]. Regarding the interface between a gel polymer electrolyte (GPE) and a garnet-type SSE, the results from L. Hu' group showed that the GPE/garnet interface resistance was $10^2\ \Omega/cm^2$, which was higher than that of garnet SSE bulk resistance and thus it cannot be negligible in SSLBs [316]. So far, there are a few reports about the chemistry at the SPE/oxide SSE interface. Nevertheless, the SPE/oxide SSE interfacial resistance is still too significant to be neglected in SSLBs.

In conclusion, many efforts have been dedicated to developing SSLBs with oxide-based SSEs, especially interfacial engineering for the SSE/electrode interface using a small amount of liquid electrolyte or SPE interfacial layers. Achievements are promising. However, the multilayer structured hybrid electrolytes still require Li^+ ion transport across different electrolyte phases that involve different Li^+ ion transport mechanisms and cause extra interface resistance. The interfacial resistance may pose drawbacks to the overall SSLB performance in terms of rate performance and energy density. Research efforts on interphase formation mechanism and reducing the thickness of the hybrid electrolytes are urgent in this field.

4. Conclusions and perspectives

SSEs are essential to the development of SSLBs, serving as both separator and ionic conductor. SPEs, oxide-based SSEs, and sulfide-based SSEs are typical categories of common SSEs for SSLBs, inheriting different pros and cons. SPEs usually have good flexibility and softness that enable low interfacial resistance towards electrodes, but the low ionic conductivity at RT and relatively narrow electrochemical stability window limit their practical applications. Oxide-based and sulfide-based SSEs exhibit relatively high ionic conductivities at RT compared to SPEs, but the rigid and brickle properties cause difficulties in maintaining sufficient contact with electrodes. Rational combinations of liquid electrolyte, SPE, and inorganic SSEs is a promising strategy to maximize the advantages and compensate the disadvantages of each constituent. Studies have shown that inorganic SSE fillers in SPEs can increase the ionic conductivity up to 10^{-4} S/cm at RT, which is higher than that of regular SPEs by several orders of magnitude. Additionally, the size, concentration, and shape of SSE fillers have great influences on the performance of hybrid electrolytes. Nano-size fillers and interconnected Li^+ ion conducting networks can significantly increase the ionic conductivity of hybrid electrolytes.

Studies on Li^+ ion conduction mechanism in hybrid electrolytes are important for hybrid electrolyte designs. IR and Raman spectroscopies are often used to study the effects of ceramic fillers in composite electrolytes by characterizing the evolution of salt anions. NMR is another powerful tool to track Li^+ ion pathways in SSEs. Using NMR, the higher ionic conductivity phase in hybrid electrolytes is identified as a preferential Li^+ ion conduction pathway over the lower ionic conductivity phase. However, Li^+ ion transportation across two electrolytes interface and electrolyte/electrode interface are remained unclear.

In addition to the bulk ionic conductivity, interfacial problems between SSEs and electrodes are not yet fully addressed by an individual SSE. Mismatch, instability, SCL, and lithium dendrite formation are common problems. Composite electrolytes are promising solutions for addressing mismatch in SSLBs. A soft electrolyte component can ensure good electrode wettability, while rigid SSE components can enhance the mechanical strength and electrochemical window. In liquid-oxide and SPE-oxide multilayer hybrid electrolytes, the liquid/SPE layers serve as flexible interfaces towards electrodes, enabling low interfacial resistance and dendrite-free lithium anodes; the inorganic SSE interlayer can block anions and redox matters from migrating across the electrolyte. However, one challenge for multilayer electrolytes is the extra interfacial resistance caused by extra electrolyte/electrolyte interfaces. More importantly, the introduction of SPEs often lowers the RT ionic conductivity of hybrid electrolytes, which limits the working temperature range of the SSLBs.

Although significant progresses have been achieved on hybrid electrolytes in SSLBs, there are still challenges to be overcome for the development of practical SSLBs. Deeper understandings on different SSEs in terms of ionic conduction mechanisms, origin of chemical and electrochemical instabilities, and possible interface modifications need to be obtained in the future. For practical SSLBs to be applied in EVs, the energy density and working temperature are the major concerns. Potential research efforts and solutions are proposed as follows:

(1) Understanding the Li^+ ion transport mechanisms in hybrid electrolytes and SSEs is important for the development of advanced SSEs. Advanced characterization techniques such as NMR, STXM (synchrotron scanning transmission X-ray microscopy) [324] and neutron diffraction [325] are powerful tools for the Li^+ ion transport mechanisms studies. In particularly, in-situ analyses on Li^+ ion transport across inorganic SSEs and SPE interface are vital for understanding the ionic conduction mechanisms in hybrid electrolytes, more studies are expected to be done in this field.

(2) In order to achieve high-energy-density for practical SSLBs, it is necessary to minimize the weight percentage of SSEs and maximize the active materials content. Theoretical calculations pointed out that the thickness of SPEs should be below 90 μm to achieve a comparable energy density to liquid-based lithium battery [326]. The inorganic SSEs, for example LLZO, need to be 4 times thinner for a comparable energy density due to their higher mass density [30]. Therefore, more research efforts should focus on advanced fabrication techniques such as sputtering [327], tape casting [328] and 3D printing [203,211] to prepared thin SSEs. Meanwhile, high active materials loading for high-energy-density could lead to poor electronic and ionic conduction problems, which are more serious in solid-state batteries. Novel electrode designs with high electronic and ionic conductivity are crucial for practical SSLBs.

(3) In order to boost the energy density of SSLBs for EVs applications, implementation of high-voltage and high-capacity cathodes are necessary. However, most of the SSEs such as PEO-based SPEs and sulfide-based SSEs are not stable at high voltage (e.g. $>$ 4.0 V). There is an urgent need for developing high-voltage stable SSEs for high-energy-density SSLBs. Composite electrolytes with an enhanced electrochemical stable window compared to bare SPEs can be a superior SSE candidate for high-energy-density SSLBs. On the other hand, engineering the SSE/active materials interface with an artificial solid electrolyte interphase can enhance the interfacial stability, which have been extensively studied in SPE and sulfide-based SSLBs [100–102,161,329]. However, the performance is still far away from practical applications. More investigations on interfacial engineering using advanced coating techniques are desired for further enhancing the performance of SSLBs. Atomic layer deposition (ALD) and molecule layer deposition (MLD), the powerful techniques for fabricating conformal coatings with controlled thickness, are perfect tools [318,330,331]. Another ultimate approach for high-voltage SSLBs is the pursuit of high voltage stable SSEs. PEO-based SPE and sulfide-based SSEs are reported to have low electrochemical oxidation window, while NASICON-type SSEs (LATP, LAGP) possess a high electrochemical oxidation voltage limit. Implementing NASICON-type SSEs or searching for other high voltage stable SSEs are an important direction for practical and high-energy-density SSLBs.

(4) Implementing sulfur cathodes is another approach for obtaining high-energy-density SSLBs, based on the high theoretical specific capacity of 1672 mAh/g for sulfur. However, there are still many challenges need to be overcome, including the incompatibility between sulfur cathode and SSEs, polysulfide shuttling effects, the volumetric expansion, and the poor ionic/electronic conductivities of sulfur and discharge products. Mechanism studies and the innovative sulfur cathode designs are urgent for developing high-performance solid-state Li-S batteries.

(5) The mechanical properties of the SSEs have great influence on the SSLB performance. To achieve a practical SSLB, a SSE with suitable mechanical properties to accommodate the volumetric expansion of active materials and maintain intimate SSE/active materials contact is critical. Up to date, tremendous research work were dedicated to understanding the basic mechanical properties of available SSEs. In the future, inspiring studies on controlling the mechanical properties of the SSEs or developing new SSEs with suitable mechanical properties should receive more attentions. Hybrid electrolytes with polymer-inorganic composite is a favorable strategy to tune the mechanical properties of SSEs. Hybrid electrolytes shall play an important role in practical SSLBs

(6) The working temperature range of SSEs is important for SSLBs. Although the thermal properties of SSEs are much better than conventional liquid electrolytes, most SSEs have not yet achieved practical performance for SSLBs at low temperature. The development of SSEs with a high ionic conductivity and a low activation

energy as well as designs of novel electrode structures for good electronic/ionic conductivities are highlighted directions.

(7) SSE/active materials interface is the most important topic in SSLBs. The understanding of the interfacial ion transport would be helpful for developing high-performance SSLBs. Advanced characterization techniques such as NMR, synchrotron radiation-based X-ray techniques (XAS, STXM, X-ray computed tomography), HR-TEM, Rutherford backscattering spectroscopy, etc., are very powerful tools for studying the interfacial engineering mechanism and interfacial ions transport. Especially, in-situ study at the interface shall give fundamental understandings and guidance for interfacial engineering designs [40,47,332–335].

Acknowledgments

This work is supported by China Automotive Battery Research Institute, Ontario Research Fund (ORF), Natural Sciences and Engineering Research Council of Canada, Canada Research Chair Program (CRC), and University of Western Ontario. Jianneng Liang is supported by China Scholarship Council for PhD study.

References

[1] T. Nagaura, K. Tozawa, Prog. Batt. Solar Cells 9 (1990) 209–217.
[2] A. Manthiram, B. Song, W. Li, Energy Storage Mater 6 (2017) 125–139.
[3] X. Li, J. Liu, M.N. Banis, A. Lushington, R. Li, M. Cai, X. Sun, Energy Environ. Sci. 7 (2014) 768–778.
[4] B. Xiao, B. Wang, J. Liu, K. Kaliyappan, Q. Sun, Y. Liu, G. Dadheech, M.P. Balogh, L. Yang, T.-K. Sham, R. Li, M. Cai, X. Sun, Nano Energy 34 (2017) 120–130.
[5] S. Hy, J.-H. Cheng, J.-Y. Liu, C.-J. Pan, J. Rick, J.-F. Lee, J.-M. Chen, B.J. Hwang, Chem. Mater. 26 (2014) 6919–6927.
[6] C. Chen, J. Liu, M. Stoll, G. Henriksen, D. Vissers, K. Amine, J. Power Sources 128 (2004) 278–285.
[7] M. Jo, M. Noh, P. Oh, Y. Kim, J. Cho, Adv. Energy Mater. 4 (2014) 1301583.
[8] X. Ji, K.T. Lee, L.F. Nazar, Nat. Mater. 8 (2009) 500–506.
[9] X. Li, A. Lushington, Q. Sun, W. Xiao, J. Liu, B. Wang, Y. Ye, K. Nie, Y. Hu, Q. Xiao, R. Li, J. Guo, T.-K. Sham, X. Sun, Nano Lett. 16 (2016) 3545–3549.
[10] C. Zhao, J. Liang, Q. Sun, J. Luo, Y. Liu, X. Lin, Y. Zhao, H. Yadegari, M.N. Banis, R. Li, H. Huang, L. Zhang, R. Yang, S. Lu, X. Sun, Small Methods 3 (2019) 1800437.
[11] H.-G. Jung, J. Hassoun, J.-B. Park, Y.-K. Sun, B. Scrosati, Nat. Chem. 4 (2012) 579–585.
[12] X. Li, M.N. Banis, A. Lushington, X. Yang, Q. Sun, Y. Zhao, C. Liu, Q. Li, B. Wang, W. Xiao, C. Wang, M. Li, J. Liang, R. Li, Y. Hu, L. Goncharova, H. Zhang, T.-K. Sham, X. Sun, Nat. Commun. 9 (2018) 4509.
[13] S. Hess, M. Wohlfahrt-Mehrens, M. Wachtler, J. Electrochem. Soc. 162 (2015) A3084–A3097.
[14] Q. Li, J. Chen, L. Fan, X. Kong, Y. Lu, Green Energy Environ 1 (2016) 18–42.
[15] D. Di Lecce, L. Carbone, V. Gancitano, J. Hassoun, J. Power Sources 334 (2016) 146–153.
[16] Q. Wang, L. Jiang, Y. Yu, J. Sun, Nano Energy 55 (2019) 93–114.
[17] Y. Sun, Y. Zhao, J. Wang, J. Liang, C. Wang, Q. Sun, X. Lin, K.R. Adair, J. Luo, D. Wang, R. Li, C. Mai, T.-K. Sham, X. Sun, Adv. Mater. 31 (2018) 1806541.
[18] Y. Zhao, X. Yang, L.Y. Kuo, P. Kaghazchi, Q. Sun, J. Liang, B. Wang, A. Lushington, R. Li, H. Zhang, X. Sun, Small 14 (2018) 1703717.
[19] J. Liang, X. Li, Y. Zhao, L.V. Goncharova, G. Wang, K.R. Adair, C. Wang, R. Li, Y. Zhu, Y. Qian, L. Zhang, R. Yang, S. Lu, X. Sun, Adv. Mater. 30 (2018) 1804684.
[20] X. Tang, D. Zhou, P. Li, X. Guo, C. Wang, F. Kang, B. Li, G. Wang, ACS Cent. Sci. 5 (2019) 365–373.
[21] D. Zhou, A. Tkacheva, X. Tang, B. Sun, D. Shanmukaraj, P. Li, F. Zhang, M. Armand, G. Wang, Angew. Chem. Int. Ed. 58 (2019) 6001–6006.
[22] H. Morimoto, H. Awano, J. Terashima, Y. Shindo, S. Nakanishi, N. Ito, K. Ishikawa, S.-i. Tobishima, J. Power Sources 240 (2013) 636–643.
[23] D. Safanama, N. Sharma, R.P. Rao, H.E. Brand, S. Adams, J. Mater. Chem. A 4 (2016) 7718–7726.
[24] R. Murugan, V. Thangadurai, W. Weppner, Angew. Chem. Int. Ed. 46 (2007) 7778–7781.
[25] W.J. Kwon, H. Kim, K.-N. Jung, W. Cho, S.H. Kim, J.-W. Lee, M.-S. Park, J. Mater. Chem. A 5 (2017) 6257–6262.
[26] J. Haruyama, K. Sodeyama, L. Han, K. Takada, Y. Tateyama, Chem. Mater. 26 (2014) 4248–4255.
[27] X. Tao, Y. Liu, W. Liu, G. Zhou, J. Zhao, D. Lin, C. Zu, O. Sheng, W. Zhang, H.-W. Lee, Y. Cui, Nano Lett. 17 (2017) 2967–2972.
[28] K.K. Fu, Y. Gong, J. Dai, A. Gong, X. Han, Y. Yao, C. Wang, Y. Wang, Y. Chen, C. Yan, Y. Li, E.D. Wachsman, L. Hu, Proc. Natl. Acad. Sci. U.S.A. 113 (2016) 7094–7099.
[29] K.J. Harry, D.T. Hallinan, D.Y. Parkinson, A.A. MacDowell, N.P. Balsara, Nat. Mater. 13 (2014) 69–73.
[30] M. Keller, A. Varzi, S. Passerini, J. Power Sources 392 (2018) 206–225.
[31] X. Liu, X. Li, H. Li, H.B. Wu, Chem. Eur J. 24 (2018) 18293–18306.
[32] L.Z. Long, S.J. Wang, M. Xiao, Y.Z. Meng, J. Mater. Chem. A 4 (2016) 10038–10069.
[33] S. Chen, D. Xie, G. Liu, J.P. Mwizerwa, Q. Zhang, Y. Zhao, X. Xu, X. Yao, Energy Storage Mater 14 (2018) 58–74.
[34] Z. Gao, H. Sun, L. Fu, F. Ye, Y. Zhang, W. Luo, Y. Huang, Adv. Mater. 30 (2018) 1705702.
[35] K. Kerman, A. Luntz, V. Viswanathan, Y.-M. Chiang, Z. Chen, J. Electrochem. Soc. 164 (2017) A1731–A1744.
[36] R. Chen, W. Qu, X. Guo, L. Li, F. Wu, Mater. Horiz. 3 (2016) 487–516.
[37] Z. Zhang, Y. Shao, B.V. Lotsch, Y.-S. Hu, H. Li, J. Janek, C. Nan, L. Nazar, J. Maier, M. Armand, L. Chen, Energy Environ. Sci. 11 (2018) 1945–1976.
[38] Y.-Z. Sun, J.-Q. Huang, C.-Z. Zhao, Q. Zhang, Sci. China Chem. 60 (2017) 1508–1526.
[39] Ö.U. Kudu, T. Famprikis, B. Fleutot, M.-D. Braida, T. Le Mercier, M.S. Islam, C. Masquelier, J. Power Sources 407 (2018) 31–43.
[40] X. Liu, L. Gu, Small Methods 2 (2018) 1800006.
[41] L. Yue, J. Ma, J. Zhang, J. Zhao, S. Dong, Z. Liu, G. Cui, L. Chen, Energy Storage Mater 5 (2016) 139–164.
[42] A. Varzi, R. Raccichini, S. Passerini, B. Scrosati, J. Mater. Chem. A 4 (2016) 17251–17259.
[43] A.M. Nolan, Y. Zhu, X. He, Q. Bai, Y. Mo, Joule 2 (2018) 2016–2046.
[44] X. Yu, A. Manthiram, Acc. Chem. Res. 50 (2017) 2653–2660.
[45] J.C. Bachman, S. Muy, A. Grimaud, H.-H. Chang, N. Pour, S.F. Lux, O. Paschos, F. Maglia, S. Lupart, P. Lamp, L. Giordano, Y. Shao-Horn, Chem. Rev. 116 (2016) 140–162.
[46] J. Dai, C. Yang, C. Wang, G. Pastel, L. Hu, Adv. Mater. 30 (2018) 1802068.
[47] L. Xu, S. Tang, Y. Cheng, K. Wang, J. Liang, C. Liu, Y.-C. Cao, F. Wei, L. Mai, Joule 2 (2018) 1991–2015.
[48] R. Xu, X. Xia, S. Zhang, D. Xie, X. Wang, J. Tu, Electrochim. Acta 284 (2018) 177–187.
[49] J. Gao, Y.-S. Zhao, S.-Q. Shi, H. Li, Chin. Phys. B 25 (2016) 018211.
[50] B. Zhang, R. Tan, L. Yang, J. Zheng, K. Zhang, S. Mo, Z. Lin, F. Pan, Energy Storage Mater 10 (2018) 139–159.
[51] G. Ceder, S.P. Ong, Y. Wang, MRS Bull. 43 (2018) 746–751.
[52] Z. Ma, H.-G. Xue, S.-P. Guo, J. Mater. Sci. 53 (2018) 3927–3938.
[53] S.-J. Tan, X.-X. Zeng, Q. Ma, X.-W. Wu, Y.-G. Guo, Electrochem. Energy Rev. 1 (2018) 113–138.
[54] C. Sun, J. Liu, Y. Gong, D.P. Wilkinson, J. Zhang, Nano Energy 33 (2017) 363–386.
[55] X.-B. Cheng, C.-Z. Zhao, Y.-X. Yao, H. Liu, Q. Zhang, Chem 5 (2019) 74–96.
[56] M. Shoji, E.J. Cheng, T. Kimura, K. Kanamura, J. Phys. D Appl. Phys. 52 (2019) 103001.
[57] L. Fan, S. Wei, S. Li, Q. Li, Y. Lu, Adv. Energy Mater. 8 (2018) 1702657.
[58] F. Zheng, M. Kotobuki, S. Song, M.O. Lai, L. Lu, J. Power Sources 389 (2018) 198–213.
[59] J.B. Goodenough, P. Singh, J. Electrochem. Soc. 162 (2015) A2387–A2392.
[60] H. Zhang, C. Li, M. Piszcz, E. Coya, T. Rojo, L.M. Rodriguez-Martinez, M. Armand, Z. Zhou, Chem. Soc. Rev. 46 (2017) 797–815.
[61] J. Yi, S. Guo, P. He, H. Zhou, Energy Environ. Sci. 10 (2017) 860–884.
[62] J. Lau, R.H. DeBlock, D.M. Butts, D.S. Ashby, C.S. Choi, B.S. Dunn, Adv. Energy Mater. 8 (2018) 1800933.
[63] Y. Shen, Y. Zhang, S. Han, J. Wang, Z. Peng, L. Chen, Joule 2 (2018) 1674–1689.
[64] K. Liu, Y. Liu, D. Lin, A. Pei, Y. Cui, Sci. Adv. 4 (2018) eaas9820.
[65] K.K. Fu, Y. Gong, B. Liu, Y. Zhu, S. Xu, Y. Yao, W. Luo, C. Wang, S.D. Lacey, J. Dai, Sci. Adv. 3 (2017) e1601659.
[66] Y. Zhang, F. Chen, D. Yang, W. Zha, J. Li, Q. Shen, X. Zhang, L. Zhang, J. Electrochem. Soc. 164 (2017) A1695–A1702.
[67] F. Han, Y. Zhu, X. He, Y. Mo, C. Wang, Adv. Energy Mater. 6 (2016) 1501590.
[68] A. Hayashi, A. Sakuda, M. Tatsumisago, Front. Energy Res. 4 (2016) 25.
[69] Y. Xia, T. Fujieda, K. Tatsumi, P.P. Prosini, T. Sakai, J. Power Sources 92 (2001) 234–243.
[70] Y. Zhu, X. He, Y. Mo, ACS Appl. Mater. Interfaces 7 (2015) 23685–23693. https://pubs.acs.org/doi/10.1021/acsami.5b07517.
[71] L. Chen, Y. Li, S.-P. Li, L.-Z. Fan, C.-W. Nan, J.B. Goodenough, Nano Energy 46 (2018) 176–184.
[72] Z. Zhang, Y. Zhao, S. Chen, D. Xie, X. Yao, P. Cui, X. Xu, J. Mater. Chem. A 5 (2017) 16984–16993.
[73] W. Zhou, S. Wang, Y. Li, S. Xin, A. Manthiram, J.B. Goodenough, J. Am. Chem. Soc. 138 (2016) 9385–9388.
[74] A. Manthiram, X. Yu, S. Wang, Nat. Rev. Mater. 2 (2017) 16103.
[75] D. Fenton, J. Parker, P. Wright, Polymer 14 (1973) 589.
[76] F. Croce, G. Appetecchi, L. Persi, B. Scrosati, Nature 394 (1998) 456–458.
[77] G.S. MacGlashan, Y.G. Andreev, P.G. Bruce, Nature 398 (1999) 792–794.
[78] Z. Gadjourova, Y.G. Andreev, D.P. Tunstall, P.G. Bruce, Nature 412 (2001) 520–523.
[79] K. Zaghib, K. Kinoshita, J. Power Sources 125 (2004) 214–220.
[80] K. Zaghib, Y. Choquette, A. Guerfi, M. Simoneau, A. Belanger, M. Gauthier, J. Power Sources 68 (1997) 368–371.
[81] K. Zaghib, M. Simoneau, M. Armand, M. Gauthier, J. Power Sources 81 (1999) 300–305.
[82] H. Marceau, C.-S. Kim, A. Paolella, S. Ladouceur, M. Lagacé, M. Chaker, A. Vijh, A. Guerfi, C.M. Julien, A. Mauger, M. Armand, P. Hovington, K. Zaghib, J. Power Sources 319 (2016) 247–254.

[83] J.-C. Daigle, A. Vijh, P. Hovington, C. Gagnon, J. Hamel-Pâquet, S. Verreault, N. Turcotte, D. Clément, A. Guerfi, K. Zaghib, J. Power Sources 279 (2015) 372–383.
[84] P. Hovington, M. Lagacé, A. Guerfi, P. Bouchard, A. Mauger, C. Julien, M. Armand, K. Zaghib, Nano Lett. 15 (2015) 2671–2678.
[85] Y. Chen, Y. Chuang, J. Su, H. Yu, Y. Chen-Yang, J. Power Sources 196 (2011) 2802–2809.
[86] C. Yang, H. Ywi Chen, F. Lin, C. Chen, Solid State Ionics 150 (2002) 327–335.
[87] H. Choe, B. Carroll, D. Pasquariello, K. Abraham, Chem. Mater. 9 (1997) 369–379.
[88] H.-W. Chen, T.-P. Lin, F.-C. Chang, Polymer 43 (2002) 5281–5288.
[89] S. Ahmad, T. Saxena, S. Ahmad, S. Agnihotry, J. Power Sources 159 (2006) 205–209.
[90] D. Saikia, A. Kumar, Electrochim. Acta 49 (2004) 2581–2589.
[91] R. Miao, B. Liu, Z. Zhu, Y. Liu, J. Li, X. Wang, Q. Li, J. Power Sources 184 (2008) 420–426.
[92] D. Zhou, R. Zhou, C. Chen, W.-A. Yee, J. Kong, G. Ding, X. Lu, J. Phys. Chem. B 117 (2013) 7783–7789.
[93] J. Zhang, X. Zang, H. Wen, T. Dong, J. Chai, Y. Li, B. Chen, J. Zhao, S. Dong, J. Ma, J. Mater. Chem. A 5 (2017) 4940–4948.
[94] L. Meabe, T.V. Huynh, N. Lago, H. Sardon, C. Li, L.A. O'Dell, M. Armand, M. Forsyth, D. Mecerreyes, Electrochim. Acta 264 (2018) 367–375.
[95] N.S. Schauser, K.J. Harry, D.Y. Parkinson, H. Watanabe, N.P. Balsara, J. Electrochem. Soc. 162 (2015) A398–A405.
[96] P. Barai, K. Higa, V. Srinivasan, Phys. Chem. Chem. Phys. 19 (2017) 20493–20505.
[97] R. Khurana, J.L. Schaefer, L.A. Archer, G.W. Coates, J. Am. Chem. Soc. 136 (2014) 7395–7402.
[98] A. Mauger, M. Armand, C. Julien, K. Zaghib, J. Power Sources 353 (2017) 333–342.
[99] C. Monroe, J. Newman, J. Electrochem. Soc. 152 (2005) A396–A404.
[100] H. Miyashiro, Y. Kobayashi, S. Seki, Y. Mita, A. Usami, M. Nakayama, M. Wakihara, Chem. Mater. 17 (2005) 5603–5605.
[101] J. Ma, Z. Liu, B. Chen, L. Wang, L. Yue, H. Liu, J. Zhang, Z. Liu, G. Cui, J. Electrochem. Soc. 164 (2017) A3454–A3461.
[102] S. Seki, Y. Kobayashi, H. Miyashiro, Y. Mita, T. Iwahori, Chem. Mater. 17 (2005) 2041–2045.
[103] Z. Gadjourova, Y.G. Andreev, D.P. Tunstall, P.G. Bruce, Nature 412 (2001) 520.
[104] Y. Tominaga, K. Yamazaki, Chem. Commun. 50 (2014) 4448–4450.
[105] C.R. Mariappan, C. Yada, F. Rosciano, B. Roling, J. Power Sources 196 (2011) 6456–6464.
[106] B. Kumar, D. Thomas, J. Kumar, J. Electrochem. Soc. 156 (2009) A506–A513.
[107] V. Thangadurai, S. Narayanan, D. Pinzaru, Chem. Soc. Rev. 43 (2014) 4714–4727.
[108] M.P. O'Callaghan, D.R. Lynham, E.J. Cussen, G.Z. Chen, Chem. Mater. 18 (2006) 4681–4689.
[109] V. Thangadurai, H. Kaack, W.J. Weppner, J. Am. Ceram. Soc. 86 (2003) 437–440.
[110] V. Thangadurai, W. Weppner, J. Am. Ceram. Soc. 88 (2005) 411–418.
[111] D. Rettenwander, G.n. Redhammer, F. Preishuber-Pflügl, L. Cheng, L. Miara, R. Wagner, A. Welzl, E. Suard, M.M. Doeff, M. Wilkening, J. Fleig, G. Amthauer, Chem. Mater. 28 (2016) 2384–2392.
[112] R. Jalem, M. Rushton, W. Manalastas Jr., M. Nakayama, T. Kasuga, J.A. Kilner, R.W. Grimes, Chem. Mater. 27 (2015) 2821–2831.
[113] D. Wang, G. Zhong, W.K. Pang, Z. Guo, Y. Li, M.J. McDonald, R. Fu, J.-X. Mi, Y. Yang, Chem. Mater. 27 (2015) 6650–6659.
[114] L. Truong, V. Thangadurai, Chem. Mater. 23 (2011) 3970–3977.
[115] Y. Ren, Y. Shen, Y. Lin, C.-W. Nan, Electrochem. Commun. 57 (2015) 27–30.
[116] L. Porz, T. Swamy, B.W. Sheldon, D. Rettenwander, T. Frömling, H.L. Thaman, S. Berendts, R. Uecker, W.C. Carter, Y.M. Chiang, Adv. Energy Mater. 7 (2017) 1701003.
[117] T. Takahashi, H. Iwahara, Energy Convers. 11 (1971) 105–111.
[118] Y. Inaguma, C. Liquan, M. Itoh, T. Nakamura, T. Uchida, H. Ikuta, M. Wakihara, Solid State Commun. 86 (1993) 689–693.
[119] S.D. Jackman, R.A. Cutler, J. Power Sources 218 (2012) 65–72.
[120] S. Yu, R.D. Schmidt, R. Garcia-Mendez, E. Herbert, N.J. Dudney, J.B. Wolfenstine, J. Sakamoto, D.J. Siegel, Chem. Mater. 28 (2016) 197–206.
[121] K.G. Schell, F. Lemke, E.C. Bucharsky, A. Hintennach, M. Hoffmann, J. Mater. Sci. 52 (2017) 2232–2240.
[122] W. Luo, Y. Gong, Y. Zhu, Y. Li, Y. Yao, Y. Zhang, K.K. Fu, G. Pastel, C.F. Lin, Y. Mo, E.D. Wachsman, L. Hu, Adv. Mater. 29 (2017) 1606042.
[123] X. Han, Y. Gong, K.K. Fu, X. He, G.T. Hitz, J. Dai, A. Pearse, B. Liu, H. Wang, G. Rubloff, Y. Mo, V. Thangadurai, E.D. Wachsman, L. Hu, Nat. Mater. 16 (2017) 572–579.
[124] C. Wang, Y. Gong, B. Liu, K. Fu, Y. Yao, E. Hitz, Y. Li, J. Dai, S. Xu, W. Luo, E.D. Wachsman, L. Hu, Nano Lett. 17 (2016) 565–571.
[125] S. Ohta, S. Komagata, J. Seki, T. Saeki, S. Morishita, T. Asaoka, J. Power Sources 238 (2013) 53–56.
[126] F. Han, J. Yue, C. Chen, N. Zhao, X. Fan, Z. Ma, T. Gao, F. Wang, X. Guo, C. Wang, Joule 2 (2018) 497–508.
[127] J. Van Den Broek, S. Afyon, J.L. Rupp, Adv. Energy Mater. 6 (2016) 1600736.
[128] S. Ohta, J. Seki, Y. Yagi, Y. Kihira, T. Tani, T. Asaoka, J. Power Sources 265 (2014) 40–44.
[129] K. Park, B.-C. Yu, J.-W. Jung, Y. Li, W. Zhou, H. Gao, S. Son, J.B. Goodenough, Chem. Mater. 28 (2016) 8051–8059.
[130] M. Shoji, H. Munakata, K. Kanamura, Front. Energy Res. 4 (2016) 32.
[131] K.K. Fu, Y. Gong, G.T. Hitz, D.W. McOwen, Y. Li, S. Xu, Y. Wen, L. Zhang, C. Wang, G. Pastel, J. Dai, B. Liu, H. Xie, Y. Yao, E.D. Wachsman, L. Hu, Energy Environ. Sci. 10 (2017) 1568–1575.
[132] R. Koerver, W. Zhang, L. de Biasi, S. Schweidler, A. Kondrakov, S. Kolling, T. Brezesinski, P. Hartmann, W. Zeier, J. Janek, Energy Environ. Sci. 11 (2018) 2142–2158.
[133] H. Huo, J. Sun, X. Meng, M. He, N. Zhao, X. Guo, J. Power Sources 383 (2018) 150–156.
[134] X. Yao, N. Huang, F. Han, Q. Zhang, H. Wan, J.P. Mwizerwa, C. Wang, X. Xu, Adv. Energy Mater. 7 (2017) 1602923.
[135] K.H. Kim, Y. Iriyama, K. Yamamoto, S. Kumazaki, T. Asaka, K. Tanabe, C.A. Fisher, T. Hirayama, R. Murugan, Z. Ogumi, J. Power Sources 196 (2011) 764–767.
[136] F. Han, A.S. Westover, J. Yue, X. Fan, F. Wang, M. Chi, D.N. Leonard, N.J. Dudney, H. Wang, C. Wang, Nat. Energy 4 (2019) 187–196.
[137] Y. Song, L. Yang, W. Zhao, Z. Wang, Y. Zhao, Z. Wang, Q. Zhao, H. Liu, F. Pan, Adv. Energy Mater. 12 (2019) 1900671.
[138] Y. Liu, Q. Sun, Y. Zhao, B. Wang, P. Kaghazchi, K.R. Adair, R. Li, C. Zhang, J. Liu, L.-Y. Kuo, Y. Hu, T.-K. Sham, L. Zhang, R. Yang, S. Lu, X. Song, X. Sun, ACS Appl. Mater. Interfaces 10 (2018) 31240–31248.
[139] Y. Liu, P. He, H. Zhou, Adv. Energy Mater. 8 (2018) 1701602.
[140] N.M. Asl, J. Keith, C. Lim, L. Zhu, Y. Kim, Electrochim. Acta 79 (2012) 8–16.
[141] A. Hayashi, S. Hama, H. Morimoto, M. Tatsumisago, T. Minami, J. Am. Ceram. Soc. 84 (2001) 477–479.
[142] S. Kondo, K. Takada, Y. Yamamura, Solid State Ionics 53 (1992) 1183–1186.
[143] M. Tachez, J.-P. Malugani, R. Mercier, G. Robert, Solid State Ionics 14 (1984) 181–185.
[144] R. Kanno, T. Hata, Y. Kawamoto, M. Irie, Solid State Ionics 130 (2000) 97–104.
[145] R. Kanno, M. Murayama, J. Electrochem. Soc. 148 (2001) A742–A746.
[146] N. Kamaya, K. Homma, Y. Yamakawa, M. Hirayama, R. Kanno, M. Yonemura, T. Kamiyama, Y. Kato, S. Hama, K. Kawamoto, A. Mitsui, Nat. Mater. 10 (2011) 682–686.
[147] M. Murayama, N. Sonoyama, A. Yamada, R. Kanno, Solid State Ionics 170 (2004) 173–180.
[148] X. Yao, D. Liu, C. Wang, P. Long, G. Peng, Y.-S. Hu, H. Li, L. Chen, X. Xu, Nano Lett. 16 (2016) 7148–7154.
[149] Y. Kato, S. Hori, T. Saito, K. Suzuki, M. Hirayama, A. Mitsui, M. Yonemura, H. Iba, R. Kanno, Nat. Energy 1 (2016) 16030.
[150] A. Kuhn, O. Gerbig, C. Zhu, F. Falkenberg, J. Maier, B.V. Lotsch, Phys. Chem. Chem. Phys. 16 (2014) 14669–14674.
[151] C. Wang, Y. Zhao, Q. Sun, X. Li, Y. Liu, J. Liang, X. Li, X. Lin, R. Li, K.R. Adair, L. Zhang, R. Yang, S. Lu, X. Sun, Nano Energy 53 (2018) 168–174.
[152] W.D. Richards, L.J. Miara, Y. Wang, J.C. Kim, G. Ceder, Chem. Mater. 28 (2015) 266–273.
[153] S. Wenzel, S. Randau, T. Leichtweiß, D.A. Weber, J. Sann, W.G. Zeier, J.r. Janek, Chem. Mater. 28 (2016) 2400–2407.
[154] Y. Zhu, X. He, Y. Mo, J. Mater. Chem. A 4 (2016) 3253–3266.
[155] F. Han, T. Gao, Y. Zhu, K.J. Gaskell, C. Wang, Adv. Mater. 27 (2015) 3473–3483.
[156] M. Nagao, A. Hayashi, M. Tatsumisago, Electrochemistry 80 (2012) 734–736.
[157] Z. Zhang, S. Chen, J. Yang, J. Wang, L. Yao, X. Yao, P. Cui, X. Xu, ACS Appl. Mater. Interfaces 10 (2018) 2556–2565.
[158] R. Xu, F. Han, X. Ji, X. Fan, J. Tu, C. Wang, Nano Energy 53 (2018) 958–966.
[159] F. Han, J. Yue, X. Zhu, C. Wang, Adv. Energy Mater. 8 (2018) 1703644.
[160] A. Sakuda, A. Hayashi, M. Tatsumisago, Chem. Mater. 22 (2009) 949–956.
[161] J.H. Woo, J.E. Trevey, A.S. Cavanagh, Y.S. Choi, S.C. Kim, S.M. George, K.H. Oh, S.-H. Lee, J. Electrochem. Soc. 159 (2012) A1120–A1124.
[162] N. Ohta, K. Takada, L. Zhang, R. Ma, M. Osada, T. Sasaki, Adv. Mater. 18 (2006) 2226–2229.
[163] R. Koerver, I. Aygün, T. Leichtweiß, C. Dietrich, W. Zhang, J.O. Binder, P. Hartmann, W.G. Zeier, J.r. Janek, Chem. Mater. 29 (2017) 5574–5582.
[164] Z. Deng, Z. Wang, I.-H. Chu, J. Luo, S.P. Ong, J. Electrochem. Soc. 163 (2016) A67–A74.
[165] A. Kato, M. Nose, M. Yamamoto, A. Sakuda, A. Hayashi, M. Tatsumisago, J. Ceram. Soc. Jpn. 126 (2018) 719–727.
[166] G. Bucci, T. Swamy, Y.-M. Chiang, W.C. Carter, J. Mater. Chem. A 5 (2017) 19422–19430.
[167] G. Bucci, B. Talamini, A.R. Balakrishna, Y.-M. Chiang, W.C. Carter, Phys. Rev. Mater. 2 (2018) 105407.
[168] A. Sakuda, A. Hayashi, M. Tatsumisago, Sci. Rep. 3 (2013) 2261.
[169] T. Swamy, R. Park, B.W. Sheldon, D. Rettenwander, L. Porz, S. Berendts, R. Uecker, W.C. Carter, Y.-M. Chiang, J. Electrochem. Soc. 165 (2018) A3648–A3655.
[170] A. Kato, M. Yamamoto, A. Sakuda, A. Hayashi, M. Tatsumisago, ACS Appl. Energy Mater. 1 (2018) 1002–1007.
[171] J.E. Ni, E.D. Case, J.S. Sakamoto, E. Rangasamy, J.B. Wolfenstine, J. Mater. Sci. 47 (2012) 7978–7985.
[172] Y. Kim, H. Jo, J.L. Allen, H. Choe, J. Wolfenstine, J. Sakamoto, J. Am. Ceram. Soc. 99 (2016) 1367–1374.
[173] J. Wolfenstine, H. Jo, Y.-H. Cho, I.N. David, P. Askeland, E.D. Case, H. Kim, H. Choe, J. Sakamoto, Mater. Lett. 96 (2013) 117–120.
[174] Y.-H. Cho, J. Wolfenstine, E. Rangasamy, H. Kim, H. Choe, J. Sakamoto, J. Mater. Sci. 47 (2012) 5970–5977.
[175] C. Cooper, A.C. Sutorik, J. Wright, E.A. Luoto III, G. Gilde, J. Wolfenstine, Adv. Eng. Mater. 16 (2014) 755–759.
[176] A. Sakuda, A. Hayashi, Y. Takigawa, K. Higashi, M. Tatsumisago, J. Ceram. Soc. Jpn. 121 (2013) 946–949.
[177] F.P. McGrogan, T. Swamy, S.R. Bishop, E. Eggleton, L. Porz, X. Chen, Y.-M. Chiang, K.J. Van Vliet, Adv. Energy Mater. 7 (2017) 1602011.
[178] Z. Wang, M. Wu, G. Liu, X. Lei, B. Xu, C. Ouyang, Int. J. Electrochem. Sci 9 (2014) 562–568.

[179] E.G. Herbert, W.E. Tenhaeff, N.J. Dudney, G.M. Pharr, Thin Solid Films 520 (2011) 413–418.
[180] J. Ji, B. Li, W.-H. Zhong, J. Phys. Chem. B 114 (2010) 13637–13643.
[181] C. Wang, Y. Yang, X. Liu, H. Zhong, H. Xu, Z. Xu, H. Shao, F. Ding, ACS Appl. Mater. Interfaces 9 (2017) 13694–13702.
[182] J. Xie, R.G. Duan, Y. Han, J.B. Kerr, Solid State Ionics 175 (2004) 755–758.
[183] S. Ramesh, T. Winie, A.K. Arof, J. Mater. Sci. 45 (2010) 1280–1283.
[184] P. Raghavan, X. Zhao, J.-K. Kim, J. Manuel, G.S. Chauhan, J.-H. Ahn, C. Nah, Electrochim. Acta 54 (2008) 228–234.
[185] N. Shubha, R. Prasanth, H.H. Hng, M. Srinivasan, J. Power Sources 267 (2014) 48–57.
[186] I. Villaluenga, K.H. Wujcik, W. Tong, D. Devaux, D.H. Wong, J.M. DeSimone, N.P. Balsara, Proc. Natl. Acad. Sci. U.S.A. 113 (2016) 52–57.
[187] H. Huo, B. Wu, T. Zhang, X. Zheng, L. Ge, T. Xu, X. Guo, X. Sun, Energy Storage Mater., 2019.
[188] J. Zhang, L. Yue, Q. Kong, Z. Liu, X. Zhou, C. Zhang, Q. Xu, B. Zhang, G. Ding, B. Qin, Y. Duan, Q. Wang, J. Yao, G. Cui, L. Chen, Sci. Rep. 4 (2014) 3935.
[189] D. Li, L. Chen, T. Wang, L.-Z. Fan, ACS Appl. Mater. Interfaces 10 (2018) 7069–7078.
[190] R. Khurana, J.L. Schaefer, L.A. Archer, G.W. Coates, J. Am. Chem. Soc. 136 (2014) 7395–7402.
[191] W. Zhou, Z. Wang, Y. Pu, Y. Li, S. Xin, X. Li, J. Chen, J.B. Goodenough, Adv. Mater. 31 (2019) 1805574.
[192] J.-F. Wu, B.-W. Pu, D. Wang, S.-Q. Shi, N. Zhao, X. Guo, X. Guo, ACS Appl. Mater. Interfaces 11 (2019) 898–905.
[193] D. Wang, Q. Sun, J. Luo, J. Liang, Y. Sun, R. Li, K. Adair, L. Zhang, R. Yang, S. Lu, H. Huang, X. Sun, ACS Appl. Mater. Interfaces 11 (2019) 4954–4961.
[194] F. Lu, Y. Pang, M. Zhu, F. Han, J. Yang, F. Fang, D. Sun, S. Zheng, C. Wang, Adv. Funct. Mater. 29 (2019) 1809219.
[195] T. Lapp, S. Skaarup, A. Hooper, Solid State Ionics 11 (1983) 97–103.
[196] J. Bates, N. Dudney, B. Neudecker, A. Ueda, C. Evans, Solid State Ionics 135 (2000) 33–45.
[197] D. Lin, W. Liu, Y. Liu, H.R. Lee, P.-C. Hsu, K. Liu, Y. Cui, Nano Lett. 16 (2015) 459–465.
[198] Y. Liu, J.Y. Lee, L. Hong, J. Appl. Polym. Sci. 89 (2003) 2815–2822.
[199] C. Galven, J.-L. Fourquet, M.-P. Crosnier-Lopez, F.o. Le Berre, Chem. Mater. 23 (2011) 1892–1900.
[200] G. Sahu, Z. Lin, J. Li, Z. Liu, N. Dudney, C. Liang, Energy Environ. Sci. 7 (2014) 1053–1058.
[201] Y.G. Zhang, Y. Zhao, D. Gosselink, P. Chen, Ionics 21 (2015) 381–385.
[202] M. Keller, G.B. Appetecchi, G.-T. Kim, V. Sharova, M. Schneider, J. Schuhmacher, A. Roters, S. Passerini, J. Power Sources 353 (2017) 287–297.
[203] D.W. McOwen, S. Xu, Y. Gong, Y. Wen, G.L. Godbey, J.E. Gritton, T.R. Hamann, J. Dai, G.T. Hitz, L. Hu, Adv. Mater. 30 (2018) 1707132.
[204] A. Hayashi, T. Harayama, F. Mizuno, M. Tatsumisago, J. Power Sources 163 (2006) 289–293.
[205] E. Rangasamy, G. Sahu, J.K. Keum, A.J. Rondinone, N.J. Dudney, C. Liang, J. Mater. Chem. A 2 (2014) 4111–4116.
[206] R.-J. Chen, Y.-B. Zhang, T. Liu, B.-Q. Xu, Y.-H. Lin, C.-W. Nan, Y. Shen, ACS Appl. Mater. Interfaces 9 (2017) 9654–9661.
[207] H. Zhai, P. Xu, M. Ning, Q. Cheng, J. Mandal, Y. Yang, Nano Lett. 17 (2017) 3182–3187.
[208] J. Bae, Y. Li, J. Zhang, X. Zhou, F. Zhao, Y. Shi, J.B. Goodenough, G. Yu, Angew. Chem. Int. Ed. 57 (2018) 2096–2100.
[209] K. Fu, Y. Wang, C. Yan, Y. Yao, Y. Chen, J. Dai, S. Lacey, Y. Wang, J. Wan, T. Li, Z. Wang, Y. Xu, L. Hu, Adv. Mater. 28 (2016) 2587–2594.
[210] J. Li, M.C. Leu, R. Panat, J. Park, Mater. Des. 119 (2017) 417–424.
[211] X. Gao, Q. Sun, X. Yang, J. Liang, A. Koo, W. Li, J. Liang, J. Wang, R. Li, F.B. Holness, A.D. Price, S. Yang, T.-K. Sham, X. Sun, Nano Energy 56 (2019) 595–603.
[212] A.J. Blake, R.R. Kohlmeyer, J.O. Hardin, E.A. Carmona, B. Maruyama, J.D. Berrigan, H. Huang, M.F. Durstock, Adv. Energy Mater. 7 (2017) 1602920.
[213] M. Cheng, Y. Jiang, W. Yao, Y. Yuan, R. Deivanayagam, T. Foroozan, Z. Huang, B. Song, R. Rojaee, T. Shokuhfar, Y. Pan, J. Lu, R. Shahbazian-Yassar, Adv. Mater. 30 (2018) 1800615.
[214] K. Sun, T.-S. Wei, B.Y. Ahn, J.Y. Seo, S.J. Dillon, J.A. Lewis, Adv. Mater. 25 (2013) 4539–4543.
[215] K. Fu, Y. Yao, J. Dai, L. Hu, Adv. Mater. 29 (2017) 1603486.
[216] X. Tian, J. Jin, S. Yuan, C.K. Chua, S.B. Tor, K. Zhou, Adv. Energy Mater. 7 (2017) 1700127.
[217] J.E. Weston, B.C.H. Steele, Solid State Ion 7 (1982) 75–79.
[218] F. Croce, L. Persi, F. Ronci, B. Scrosati, Solid State Ionics 135 (2000) 47–52.
[219] C.W. Lin, C.L. Hung, M. Venkateswarlu, B.J. Hwang, J. Power Sources 146 (2005) 397–401.
[220] S. Jayanthi, K. Kulasekarapandian, A. Arulsankar, K. Sankaranarayanan, B. Sundaresan, J. Compos. Mater. 49 (2015) 1035–1045.
[221] O. Sheng, C. Jin, J. Luo, H. Yuan, C. Fang, H. Huang, Y. Gan, J. Zhang, Y. Xia, C. Liang, W. Zhang, X. Tao, J. Mater. Chem. A 5 (2017) 12934–12942.
[222] K. Liu, F. Ding, Q.W. Lu, J.Q. Liu, Q.Q. Zhang, X.J. Liu, Q. Xu, Solid State Ionics 289 (2016) 1–8.
[223] A.M. Stephan, T.P. Kumar, M.A. Kulandainathan, N.A. Laksh, J. Phys. Chem. B 113 (2009) 1963–1971.
[224] J.L. Schaefer, D.A. Yanga, L.A. Archer, Chem. Mater. 25 (2013) 834–839.
[225] Z. Wang, S. Wang, A. Wang, X. Liu, J. Chen, Q. Zeng, L. Zhang, W. Liu, L. Zhang, J. Mater. Chem. A 6 (2018) 17227–17234.
[226] C. Yuan, J. Li, P. Han, Y. Lai, Z. Zhang, J. Liu, J. Power Sources 240 (2013) 653–658.
[227] C. Gerbaldi, J.R. Nair, M.A. Kulandainathan, R.S. Kumar, C. Ferrara, P. Mustarellic, A.M. Stephan, J. Mater. Chem. A 2 (2014) 9948–9954.
[228] K. Zhu, Y. Liu, J. Liu, RSC Adv. 4 (2014) 42278–42284.
[229] Y.J. Wang, Y. Pan, L. Wang, M.J. Pang, L. Chen, J. Appl. Polym. Sci. 102 (2006) 4269–4275.
[230] Y.J. Wang, Y. Pan, D. Kim, J. Power Sources 159 (2006) 690–701.
[231] S.-K. Kim, Y.-C. Jung, D.-H. Kim, W.-C. Shin, M. Ue, D.-W. Kim, J. Electrochem. Soc. 163 (2016) A974–A980.
[232] Y.-C. Jung, M.-S. Park, C.-H. Doh, D.-W. Kim, Electrochim. Acta 218 (2016) 271–277.
[233] Y. Zhao, Z. Huang, S. Chen, B. Chen, J. Yang, Q. Zhang, F. Ding, Y. Chen, X. Xu, Solid State Ionics 295 (2016) 65–71.
[234] W. Liu, N. Liu, J. Sun, P.-C. Hsu, Y. Li, H.-W. Lee, Y. Cui, Nano Lett. 15 (2015) 2740–2745.
[235] S. Ohta, T. Kobayashi, T. Asaoka, J. Power Sources 196 (2011) 3342–3345.
[236] J.H. Choi, C.H. Lee, J.H. Yu, C.H. Doh, S.M. Lee, J. Power Sources 274 (2015) 458–463.
[237] J. Zhang, N. Zhao, M. Zhang, Y. Li, P.K. Chu, X. Guo, Z. Di, X. Wang, H. Li, Nano Energy 28 (2016) 447–454.
[238] Z. He, L. Chen, B. Zhang, Y. Liu, L.-Z. Fan, J. Power Sources 392 (2018) 232–238.
[239] X. Zhang, T. Liu, S. Zhang, X. Huang, B. Xu, Y. Lin, B. Xu, L. Li, C.-W. Nan, Y. Shen, J. Am. Chem. Soc. 139 (2017) 13779–13785.
[240] J. Yu, S.C.T. Kwok, Z. Lu, M.B. Effat, Y.-Q. Lyu, M.M.F. Yuen, F. Ciucci, Chemelectrochem 5 (2018) 2873–2881.
[241] K. Kimura, H. Matsumoto, J. Hassoun, S. Panero, B. Scrosati, Y. Tominaga, Electrochim. Acta 175 (2015) 134–140.
[242] W. Zhang, J. Nie, F. Li, Z.L. Wang, C. Sun, Nano Energy 45 (2018) 413–419.
[243] H. Huo, Y. Chen, J. Luo, X. Yang, X. Guo, X. Sun, Adv. Energy Mater. 9 (2019) 1804004.
[244] Y. Zhao, C. Wu, G. Peng, X. Chen, X. Yao, Y. Bai, F. Wu, S. Chen, X. Xu, J. Power Sources 301 (2016) 47–53.
[245] S. Chen, J. Wang, Z. Zhang, L. Wu, L. Yao, Z. Wei, Y. Deng, D. Xie, X. Yao, X. Xu, J. Power Sources 387 (2018) 72–80.
[246] J. Wolfenstine, J.L. Allen, J. Sakamoto, D.J. Siegel, H. Choe, Ionics 24 (2018) 1271–1276.
[247] S. Bi, C.N. Sun, T.A. Zawodzinski, F. Ren, J.K. Keum, S.K. Ahn, D. Li, J. Chen, J. Polym. Sci., Part B: Polym. Phys. 53 (2015) 1450–1457.
[248] S. Kohjiya, T. Kitade, Y. Ikeda, A. Hayashi, A. Matsuda, M. Tatsumisago, T. Minami, Solid State Ionics 154 (2002) 1–6.
[249] D.H. Wong, J.L. Thelen, Y. Fu, D. Devaux, A.A. Pandya, V.S. Battaglia, N.P. Balsara, J.M. DeSimone, Proc. Natl. Acad. Sci. U.S.A. 111 (2014) 3327–3331.
[250] H. Aono, E. Sugimoto, Y. Sadaaka, N. Imanaka, G. Adachi, J. Electrochem. Soc. 136 (1989) 590–591.
[251] X. Xu, Z. Wen, X. Yang, J. Zhang, Z. Gu, Solid State Ionics 177 (2006) 2611–2615.
[252] P. Knauth, Solid State Ionics 180 (2009) 911–916.
[253] K. Takada, M. Tansho, I. Yanase, T. Inada, A. Kajiyama, M. Kouguchi, S. Kondo, M. Watanabe, Solid State Ionics 139 (2001) 241–247.
[254] K. Arbi, S. Mandal, J. Rojo, J. Sanz, Chem. Mater. 14 (2002) 1091–1097.
[255] M. Kotobuki, M. Koishi, Ceram. Int. 39 (2013) 4645–4649.
[256] H. Chung, B. Kang, Solid State Ionics 263 (2014) 125–130.
[257] V. Thangadurai, W. Weppner, J. Solid State Chem. 179 (2006) 974–984.
[258] Y. Gao, X. Wang, W. Wang, Z. Zhuang, D. Zhang, Q. Fang, Solid State Ionics 181 (2010) 1415–1419.
[259] H. Xie, Y. Li, J. Han, Y. Dong, M.P. Paranthaman, L. Wang, M. Xu, A. Gupta, Z. Bi, C.A. Bridges, M. Nakanishui, A.P. Sokolov, J.B. Goodenough, J. Electrochem. Soc. 159 (2012) A1148–A1151.
[260] Y. Li, J.-T. Han, C.-A. Wang, H. Xie, J.B. Goodenough, J. Mater. Chem. 22 (2012) 15357–15361.
[261] V. Thangadurai, W. Weppner, J. Electrochem. Soc. 151 (2004). H1-H6.
[262] M. Itoh, Y. Inaguma, W.-H. Jung, L. Chen, T. Nakamura, Solid State Ionics 70 (1994) 203–207.
[263] V. Thangadurai, W. Weppner, Ionics 6 (2000) 70–77.
[264] K. Mizumoto, S. Hayashi, Solid State Ionics 116 (1999) 263–269.
[265] S. Garcıa-Martın, J. Rojo, H. Tsukamoto, E. Morán, M. Alario-Franco, Solid State Ionics 116 (1999) 11–18.
[266] S. Stramare, V. Thangadurai, W. Weppner, Chem. Mater. 15 (2003) 3974–3990.
[267] P. Bron, S. Johansson, K. Zick, J.r. Schmedt auf der Günne, S. Dehnen, B. Roling, J. Am. Chem. Soc. 135 (2013) 15694–15697.
[268] Y. Seino, T. Ota, K. Takada, A. Hayashi, M. Tatsumisago, Energy Environ. Sci. 7 (2014) 627–631.
[269] H. Yamane, M. Shibata, Y. Shimane, T. Junke, Y. Seino, S. Adams, K. Minami, A. Hayashi, M. Tatsumisago, Solid State Ionics 178 (2007) 1163–1167.
[270] Z. Liu, W. Fu, E.A. Payzant, X. Yu, Z. Wu, N.J. Dudney, J. Kiggans, K. Hong, A.J. Rondinone, C. Liang, J. Am. Chem. Soc. 135 (2013) 975–978.
[271] M. Tatsumisago, Solid State Ionics 175 (2004) 13–18.
[272] E. Rietman, M. Kaplan, R. Cava, Solid State Ionics 25 (1987) 41–44.
[273] S.K. Fullerton-Shirey, J.K. Maranas, J. Phys. Chem. C 114 (2010) 9196–9206.
[274] S.H.-S. Cheng, K.-Q. He, Y. Liu, J.-W. Zha, M. Kamruzzaman, R.L.-W. Ma, Z.-M. Dang, R.K. Li, C. Chung, Electrochim. Acta 253 (2017) 430–438.
[275] C.-Z. Zhao, X.-Q. Zhang, X.-B. Cheng, R. Zhang, R. Xu, P.-Y. Chen, H.-J. Peng, J.-Q. Huang, Q. Zhang, Proc. Natl. Acad. Sci. U.S.A. 114 (2017) 11069–11074.
[276] M. Dissanayake, P. Jayathilaka, R. Bokalawala, I. Albinsson, B.-E. Mellander, J. Power Sources 119 (2003) 409–414.

[277] F. Croce, L. Persi, B. Scrosati, F. Serraino-Fiory, E. Plichta, M. Hendrickson, Electrochim. Acta 46 (2001) 2457–2461.
[278] Z. Wang, X. Huang, L. Chen, Electrochem. Solid State Lett. 6 (2003) E40–E44.
[279] J. Shin, S. Passerini, J. Electrochem. Soc. 151 (2004) A238–A245.
[280] G. Appetecchi, F. Croce, L. Persi, F. Ronci, B. Scrosati, Electrochim. Acta 45 (2000) 1481–1490.
[281] J. Zheng, M. Tang, Y.Y. Hu, Angew. Chem. 128 (2016) 12726–12730.
[282] W. Gang, J. Roos, D. Brinkmann, F. Capuano, F. Croce, B. Scrosati, Solid State Ionics 53 (1992) 1102–1105.
[283] E.M. Masoud, A.A. El-Bellihi, W.A. Bayoumy, M.A. Mousa, J. Alloy. Comp. 575 (2013) 223–228.
[284] P. Sun, Y.H. Liao, X.Y. Luo, Z.H. Li, T.T. Chen, L.D. Xing, W.S. Li, RSC Adv. 5 (2015) 64368–64377.
[285] H. Xie, C. Yang, K. Fu, Y. Yao, F. Jiang, E. Hitz, B. Liu, S. Wang, L. Hu, Adv. Energy Mater. 8 (2018) 1703474.
[286] Y.-T. Kim, E.S. Smotkin, Solid State Ionics 149 (2002) 29–37.
[287] S. Ibrahim, M.R. Johan, Int. J. Electrochem. Sci 6 (2011) 5565–5587.
[288] H. Huo, N. Zhao, J. Sun, F. Du, Y. Li, X. Guo, J. Power Sources 372 (2017) 1–7.
[289] P.-J. Alarco, Y. Abu-Lebdeh, A. Abouimrane, M. Armand, Nat. Mater. 3 (2004) 476–481.
[290] H.T. Le, D.T. Ngo, R.S. Kalubarme, G. Cao, C.-N. Park, C.-J. Park, ACS Appl. Mater. Interfaces 8 (2016) 20710–20719.
[291] J. Zheng, H. Dang, X. Feng, P.-H. Chien, Y.-Y. Hu, J. Mater. Chem. A 5 (2017) 18457–18463.
[292] W.A. Henderson, N.R. Brooks, V.G. Young, J. Am. Chem. Soc. 125 (2003) 12098–12099.
[293] Y. Noda, K. Nakano, H. Takeda, M. Kotobuki, L. Lu, M. Nakayama, Chem. Mater. 29 (2017) 8983–8991.
[294] B. Lang, B. Ziebarth, C. Elsässer, Chem. Mater. 27 (2015) 5040–5048.
[295] E. Quartarone, P. Mustarelli, Chem. Soc. Rev. 40 (2011) 2525–2540.
[296] Q. Ma, X.X. Zeng, J. Yue, Y.X. Yin, T.T. Zuo, J.Y. Liang, Q. Deng, X.W. Wu, Y.G. Guo, Adv. Energy Mater. 9 (2019) 1803854.
[297] Z. Wan, D. Lei, W. Yang, C. Liu, K. Shi, X. Hao, L. Shen, W. Lv, B. Li, Q.-H. Yang, F. Kang, Y.-B. He, Adv. Funct. Mater. 29 (2019) 1805301.
[298] X. Chen, W. He, L.-X. Ding, S. Wang, H. Wang, Energy Environ. Sci. 12 (2019) 938–944.
[299] M. Jo, Y.-S. Hong, J. Choo, J. Cho, J. Electrochem. Soc. 156 (2009) A430–A434.
[300] D.W. Dees, K.G. Gallagher, D.P. Abraham, A.N. Jansen, J. Electrochem. Soc. 160 (2013) A478–A486.
[301] L. Wang, Y. Wang, Y. Xia, Energy Environ. Sci. 8 (2015) 1551–1558.
[302] S. Wang, Y. Ding, G. Zhou, G. Yu, A. Manthiram, ACS Energy Lett 1 (2016) 1080–1085.
[303] C. Wang, Q. Sun, Y. Liu, Y. Zhao, X. Li, X. Lin, M.N. Banis, M. Li, W. Li, K.R. Adair, D. Wang, J. Liang, R. Li, L. Zhang, R. Yang, S. Lu, X. Sun, Nano Energy 48 (2018) 35–43.
[304] A. Hayashi, T. Ohtomo, F. Mizuno, K. Tadanaga, M. Tatsumisago, Electrochem. Commun. 5 (2003) 701–705.
[305] J. Hassoun, B. Scrosati, Adv. Mater. 22 (2010) 5198–5201.
[306] A. Hayashi, R. Ohtsubo, T. Ohtomo, F. Mizuno, M. Tatsumisago, J. Power Sources 183 (2008) 422–426.
[307] M. Nagao, A. Hayashi, M. Tatsumisago, J. Mater. Chem. 22 (2012) 10015–10020.
[308] D. Zhou, Y. Chen, B. Li, H. Fan, F. Cheng, D. Shanmukaraj, T. Rojo, M. Armand, G. Wang, Angew. Chem. Int. Ed. 57 (2018) 10168–10172.
[309] X. Yu, Z. Bi, F. Zhao, A. Manthiram, ACS Appl. Mater. Interfaces 7 (2015) 16625–16631.
[310] N. Li, Z. Weng, Y. Wang, F. Li, H.-M. Cheng, H. Zhou, Energy Environ. Sci. 7 (2014) 3307–3312.
[311] X. Yu, Z. Bi, F. Zhao, A. Manthiram, Adv. Energy Mater. 6 (2016) 1601392.
[312] Q. Wang, J. Jin, X. Wu, G. Ma, J. Yang, Z. Wen, Phys. Chem. Chem. Phys. 16 (2014) 21225–21229.
[313] H. Zhou, Y. Wang, H. Li, P. He, ChemSuschem 3 (2010) 1009–1019.
[314] M.R. Busche, T. Drossel, T. Leichtweiss, D.A. Weber, M. Falk, M. Schneider, M.-L. Reich, H. Sommer, P. Adelhelm, J. Janek, Nat. Chem. 8 (2016) 426–434.
[315] Y.T. Li, B.Y. Xu, H.H. Xu, H.N. Duan, X.J. Lu, S. Xin, W.D. Zhou, L.G. Xue, G.T. Fu, A. Manthiram, J.B. Goodenough, Angew. Chem. Int. Ed. 56 (2017) 753–756.
[316] B. Liu, Y. Gong, K. Fu, X. Han, Y. Yao, G. Pastel, C. Yang, H. Xie, E.D. Wachsman, L. Hu, ACS Appl. Mater. Interfaces 9 (2017) 18809–18815.
[317] Q. Wang, Z. Wen, J. Jin, J. Guo, X. Huang, J. Yang, C. Chen, Chem. Commun. 52 (2016) 1637–1640.
[318] J. Liang, Q. Sun, Y. Zhao, Y. Sun, C. Wang, W. Li, M. Li, D. Wang, X. Li, Y. Liu, J. Mater. Chem. A 6 (2018) 23712–23719.
[319] S.-S. Chi, Y. Liu, N. Zhao, X. Guo, C.-W. Nan, L.-Z. Fan, Energy Storage Mater 17 (2019) 309–316.
[320] C. Wang, K.R. Adair, J. Liang, X. Li, Y. Sun, X. Li, J. Wang, Q. Sun, F. Zhao, X. Lin, R. Li, H. Huang, L. Zhang, R. Yang, S. Lu, X. Sun, Adv. Funct. Mater. (2019) 1900392.
[321] Y. Li, B. Xu, H. Xu, H. Duan, X. Lü, S. Xin, W. Zhou, L. Xue, G. Fu, A. Manthiram, Angew. Chem. Int. Ed. 56 (2017) 753–756.
[322] T. Abe, M. Ohtsuka, F. Sagane, Y. Iriyama, Z. Ogumi, J. Electrochem. Soc. 151 (2004) A1950–A1953.
[323] W.E. Tenhaeff, K.A. Perry, N.J. Dudney, J. Electrochem. Soc. 159 (2012) A2118–A2123.
[324] W.C. Chueh, F. El Gabaly, J.D. Sugar, N.C. Bartelt, A.H. McDaniel, K.R. Fenton, K.R. Zavadil, T. Tyliszczak, W. Lai, K.F. McCarty, Nano Lett. 13 (2013) 866–872.
[325] M. Yashima, M. Itoh, Y. Inaguma, Y. Morii, J. Am. Chem. Soc. 127 (2005) 3491–3495.
[326] C. Li, H. Zhang, L. Otaegui, G. Singh, M. Armand, L.M. Rodriguez-Martinez, J. Power Sources 326 (2016) 1–5.
[327] Y. Hamon, A. Douard, F. Sabary, C. Marcel, P. Vinatier, B. Pecquenard, A. Levasseur, Solid State Ionics 177 (2006) 257–261.
[328] R.A. Jonson, P.J. McGinn, Solid State Ionics 323 (2018) 49–55.
[329] N. Ohta, K. Takada, I. Sakaguchi, L. Zhang, R. Ma, K. Fukuda, M. Osada, T. Sasaki, Electrochem. Commun. 9 (2007) 1486–1490.
[330] Y. Zhao, X. Sun, ACS Energy Lett 3 (2018) 899–914.
[331] Y. Zhao, K. Zheng, X. Sun, Joule 2 (2018) 1–22.
[332] F. Lin, Y. Liu, X. Yu, L. Cheng, A. Singer, O.G. Shpyrko, H.L. Xin, N. Tamura, C. Tian, T.-C. Weng, X.-Q. Yang, Y.S. Meng, D. Nordlund, W. Yang, M.M. Doeff, Chem. Rev. 117 (2017) 13123–13186.
[333] J. Lu, T. Wu, K. Amine, Nat. Energy 2 (2017) 17011.
[334] Y. Yang, X. Liu, Z. Dai, F. Yuan, Y. Bando, D. Golberg, X. Wang, Adv. Mater. 29 (2017) 1606922.
[335] X. Li, H.Y. Wang, H. Yang, W. Cai, S. Liu, B. Liu, Small Methods 2 (2018) 1700395.